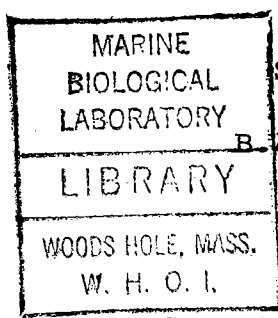


GC
7.1
L57
1977

DATA ADAPTIVE VELOCITY/DEPTH SPECTRA ESTIMATION
IN
SEISMIC WIDE ANGLE REFLECTION ANALYSIS

by



Steven John Leverette
B.A., Gettysburg College
(1972)

SUBMITTED IN PARTIAL FULFILLMENT
OF THE REQUIREMENTS FOR THE
DEGREE OF

DOCTOR OF PHILOSOPHY

at the

WOODS HOLE OCEANOGRAPHIC INSTITUTION
and the
MASSACHUSETTS INSTITUTE OF TECHNOLOGY

JOINT PROGRAM IN OCEANOGRAPHIC ENGINEERING

July 1977

Signature of Author..... *Steven J. Leverette*
Department of Ocean Engineering, July 1977

Certified by..... *Arthur B. Bayne*
Thesis Supervisor

Accepted by..... *Earl C. Hays*
Chairman, Joint Committee on Ocean Engineering

DATA ADAPTIVE VELOCITY/DEPTH SPECTRA ESTIMATION
IN
SEISMIC WIDE ANGLE REFLECTION ANALYSIS

by

STEVEN JOHN LEVERETTE

Submitted to the Department of Ocean Engineering
on July 1, 1977 in partial fulfillment of the
requirements for the degree of Doctor of Philosophy

ABSTRACT

In studying the earth with reflection seismics, one of the major unknowns is the velocity structure of the medium. Techniques used to determine the velocity structure commonly involve multi-channel arrays which measure the spatial as well as the time structure of the returning signals. The application of a data adaptive technique, the Maximum Likelihood Method, to the problem of estimating seismic velocities is described. The peculiar problems of this application are identified and investigated. The windowing of short duration signals is shown to be an important consideration, and the statistics of the MLM estimator for a single observation of the data set are presented. The adaptive estimator is applied to an ideal covariance matrix, to simulated data, and to field data. The results show the MLM

velocity/depth estimator to be a valuable tool in seismic analysis, and the windowing and statistical results should have general applications in a variety of fields.

Thesis Supervisor: Arthur B. Baggeroer, Associate Professor,
Ocean and Electrical Engineering, M.I.T.

ACKNOWLEDGEMENTS

This study was supported in part by NSF-IDOE Grant GX-4094, NOAA Contract 04-6-158-44081, ONR Contract N00014-77-6-0266, by a fellowship from the Research Laboratory of Electronics at MIT, and by the MIT/WHOI Joint Program in Ocean Engineering.

Many persons contributed with advice and guidance during the course of the project. The contributions of my advisor; Prof. Arthur Baggeroer, and committee; Prof. Owen Oakley, Dr. Woollcott Smith, and Dr. Robert Spindel were all vital to the success of the study.

The work could not have been done without the continuous support of Ken Prada and the rest of the "First Team". Their contributions of data acquisition, computer time, and moral support were invaluable. Special thanks go to Dr. Robert Ballard, who initially served on the thesis committee and spent many long hours providing a geophysical input to our early struggles in developing velocity analysis methods, and to Dr. John Grow of the USGS, who provided data for our pre-cruise development. Nancy Barnes assisted with the lengthy task of drafting innumerable figures and Lin Morse

helped type the preliminary draft.

Finally, I wish to thank my parents for providing me with the foundations and support that have enabled me to go this far.

TABLE OF CONTENTS

Title Page.....	1
Abstract.....	2
Acknowledgements.....	4
Table of Contents.....	6
Introduction.....	8
I. Travel Time Calculations.....	19
II. Estimation of the Velocity Function.....	33
The Velocity/Depth Spectrum.	
Seismic Reflection Data.	
Partitioning the Estimation Procedure.	
Conventional Estimator.	
Adaptive Estimator.	
III. Beam Patterns and Ambiguity Functions.....	57
IV. Estimation of the Cross-Spectral Correlation Matrix... 65	
4-A Windows and the Bias of Transforms.	
4-B Averaging and the Stability of the Cross-Spectral Correlation Matrix.	
V. Statistics of the Estimators.....	93
Conventional Estimator Statistics.	
MLM Estimator Statistics.	
MLM for a Singular Covariance Matrix.	
Single Observation MLM Estimator - Exact Solution.	
Statistics of Single Observation Estimators.	
Summary.	
VI. Experimental Results and Conclusions.....	116
Appendix I.....	146

TABLE OF CONTENTS, continued

Appendix II.....	150
Appendix III.....	155
Glossary of Notation and Symbols.....	157
References.....	163
Biographical Note.....	167

Introduction

This thesis considers the application of data adaptive array processing methods to the estimation of velocity/depth spectra in multi-channel seismic reflection data. The adaptive processing methods are not new; the basic techniques were developed more than a decade ago for other applications, and have been applied to a multitude of time series and array processing problems to date. The intention of the author in undertaking this study is to generalize the adaptive methods for application to non-plane wave, non-homogeneous array data, and to study the requirements and performance of the estimation methods as applied to velocity/depth spectra estimation. The application appears successful and the result is an additional tool for the geophysicist in his search for higher resolution in studying the earth's structure. This thesis presents the velocity/depth spectral estimators and compares the conventional and adaptive forms. The details of their implementation are considered and an analysis of their statistics is presented. The primary contributions of this work are the implementation of the adaptive processor to non-stationary fields, the importance and sensitivity of the time windowing to the

conflicting requirements of time and frequency resolution, and an analysis of the statistics of the adaptive estimator for a singular covariance matrix.

The concept of remotely determining seismic velocities has been used for many years (Green, 1938). Before the advent of the digital computer, the techniques involved the physical manipulation of plotted records and the fitting of curves to visually determined arrival times. Along with the digital computer came the ability to perform the velocity estimates using correlation techniques and the reality of an entire velocity/depth spectrum. A sampling of this development may be found in the literature in papers by Green (1938), Durbaum (1954), Dix (1955), LePichon, et al (1968), and Taner and Koehler (1969). The velocity/depth spectrum as we use it may be defined as an estimate of the coherent reflected signal power received from subsurface reflectors as a function of the depth (in travel time) of the reflector and the seismic RMS velocity to the reflector. The amount of effort expended in velocity analysis in seismics is justified by the fact that most of the further processing or analysis of data that is commonly performed makes use of the velocity information. In particular, common depth point stacking and migration techniques depend heavily on accurate velocity determinations.

Unlike most types of array processing, we are dealing with a medium which has non-homogeneous wave velocities. In order to correctly phase or focus the array, we must be able to relate the spatial position of the array elements to phase shifts or delay times. The velocity/depth spectrum provides the information which enables us to do this. In addition to its applications in further processing of the data, the velocity/depth information is used in stratigraphic interpretation as an aid in following layers and in determining the nature of the structure. An important use in geophysical interpretation is in differentiating between overlapping primary returns from deeper layers and multiple reflections from shallow reflectors on continuous profiling records. The normally higher velocities of deeper strata make it possible to distinguish the two types of returns.

Data adaptive processing methods have been developed in several areas which include sonar array processing (see Gabriel, 1976 for a good list of references), time series analysis (Burg 1967, Lacoss 1971), speech processing (Makhoul 1975), and communication theory (Van Trees 1968, Makhoul 1975). The development was often simultaneous, but approached in different ways. It is interesting to note that although each field has its own literature and terminology for the

methods, many of them have been shown to be equivalent (Edelblute, et al 1966, Gabriel 1976, Pusey 1975). Generally the adaptive methods may be classified as one of two types, which have come to be known as the Maximum Likelihood Method (MLM) and the Maximum Entropy Method (MEM). The MLM is attributed to Capon (1967), but has been shown to be equivalent to several earlier techniques applied to single frequencies (Edelblute, et al. 1966). The MEM includes autoregression analysis, covariance extension, prediction error filters, innovations filters, and whitening filters. The MEM techniques are attributed to Burg (1967) and Parzen (1968, 1969). Pusey (1975) demonstrates the equivalence of some of the other MEM forms.

The method we employ in our study is the Maximum Likelihood Method. The MLM is applicable to non-homogeneous fields with non-uniform sampling, whereas the MEM has not yet been generalized to cover these cases in any reasonable manner. The application of a data adaptive estimation algorithm to velocity/depth spectra estimation was first proposed by Baggeroer (1974) and Baggeroer and Leverette (1975). This thesis is a continuation and extension of that work.

The general concept behind data adaptive processing methods is that the filter coefficients or window weighting

functions are determined from the data on each application in order to minimize the effects of noise fields. In order to demonstrate this and to further motivate a study of adaptive array procedures applied to velocity/depth spectra estimation, we would like to give two examples. The first is an application of the adaptive algorithm to an array receiving plane waves. The wave number spectra of a field containing a single plane wave are given in Figures 1. and 2. Figure 1. is the spectrum as measured by the conventional array processor, and Figure 2. is the spectrum as measured by the data adaptive array processor. The remarkable increase in resolution is more easily understood if we examine the beam patterns of the two array processors. The conventional array beam pattern is given in Figure 3. For the same array with a noise field entering from various directions (k_N), the adaptive beam pattern is given in Figure 4. By adapting to the received signal and noise field, the adaptive array is able to move its peak and sidelobes away from interfering signals. This makes the adaptive processor particularly useful for sparse arrays which normally have large sidelobe structures. For the second example, Figures 5. and 6. show samples of velocity/depth spectra generated by the two estimators from data taken on Georges Bank. Figure 5. gives the

Figure 1. Response of 6 Channel Conventional Array to Field Containing One Plane Wave.

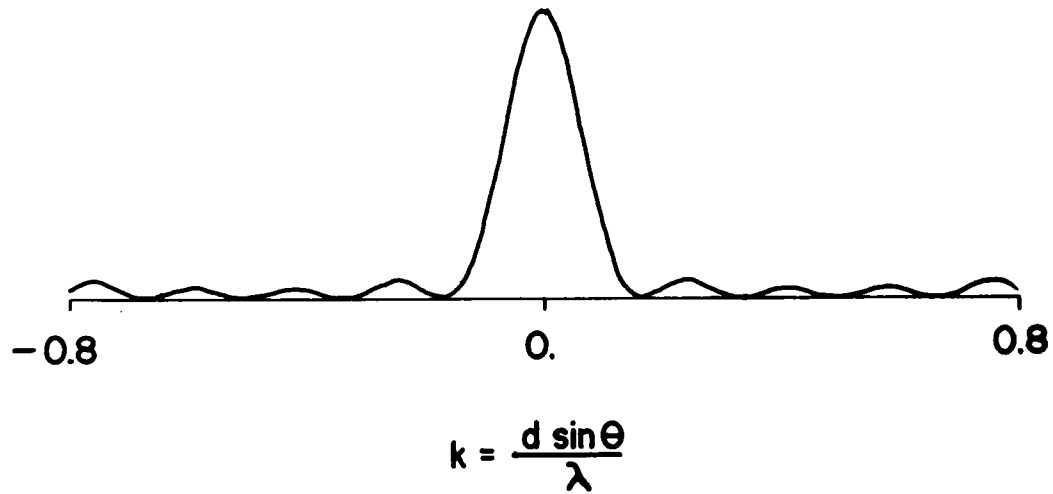


Figure 2. Response of 6 Channel Adaptive Array to Field Containing One Plane Wave and 1% White Noise. The plot shows a very sharp, narrow peak at $k=0$, indicating high resolution and noise rejection.

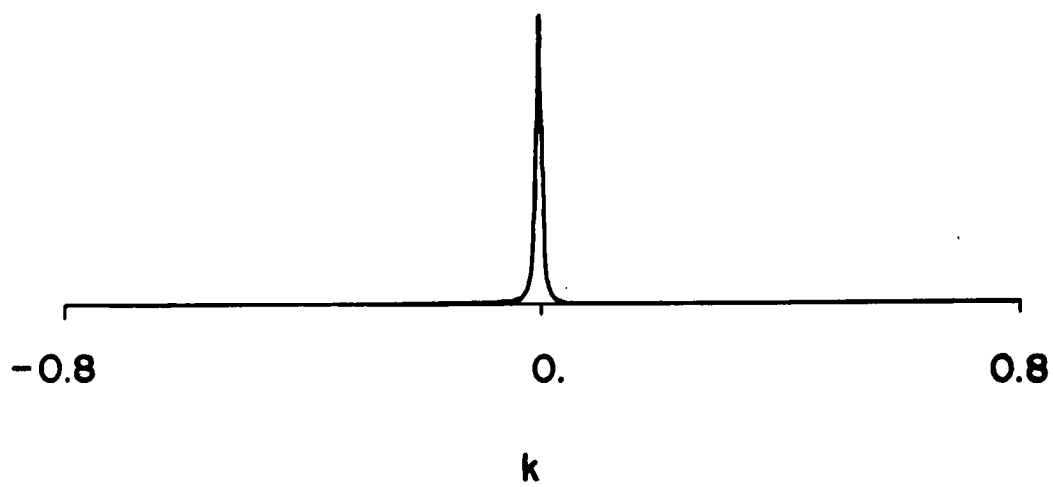


Figure 3. Beam Pattern of Conventional Array.

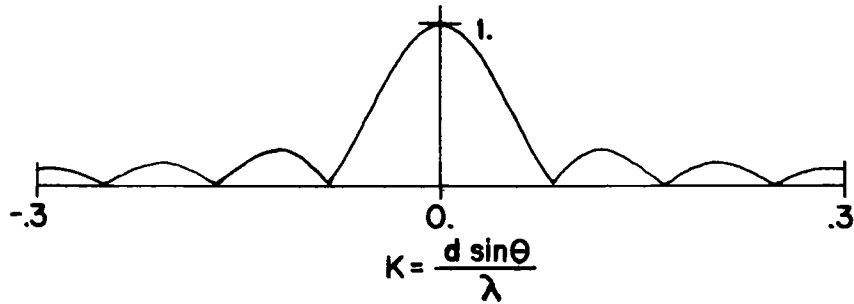


Figure 4. Beam Patterns of Adaptive Array With Various Plane Wave Inputs.

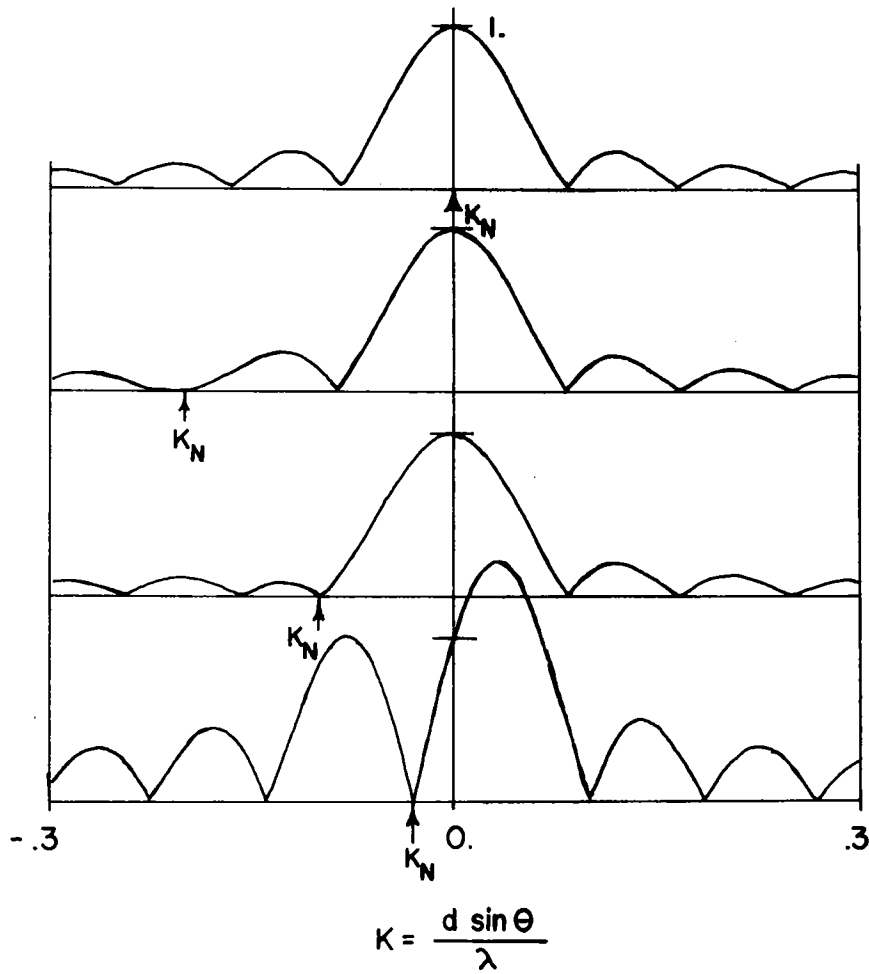


Figure 5. Conventional Velocity/Depth Spectrum.

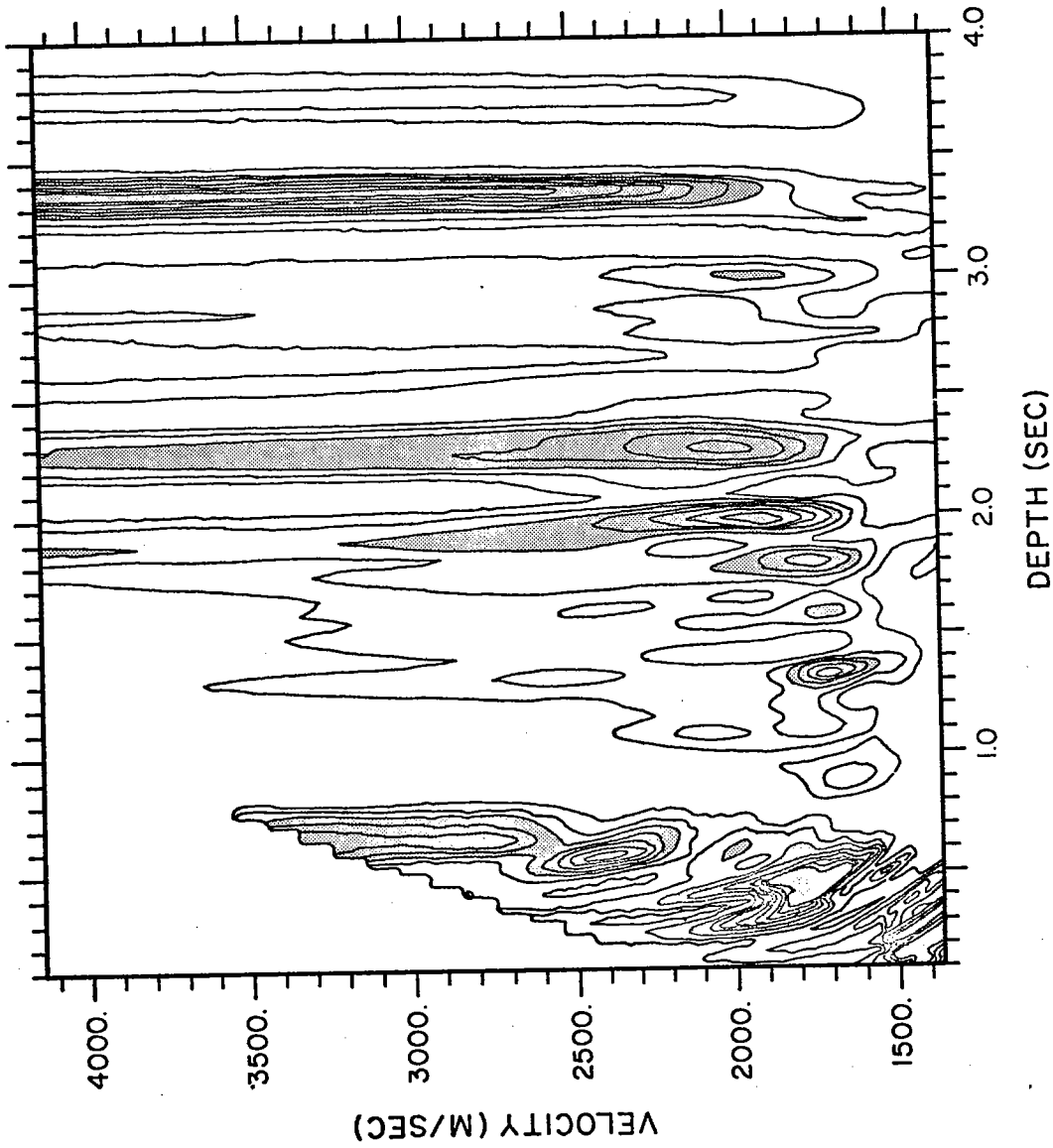
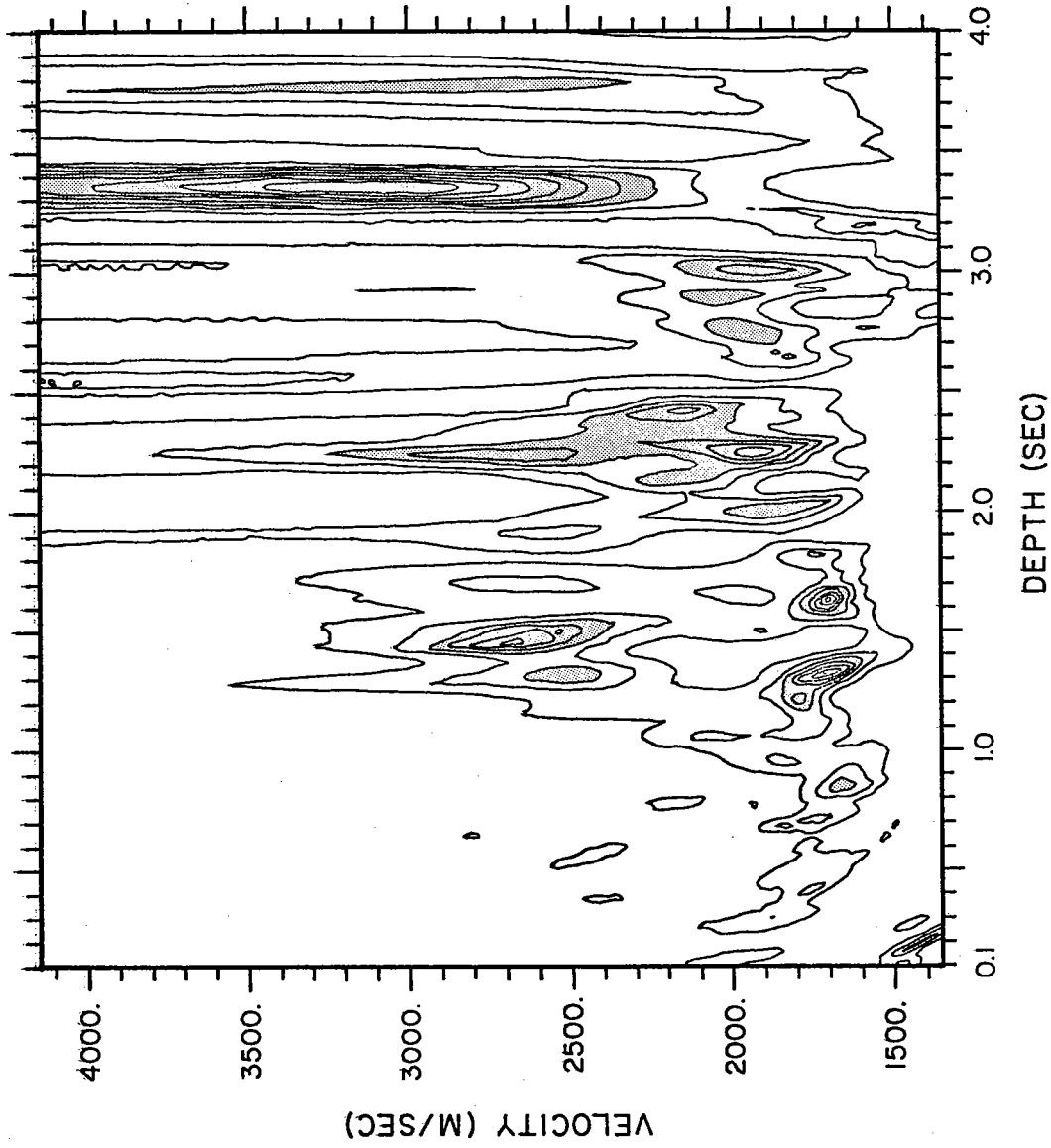


Figure 6. Data Adaptive Velocity/Depth Spectrum.



output from a conventional analysis, and Figure 6. gives the output from the data adaptive analysis. In the more complicated case of estimating velocity/depth information instead of simple plane wave vectors, the adaptive algorithm continues to exhibit a higher resolution capability.

We begin with a review of the travel time calculations and the conventional estimator. Although these may be found scattered throughout the literature, their importance to the work that follows and the relatively wide range of audience we hope to address justify a concise review. In Chapter 1 we develop the necessary background for the calculation of propagation travel times from known information about the velocity structure of the earth. In Chapter 2 we describe the inverse problem of determining seismic velocities from measured travel times, making use of the model developed in Chapter 1. The conventional estimate is presented in both the time and frequency domains and the Maximum Likelihood Method velocity/depth estimator is developed. Chapter 3 considers theoretical resolution limits of the conventional array in terms of velocity and depth. The velocity/time ambiguity function is considered, building from the work done by Kline (1976). Chapter 4 considers the problems encountered in applying the estimator to real data, specifically the

windowing and averaging requirements in forming the covariance matrix. Chapter 5 develops the statistics of the different forms of the estimators. Finally, Chapter 6 presents the experimental results and conclusions. The Appendices include some of the detailed calculations used in Chapters 4 and 5, and a glossary of symbols.

Chapter 1 Array and Travel Path Geometries and Travel Time Calculations.

Introduction

Before addressing the problem of estimation of seismic velocities, it is helpful to review some of the physical properties of the general seismic reflection problem. In this chapter we review the general array and signal path geometries and develop the commonly used RMS velocity travel time equation. The travel time, the time required for a signal to traverse a path from the source to a reflecting interface and back to a receiver, is one of the most important properties in the estimation of velocities. We calculate the travel time as a function of the source to receiver distance for a particular depth of, and RMS velocity to a reflecting surface. We can then generate a pattern of delays (or, in the frequency domain, phase shifts) that allow us to steer or phase the array to look for coherent returns as a function of velocity and depth.

Travel time calculations can become very complicated for any but the simplest geological models, and we find that simplifications of the geological models and approximate solutions are desirable and necessary for our purposes in velocity/depth spectra estimation. The RMS travel time

equation is a truncated series approximation of the travel times to interfaces in a horizontally homogeneous layered earth model. It is a particularly convenient model because it has a closed form solution and because it simplifies the velocity dependence of the delay pattern to a single average velocity rather than the entire velocity structure of the travel path.

In the remote measurement of seismic velocities, we measure the delay and curvature of a wavefront that has originated at a point source at the surface and has penetrated the earth to reflect from some lateral inhomogeneity in the substrate. The most common instrumentation used to measure the curvature of the wavefront is an array of hydrophones or geophones uniformly spaced along the surface at increasing distances from the source. The source generally gives an impulsive signal, although longer coded signals which can later be deconvolved or matched filtered are sometimes used (i.e., a chirped signal). For a single homogeneous layer the geometry is shown in Figure 1.1a. This is the exact geometry for the first return in the case of a homogeneous and horizontal first layer. In marine data, it is the water column return when there is a flat bottom. If the reflected image is unfolded (Figure 1.1b) and projected to an array

Figure 1.1a Array and Travel Path Geometries for a Single Homogeneous Layer.

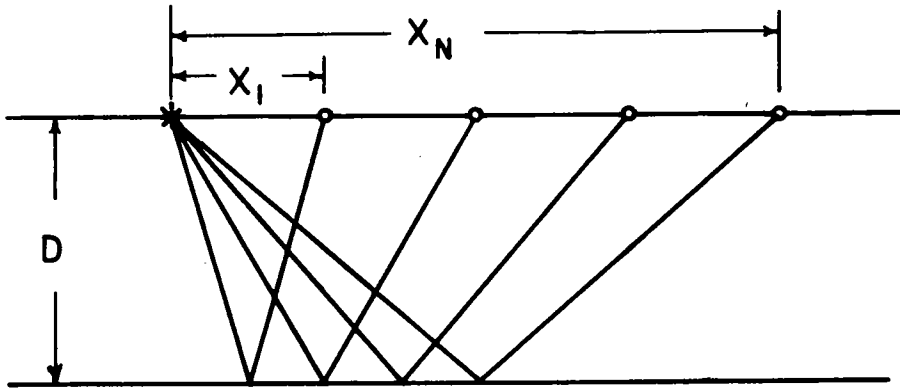
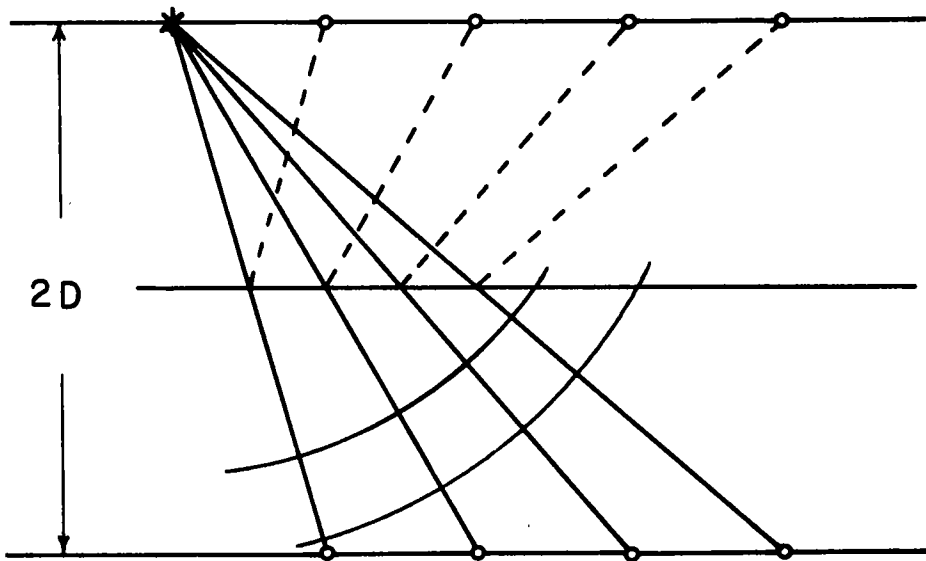


Figure 1.1b Single Layer Travel Path Unfolded.



below, it is easily seen that the wavefront is spherical and the raypaths are straight lines. The travel time to a receiver may be written as

$$T_j = \frac{1}{C} \sqrt{(2D)^2 + X_j^2} = \sqrt{T_0^2 + \frac{X_j^2}{C^2}} \quad 1.1$$

where C is the wave group velocity. We note that for convenience and in order to maintain consistency, we will use the unit of vertical two-way travel time T_0 to specify the depth of a reflector throughout the remainder of this study. Since the data is a function of time, this parameter is much easier to correlate with the data than would be depth in linear dimensions.

In the case of a non-constant sound velocity with depth, we can no longer assume straight line travel paths or perfectly spherical spreading. The rays will instead follow minimum travel time paths as given by Fermat's Principle. We can use Snell's law and ray path theory to solve for the travel time exactly, but the expression is a function of the initial angle and must be solved parametrically.

In order to generalize this exact form of travel time calculation, we consider a layered earth structure consisting of horizontal homogeneous layers. In the limit as the number

of layers goes to infinity and the layer thicknesses go to zero, this model may represent any horizontally homogeneous velocity structure. The multi-layer case is depicted in Figure 1.2. The ray parameter $\lambda = c_i / \cos \phi_i$ is preserved as the wave travels through the layers. The time through a particular layer is

$$t_i = t_{o_i} / \cos \phi_i = \lambda t_{o_i} / c_i, \quad 1.2$$

where t_{o_i} is the normal incidence travel time through the i^{th} layer. See Figure 1.3. Summing to the m^{th} layer, we obtain a two-way travel time of

$$T = 2 \sum_{i=1}^m \lambda t_{o_i} / c_i. \quad 1.3$$

The horizontal distance traveled in passing through each layer is

$$x_i = c_i t_i \sin \phi_i = t_{o_i} (\lambda^2 - c_i^2)^{1/2}. \quad 1.4$$

Summing this over a two-way trip through m layers gives us the total horizontal distance traveled.

Figure 1.2 Multi-Layer Travel Path Geometry.

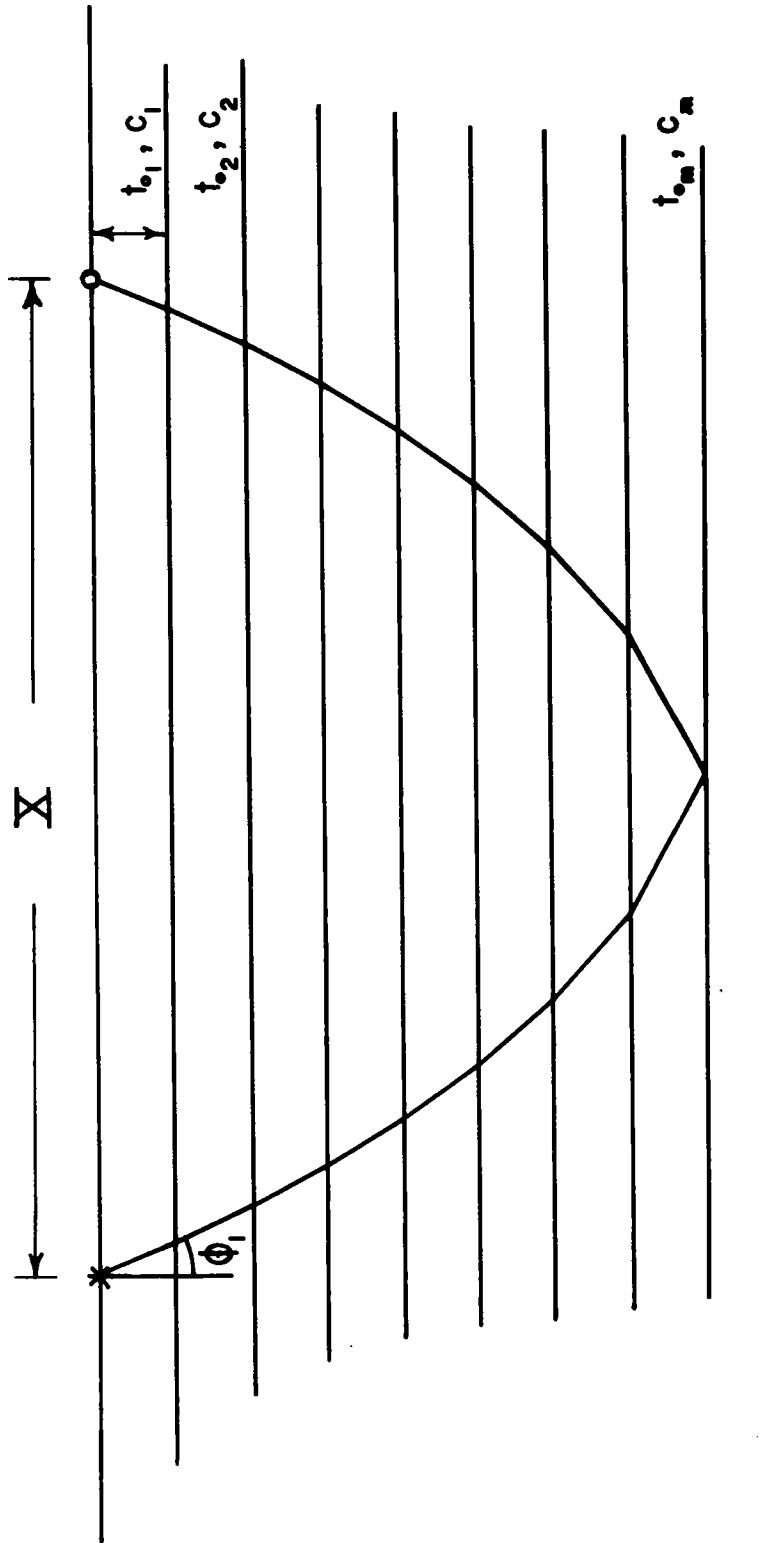
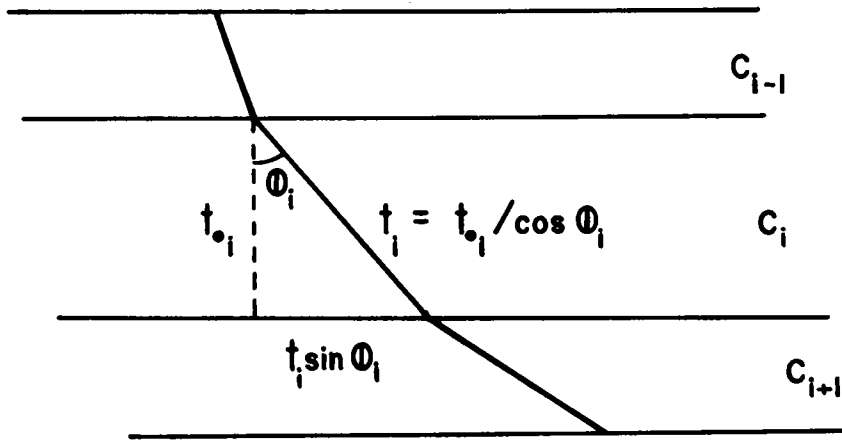


Figure 1.3 Details of One Layer of a Multi-Layer Travel Path. (Dimensions in Seismic Travel Time).



$$X = 2 \sum_{i=1}^m t_{o_i} (\lambda^2 - c_i^2)^{1/2} \quad 1.5$$

Given the source to receiver distance X_j , we can solve Equation 1.5 for λ . Inserting λ into Equation 1.3, we can then solve for the travel time T_j . For the special case where the velocity in all the layers is the same, $c_i = c_1$ for all i , the equations simplify to

$$T = \frac{\lambda}{c_1} T_0, \quad 1.6a$$

$$X = (\lambda^2 - c_1^2)^{1/2} T_0 \quad 1.6b$$

where $T_0 = \sum_{i=1}^m 2t_{o_i}$. 1.7

Solving to eliminate λ , we obtain

$$T^2 = T_0^2 + \frac{X^2}{c_1^2} \quad 1.8$$

This is identical to our result for the single layer case.

A much simpler solution was proposed by Dix (1955), which was a special case of a general solution presented by Durbaum (1954). A brief summary of the solution may be found in the appendix of Taner and Koehler (1969). We again refer

to Figure 1.2 for the travel path geometry for a separated source and receiver. Following Taner and Koehler, we write the travel time T as an infinite series in powers of X , the source to receiver distance.

$$T^2 = A_0 + A_1 X^2 + A_2 X^4 + A_3 X^6 + \dots \quad 1.9$$

Solving for the first two coefficients, we obtain

$$A_0 = \left[2 \sum_{i=1}^m t_{0i} \right]^2 = T_0^2 \quad 1.10a$$

$$A_1 = \left[A_0 \right]^{1/2} / 2 \sum_{i=1}^m c_i^2 t_{0i} = \left[2 \sum_{i=1}^m \frac{c_i^2 t_{0i}}{T_0} \right]^{-1} \quad 1.10b$$

An approximation using the first two terms of the series gives us an equation that is very similar to the expression for the travel time through a single homogeneous layer. If we define

$$\bar{C}^2 \equiv 2 \sum_{i=1}^m \frac{c_i^2 t_{0i}}{T_0}, \quad 1.11$$

where \bar{C} is a time weighted Root-Mean-Square velocity, we obtain a travel time expression of the form

$$T_j^2 = T_0^2 + \frac{1}{\bar{c}^2} X_j^2 \quad 1.12$$

This is the most common travel time expression presently in use. T_0 is the two-way normal incidence travel time to the layer of interest. \bar{c} is known as the RMS or stacking velocity. We note that it is not a true velocity, but is the first order term describing the hyperbolic curvature of the wavefront. For normal array lengths and for normally encountered seismic velocity variations, the accuracy of this approximation for the model is better than 2% (Taner and Koehler, 1969).

If it becomes necessary to go to the next term in the series, the model becomes much more complicated. The coefficient for the next term is

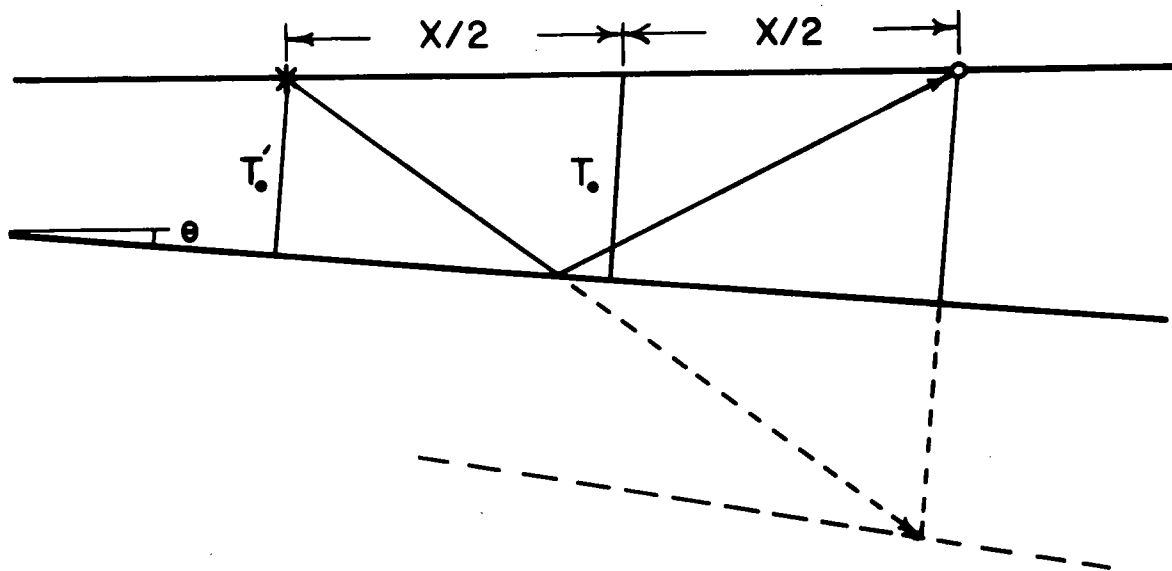
$$A_2 = \frac{\left(\sum_{i=1}^m c_i^2 t_{0i}\right)^2 - \left(\sum_{i=1}^m t_{0i}\right)\left(\sum_{i=1}^m t_{0i} c_i^4\right)}{16 \left(\sum_{i=1}^m t_{0i} c_i^2\right)^4} \quad 1.13$$

Although we can find no physical quantity corresponding directly to this term, it is a measure of the variation in layer velocities. A_2 goes to zero for $c_i = c_1$ for all i . We expect this term to be the first order variation from a hyperbolic wavefront shape. A_2 may be shown to always be less than or equal to zero by the Schwartz inequality.

The assumptions incorporated in the RMS travel time model are the horizontal homogeneity of the velocity structure, and (for A_2 to be small) an absence of extreme variations in the vertical velocity structure. In addition, all of the calculations we have considered so far require that the array length be small enough that there is always a vertical component to the velocity vector; that the travel path does not include wholly refracted segments. To put it another way, we must always be close enough to normal incidence so that the interaction with the lowest interface is strictly reflection. As the travel path deviates from vertical, the approximation in the model becomes poorer and poorer.

The most common deviation from the assumptions of the model is that there is usually some slope to the structure, both in the geology and the velocity. Solving for the first order correction to the model for uniform sloping layers, we find that the model is fairly robust to small slopes. From model studies and least squares fitting of real data, Taner and Koehler (1969) show that the returns from mildly dipping layers are still very closely hyperbolic in form. Solving for the delay times about a common central ground point for the dipping single layer case (see Figure 1.4), we obtain

Figure 1.4 Dipping Single Layer Geometry.



$$T^2 = T_0^2 + \frac{X^2}{C^2} \left(1 - \frac{\sin^2 \theta}{4} \right) \quad 1.14$$

The dipping layer always flattens the travel time curve and increases the apparent velocity. Taner and Koehler (1969) extend this to multi-layered cases. With all other parameters held constant, increased dips produce higher apparent velocities. But, although the apparent velocities vary, it is important that it is still possible to closely fit the delay pattern with a hyperbolic model.

Finally, we note that it is a simple process to take the velocity structure in RMS velocities and calculate interval velocities. The interval velocity between interface i and $i+1$ is given by

$$c_{i+1}^2 = \left[\bar{c}_{i+1}^2 - \bar{c}_i^2 \right] \frac{T_0}{2t_{i+1}} \quad 1.15$$

Summary

In the RMS travel time model we have a simple and efficient means of calculating the travel time delays for the multi-channel array. The model assumes a horizontally homogeneous acoustic velocity structure for the travel paths, although it appears to be robust to small dips. It is most accurate

near vertical incidence and for structures without major deviations in velocity. The model becomes invalid as any part of the travel path approaches a refracting (i.e. horizontal) condition. With a means of relating velocity and depth to parameters that are directly measurable, we can now look at the estimation procedure.

Chapter 2 Estimation of the Velocity Function.

Introduction

In this chapter we develop the concept of a velocity/depth spectrum and present the mechanics of its estimation. The form and general structure of the data are examined and the estimation procedure is segmented into a two step operation. The contribution of each step toward the overall resolution is examined, and areas of needed improvement identified. The first step, the windowing, is shown to be a critical, although often subtle, part of the estimation procedure. The second, a beamforming or coherent power estimate, is the operation to which we intend to apply the adaptive procedure. The conventional velocity/depth estimator is developed using a beamformer approach, and then an adaptive form of this is derived from an adaptive wave number estimator. Finally, the adaptive form is shown to be computationally similar to the conventional estimator, and the possible advantage of applying either form in the frequency domain is indicated.

The Velocity/Depth Spectrum

The concept of a velocity/depth spectrum has been well described in the literature by LePichon, Ewing, and Houtz (1968),

Taner and Koehler (1969), and others. It is an estimate of the coherent power received from a reflecting surface at a given depth and at a given RMS velocity. The data set, composed of N channels of recordings from the N surface positions, is scanned in an iterative process with the estimator. For each combination of depth and velocity the data is windowed according to the travel time model, and an estimate of the coherent power in the windows is made to form the spectral estimate. A sample spectrum is given in Figure 2.1.

There are several ways commonly used to display velocity/depth spectra; this one shows the estimated power as the displacement of plotted traces. In most of the work which follows we prefer to display the spectra in contour plots of the power levels in 6 dB increments. Because of the simplicity of the equations and the ease of correlating the spectra with the original time traces of the data, we always consider depth in the units of seconds of two-way travel time. Our units of velocity are RMS meters per second.

An idealized example of velocity/depth spectra estimation is given in Figures 2.2 and 2.3. Figure 2.2 gives the time traces from 8 channels showing reflected returns from four interfaces. As the data is scanned with the estimator, the windows are delayed according to a travel time model such

Figure 2.1 Sample Velocity/Depth Spectrum.
From USGS. Used with permission.

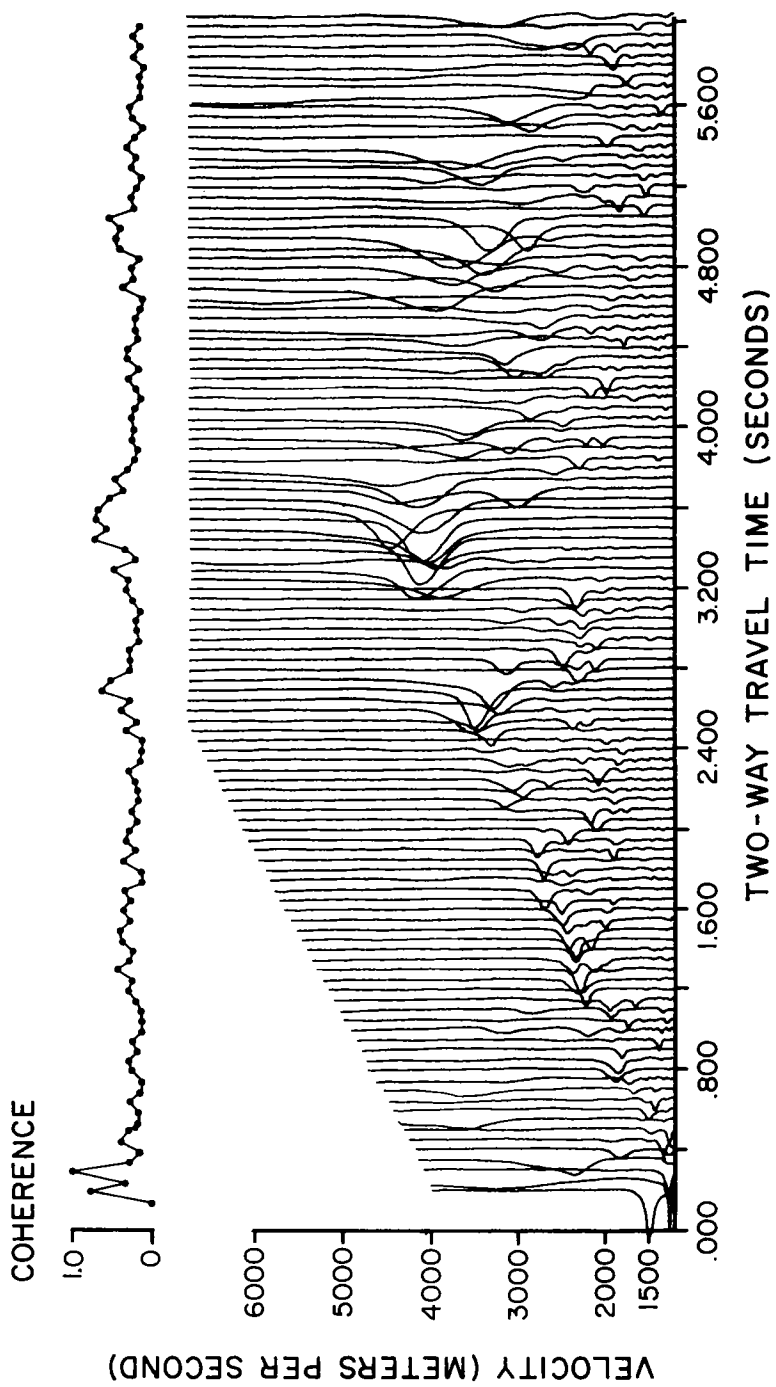


Figure 2.2 Simulated Data Set Showing Windows Properly Delayed for Third Reflector.

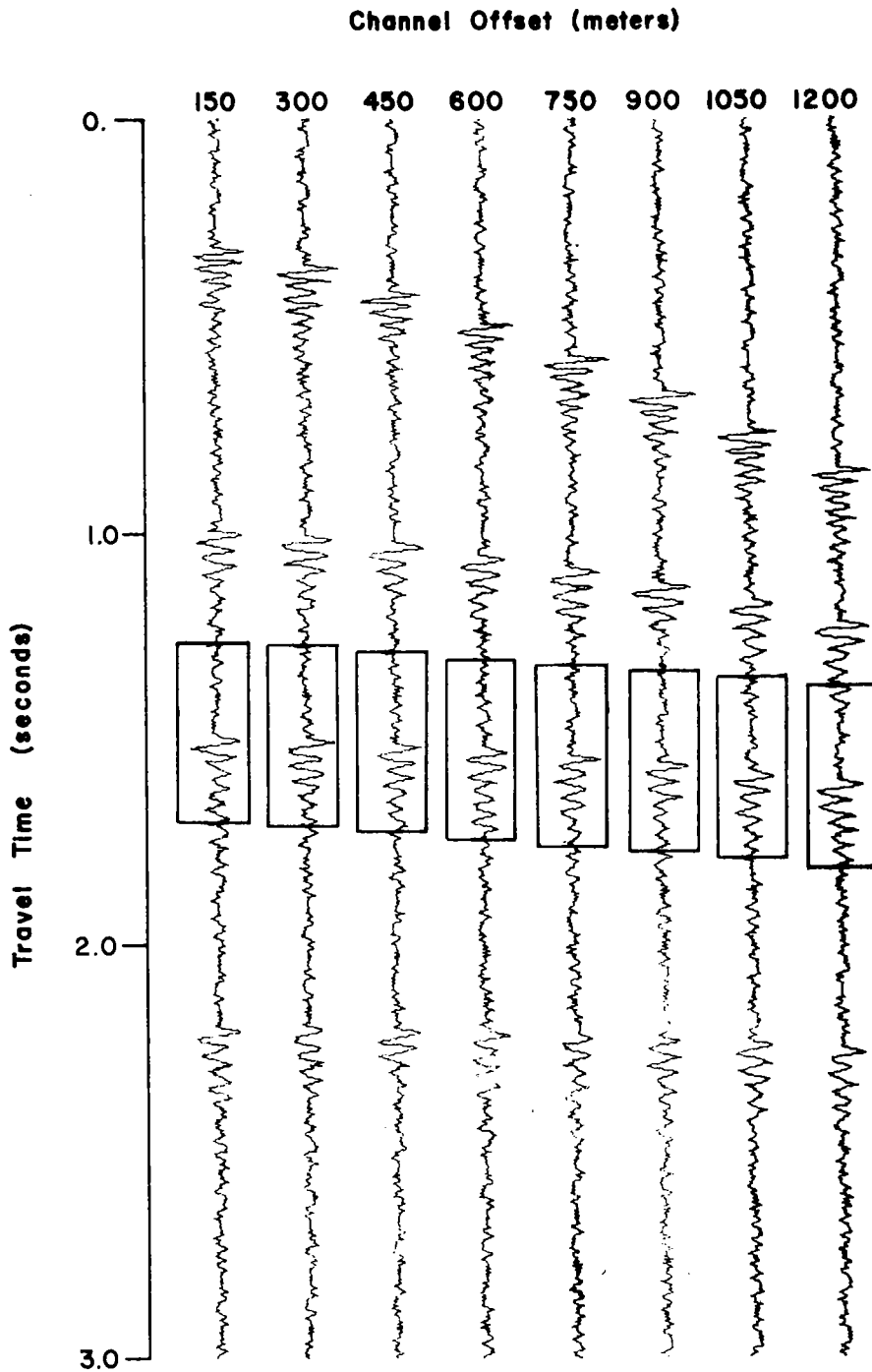


Figure 2.3a Data Windows With Velocity Too Small.

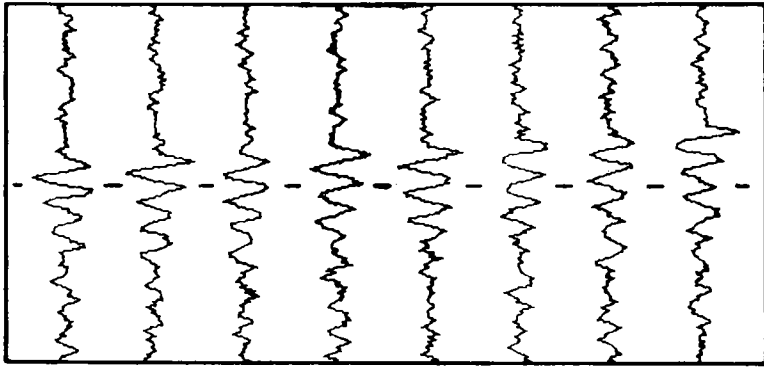


Figure 2.3b Correct Delay of Data Windows.

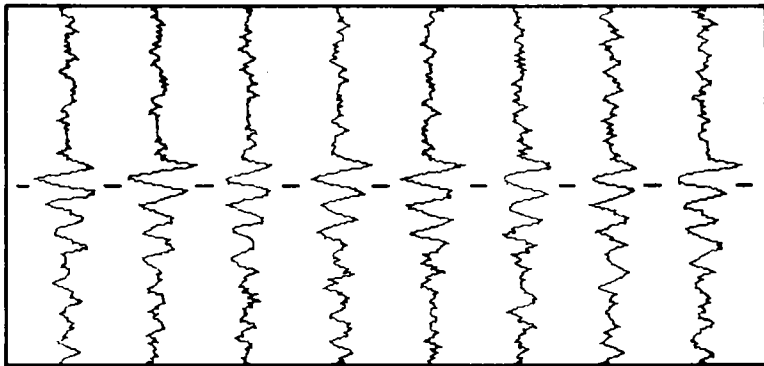


Figure 2.3c Data Windows With Velocity Too Large.

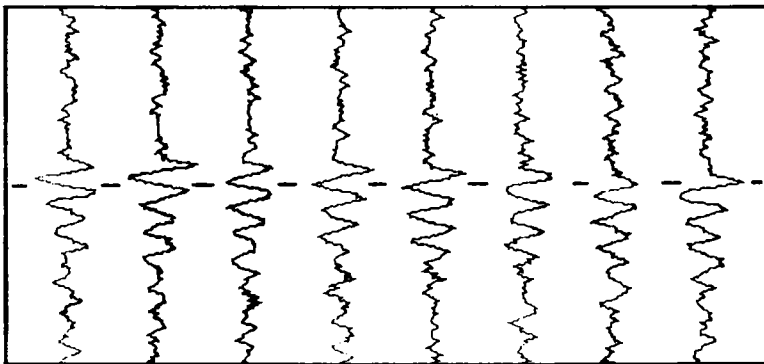
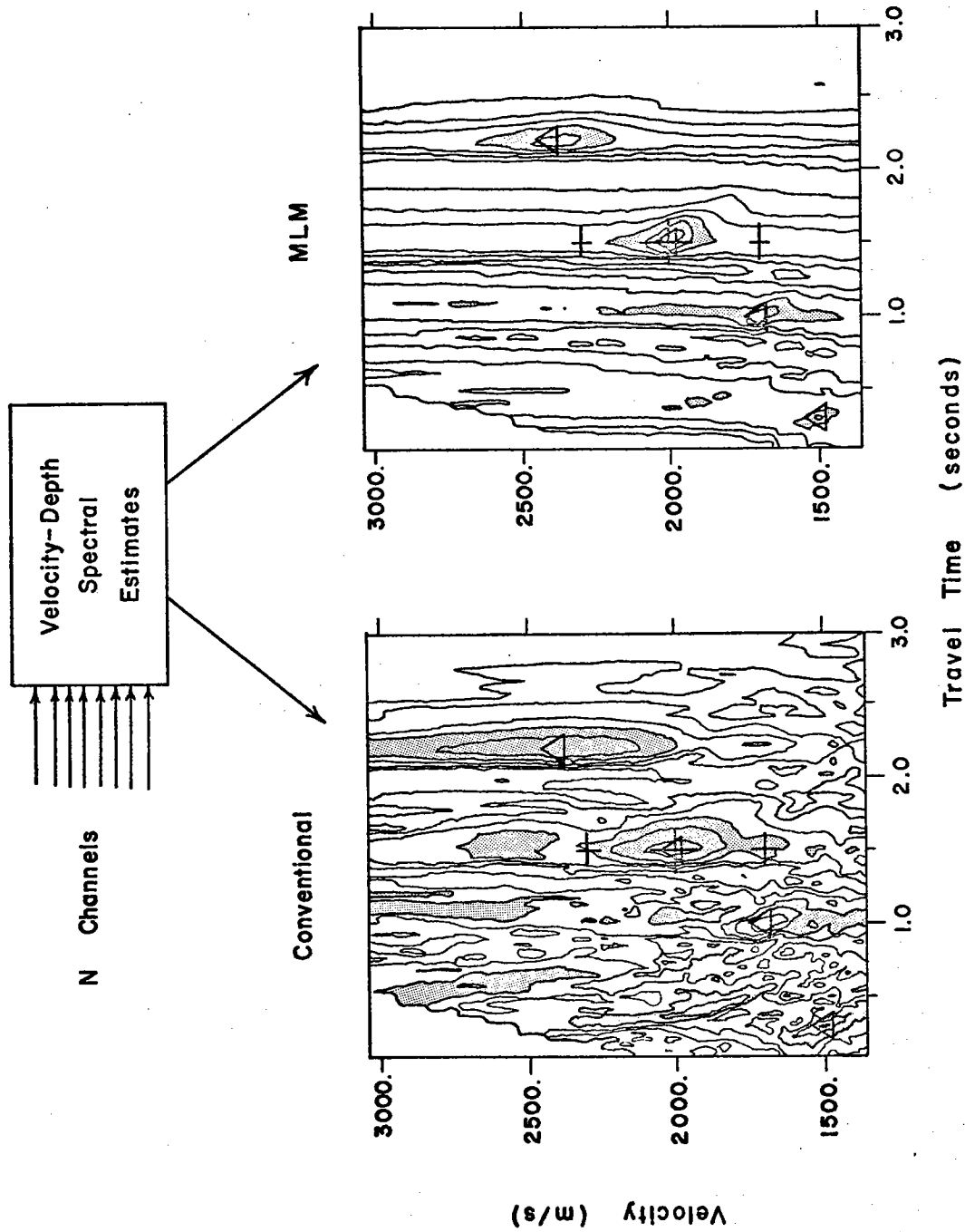


Figure 2.4 Velocity/Depth Spectral Estimates of Data in Fig. 2.2 & 2.3



as we calculated in the previous chapter. The windows in Figure 2.2 are shown delayed for a velocity and depth corresponding to the third reflector. As the velocity in the travel time model is incremented in the scanning process, the window delays are shifted appropriately. Examples of the resulting windowed data for several shifts in velocity are given in Figure 2.3a through 2.3c. Changes in the depth (normal incidence travel time) shift the windows in a similar manner, although much more uniformly up or down the trace for all the channels. For each delay pattern specified by the combination of each depth and each velocity, the data is windowed and an estimate of the coherent energy in those windows is made. The signals (though not necessarily the noise) in the windows in 2.3b are coherent across all 8 channels, and our estimate of the coherent power in these windows will be much larger than the estimate for the windows in Figures 2.3a and 2.3c. This estimate of the coherent power as a function of the velocity and depth of the delay model forms the velocity/depth spectrum. The results of the velocity/depth estimation procedure for the idealized data in Figures 2.2 and 2.3 are given in Figure 2.4. The four reflectors are indicated by \triangle and the estimates corresponding to the three sets of windows in Figure 2.3 are indicated by $+$.

Seismic Reflection Data

Before examining the estimation algorithms in any detail, we first examine the form of the data and the source signature. The entire estimation procedure, and the windowing in particular, are ultimately dependent on the expected form of the returning wave front. A typical example of data is shown in Figure 2.5. This is data taken with WHOI's 6 channel system on Georges Bank in August 1975. Reflection wavefronts are indicated in the time display by hyperbolic patterns of varying degrees of curvature. Two of these are indicated on the figure. The velocity spectrum of this data was given in Figures 5 and 6 in the Introduction. The set of returns from an interface is not always obvious, even to the trained eye. They vary for different interfaces and, to some extent, from channel to channel. The characteristics of the reflected wave are a function of the source signature and the dispersive and attenuation characteristics of the travel path medium.

The characteristics of various seismic sources have been studied and classified (Kramer, et al. 1968). The outgoing signal for our data is a pulse from an array of Bolt PAR airguns. A typical outgoing signature is given in Figure 2.6. It is a relatively wideband signal of approximately 250 to 500 ms. duration. The frequency power spectrum is

Figure 2.5 Sample 6 Channel Data.
Common Depth Point Gather.

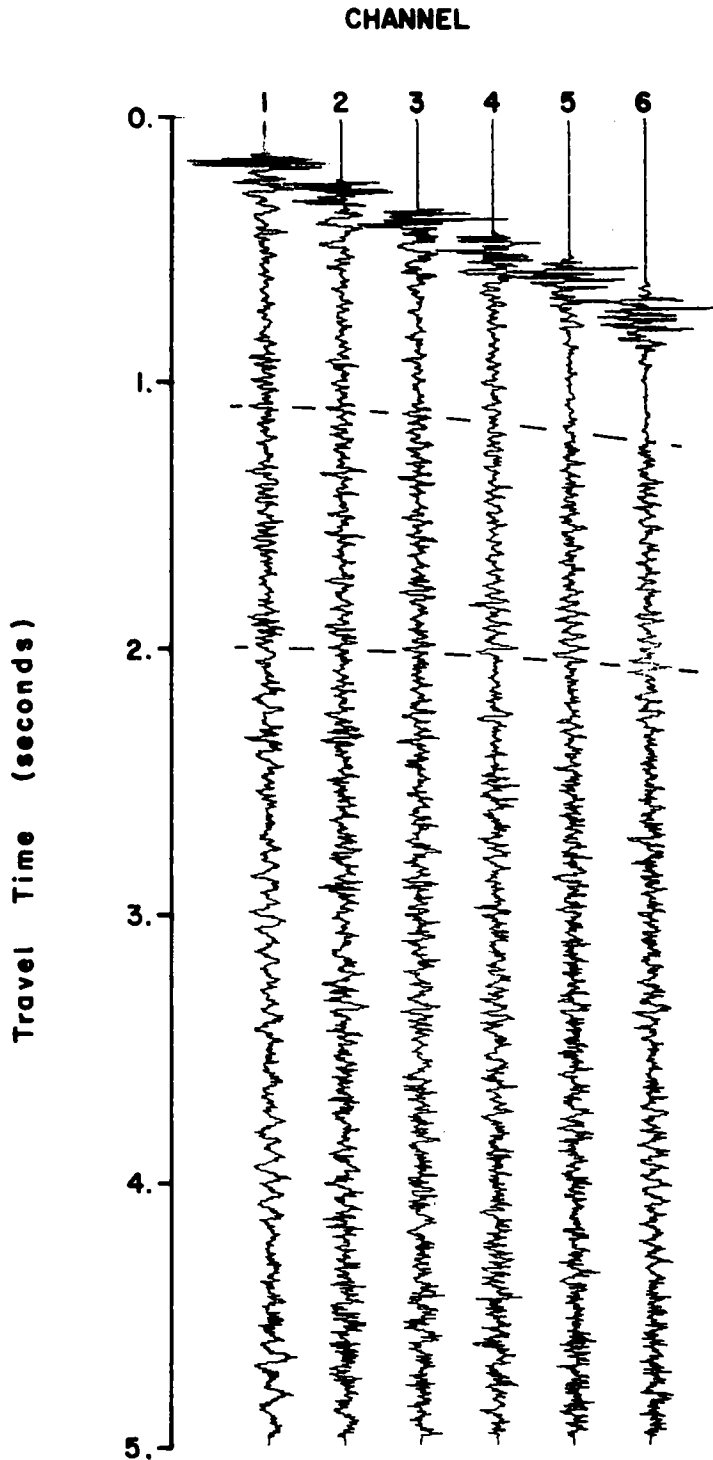


Figure 2.6 Airgun Signature. 3 gun array.
(from Kramer, et al, 1968)

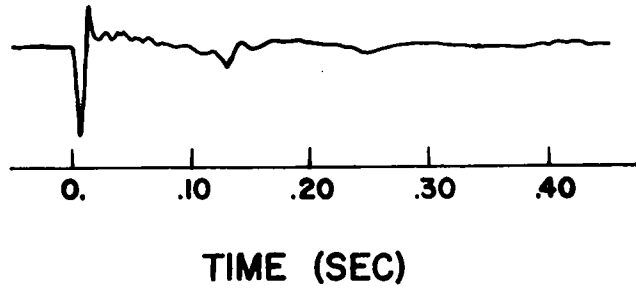
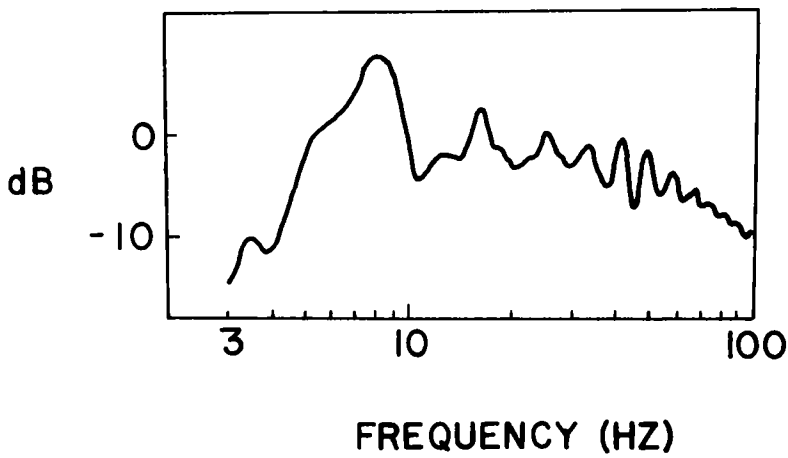


Figure 2.7 Frequency Spectrum of Gun Signature.



given in Figure 2.7. The spectrum is quite peaked at the natural compressional frequencies of the air discharge bubble. This signal undergoes phase changes, dispersion, and selective attenuation as it travels through the sediment structure. Since the travel paths for the N channels of data differ in length, and usually to some extent in composition, there will be a modification of the signal as a function of time (travel distance) that will vary somewhat from channel to channel. To the extent that the signal from a given reflector is coherent across the array, our coherent power measurement functions well. Any incoherence across the wavefront creates difficulties with its measurement which we will address later when we are considering the sensitivity of the estimation procedure to noise and signal incoherence.

Partitioning of the Estimation Procedure

In this section we look separately at the two basic operations making up the estimation procedure - the windowing and the coherent power estimate. Each can be used alone to produce a form of spectrum. Our reason for doing so is twofold. By examining each aspect separately, we can better understand the whole and how each part contributes to the overall resolution and accuracy of the complete estimator. Secondly,

our proposed processor differs from the conventional in only one of the aspects, the coherent power estimate, and an understanding of the role of this part enables us to place limits on any improvements we hope to achieve. In considering a spectral estimate without the coherent power estimate, we replace that operation with a calculation of the total power that is present in the windows. For the case of only using the coherent power estimate, we lengthen the windows until they include the entire data trace. In this way both forms are still estimates of the power in the data as a function of velocity and depth.

In Figures 2.8 and 2.9 we present the two forms of spectra run on idealized data containing four reflectors. Figure 2.8 gives a contour plot of the spectrum which relies solely on windowing for its resolution. The points of interest are the relatively sharp delineation of the reflectors in depth, but the rather poor delineation in velocity. Figure 2.9 gives the spectrum of the same reflectors calculated using only the conventional coherent power estimate. In this case there is poor resolution along a line which, as we show in the next chapter, is defined by

$$T_0 C^2 = \text{constant}$$

Figure 2.8 Velocity/Depth Spectrum Calculated From Incoherent Arrival Times. Four Reflector Simulated Data With No Noise. Linear Contour Spacing.

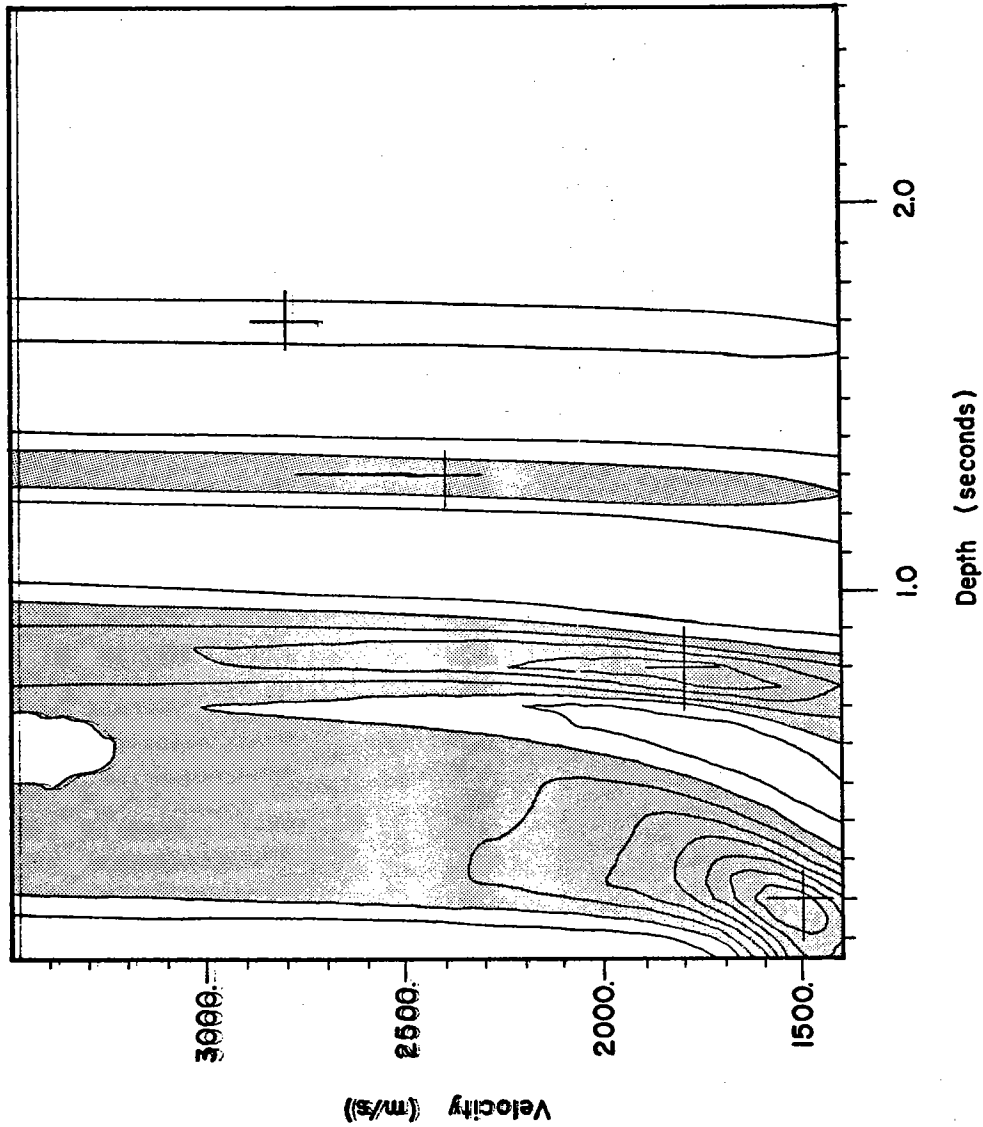
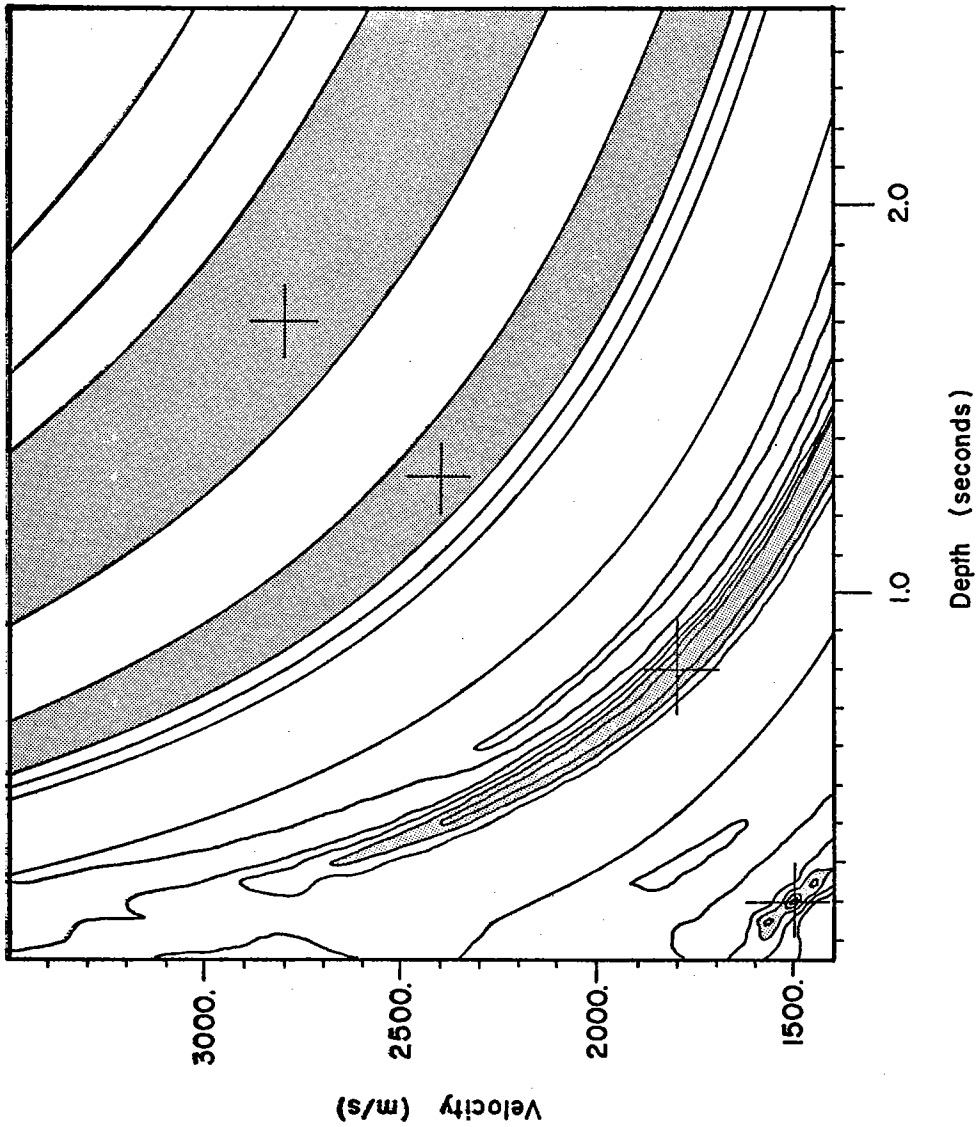


Figure 2.9 Velocity/Depth Spectrum Calculated From Conventional Phase Measurement Without Windowing. Four Reflector Simulated Data. Linear Contour Spacing.



From the general nature of the two forms of spectra and their order of application, we observe that the windowing provides most of the resolution in the time dimension, and the coherence measurement then provides the resolving power in the velocity dimension. In both of these forms of spectra we note that the resolution is significantly better at shallower depths. It is interesting that the coherence measurement alone completely determines the reflector parameters in the shallowest region. The wavefront exhibits the most curvature (as determined by the travel time equation) in the very near field of the array and the wavefront shape is unique for a given depth. In this region the focusing of the array is analogous to holographic methods. If the entire geologic region of interest were in this holographic focusing region, we could dispense with some of the stringent windowing requirements. But such is not often the case, and we recall that this is also a region where the travel time equations start to break down due to refraction effects. The area where we have the most to gain from new coherence measurement techniques is in the velocity resolution in the intermediate and far end of the Fresnel region.¹ In these regions the change

¹We define the Fresnel region as being the region where the reflectors are shallow enough that the curvature of the wavefronts is still significant over the array length, and the planewave approximations of the wavefront are not valid. The term is commonly used in optics.

in wavefront curvature for a given change in velocity is relatively small, and any improvements in resolving power effectively improve the resolution and the operating range of the array.

Conventional Estimator

In conventional array theory, a processor which calculates the coherent power received by an array is called a beamformer. A simple beamformer corrects the phase of the signal from each element to correctly "steer" the array, and then sums the outputs. Since the phasing is a function of frequency, it is often convenient to work in the frequency domain. The conventional estimate of the total coherent power is given by

$$P_c = \sum_f \left| \sum_{i=1}^N Y_i(f) e^{j2\pi f T_i} \right|^2 \quad 2.1$$

where $Y_i(f)$ is the frequency domain representation of the signal from channel i ,

and $2\pi f T_i$ is the phase correction at frequency f for channel i .

This estimator can be modified by multiplying each channel by a weighting coefficient in order to taper the array, and thus modify its resolution and sidelobe structure. But for

any form of the conventional beamformer, we note that the weights, and hence the resolution and beampatterns, are constant with respect to the data being looked at.

In the development of velocity/depth estimation, the traditional approach has been to use an algorithm in the time domain. We can easily show that our simple beamformer is equivalent to an un-normalized "semblance criteria" as developed by Taner and Koehler (1969). Applying Parseval's theorem to Equation 2.1, we obtain

$$P_c = \sum_t \left| \sum_{i=1}^N Y_i(t + T_i) \right|^2 \quad 2.2$$

The phase shifts become delays in time, and the summation in time is over the data window used by the Fourier transform when going to the frequency domain.

Returning to our frequency domain representation, we now introduce a vector notation. We let $\underline{Y}(f)$ be a vector of the data $Y_i(f)$ and $\underline{E}(f)$ be a steering vector of phase shifts $e^{j2\pi f T_i}$. Using this notation, the conventional estimator becomes

$$P_c = \sum_f \left[\underline{E}^t \underline{Y} \underline{Y}^t \underline{E} \right] \quad 2.3$$

The quantity $[\underline{Y}\underline{Y}^\dagger]$ is a matrix of products and cross products of the frequency terms from the Fourier transforms.

For Gaussian data, this is an estimate of the covariance matrix of the process (Anderson, 1958). We denote the covariance matrix by \underline{R} .

spectral covariance (?)

$$\hat{\underline{R}}(f) = \underline{Y}(f) \underline{Y}^\dagger(f) \quad 2.4$$

We note that $\underline{R}(f)$ is hermitian; it is conjugate symmetric complex, and is different for each frequency of the transform. Collectively, the set of covariance matrices contain all the relative phase information of the N data windows.

In final form, we can write

$$\underline{P}_c = \sum_f \underline{E}^\dagger \hat{\underline{R}} \underline{E} \quad 2.5$$

Adaptive Estimator

The simple beamformer has a beam pattern which is directed to look at the amount of coherent energy in the desired incoming wave through the use of the proper delays. The weights on the elements in this beamforming process are held constant, so that the basic shape of the beam pattern and the associated

sidelobe pattern for a given focus (velocity and depth) do not change. But more importantly, they do not depend upon the data in any direct manner. In order to optimize the signal-to-noise ratio when there are other wavefronts in the viewing field, we would like the beam pattern to adapt to the data being processed. By changing the weights of the array elements, the beam pattern may be controlled such that the peak and sidelobes of the pattern are kept away from the directions that may interfere with the estimation at a particular desired direction.

The data adaptive algorithm we are incorporating is called the high resolution Maximum Likelihood Method, or MLM. It was developed for wave-vector analysis for the large aperture seismic array (LASA) in Montana by Capon (1967). Our application differs from previous uses in that the field being measured does not consist of plane waves. The data field is non-homogeneous, or spatially non-stationary. This characteristic rules out most other data adaptive methods that are in popular use.

The MLM is based upon the design of a minimum noise unbiased estimator. The estimator is constrained to pass the desired wave (phase or delay pattern) with no distortion, while optimally suppressing any noise fields. The resulting

estimator is identical to the maximum likelihood estimate if the input signal field is a multi-dimensional Gaussian process.¹ The concept of the MLM of wavenumber estimation is to calculate the average power that this unbiased, or maximum likelihood, estimator has as a function of the steering wavenumber, \underline{k} . There are several ways to arrive at the MLM wavenumber estimator formula; and we present one which has an intuitive appeal based upon the unbiased array processor. Similar discussion can be found in Edelblute, et al. (1967), Capon (1969), and Lacoss (1971).

The unbiased estimator for a plane wave with a wavenumber \underline{k} operating in the presence of a noise field with a spectral cross correlation matrix, \underline{R} , is given by²

$$A(\underline{k}) = \frac{\underline{R}^{-1}(f) \underline{E}(\underline{k})}{\underline{E}^{\dagger}(\underline{k}) \underline{R}^{-1}(f) \underline{E}(\underline{k})} \quad 2.6$$

where $R_{ij}(f)$ is the cross spectra between array elements i and j at frequency f , and

¹The maximum likelihood estimator is the one which gives as its estimate the parameter set which has the maximum probability of producing the received signal. (see Van Trees, 1968)

²We use notation similar to Lacoss (1971).

$$\underline{E}(k) = \left[e^{-jk \cdot x_1}, e^{-jk \cdot x_2}, \dots, e^{-jk \cdot x_N} \right]^T$$

is a steering vector consisting of the phase shifts required for each array element. Now, if the noise field is applied to the minimum variance unbiased array processor, it passes the component in its steered direction without attenuation and rejects the rest of the field in the manner which minimizes the output variance. Ideally, then, the output variance should indicate the intensity of the component in the steering direction, and this is defined as the MLM wavenumber estimator formula.

$$\begin{aligned} S_{MLM}(k) &\triangleq \sigma^2(k) = \underline{A}^\dagger(k) \underline{R}(f) \underline{A}(k) \\ &= \left[\underline{E}^\dagger(k) \underline{R}^{-1}(f) \underline{E}(k) \right]^{-1} \end{aligned} \quad 2.7$$

The final step is to employ an estimate of the cross spectral correlation matrix.¹

$$\hat{S}_{MLM}(k) = \left[\underline{E}^\dagger(k) \hat{\underline{R}}^{-1}(f) \underline{E}(k) \right]^{-1} \quad 2.8$$

¹Capon and Goodman have derived formulae which specify the fluctuation introduced by using an estimate of the cross correlation matrix. Essentially, their results show that one loses N degrees of stability in the MLM formula when one has a multi-dimensional Gaussian process.

The form of the MLM estimator can be compared with the more conventional beamformer estimator,

$$\hat{S}_{CONV}(\underline{k}) = \left[\underline{E}^T(\underline{k}) \hat{R}(f) \underline{E}(\underline{k}) \right] \quad 2.9$$

We observe that additional computation required essentially consists of inverting the cross spectral matrix, which is a minor computational load when compared with that of estimating the matrix and scanning across the parameter set.

In modifying the MLM adaptive spectral estimation algorithm for use in estimating velocity spectra, one major modification is required, and this is the introduction of windows.¹ For depths or normal incidence times in excess of that where there is holographic resolution by the phasing across the array, the only way that one can obtain resolution in depth is to use a sequence of window sets which are positioned as a function of depth. Since the velocity also influences the position of the windows, especially at the more distant elements, these windows are positioned as a function of both depth and velocity. The net effect is that one essentially has a local estimate of the cross spectral matrix and a resulting MLM

¹Almost all previous applications of the MLM algorithm have implicitly employed windows; but here their role is more important because of the inhomogeneity of the spatial process.

velocity spectra estimate around each window position.

The presence of this windowing procedure introduces a tradeoff which turns out to be quite important in estimating the cross spectral matrix. (In fact, understanding the presence of this tradeoff proved to be one of the more subtle issues of this investigation.) The conflicting issues in this tradeoff may be summarized as follows: Good depth resolution and suppression of interference from reflectors at different depths requires multiplication by short duration windows in the time domain. This, however, implies a smearing of the data, especially the phase, across the bandwidth of the window which increases as the window is shortened. We analyze this tradeoff in more detail in Chapter 4.

With these comments on the use of windows, we define the MLM velocity/depth spectra estimate to be

$$P_{MLM}(\hat{T}_0, \hat{C}; f) = \left[E^{\dagger}(\hat{T}_0, \hat{C}; f) \hat{R}^{-1}(T, C; f) E(\hat{T}_0, \hat{C}; f) \right]^{-1} \quad 2.10$$

random function

where

$$\hat{R}(T, C; f) = \frac{1}{M} \sum_{m=1}^M \underline{Y}_m(T, C; f) \underline{Y}_m^{\dagger}(T, C; f) \quad 2.11$$

window function

which is an estimate of the covariance based upon transforms, $\underline{Y}_m(\hat{T}, \hat{C}; f)$, of the data within windows positioned around depth T and velocity C ; and where $\underline{E}(\hat{T}_0, \hat{C}; f)$ is a steering phasing vector in the direction of the desired depth and velocity parameters \hat{T}_0 and \hat{C} . If we compare the form of the MLM velocity/depth estimator to the conventional beamforming procedure based upon coherency measure, we observe that it is completely analogous to comparing the MLM and conventional wavenumber estimators.

Finally, we note that the estimator is a function of frequency and is applied to discrete frequency bands of the Fourier transform. The characteristics of seismic data are such that this partitioning of frequency is often desirable. Real reflecting horizons are often wavelength selective because of the finite thickness of the impedance transition region. Maintaining separate estimates over frequency not only gives sharper resolution of this type of reflection, but gives some insight into the nature of the reflecting surface.

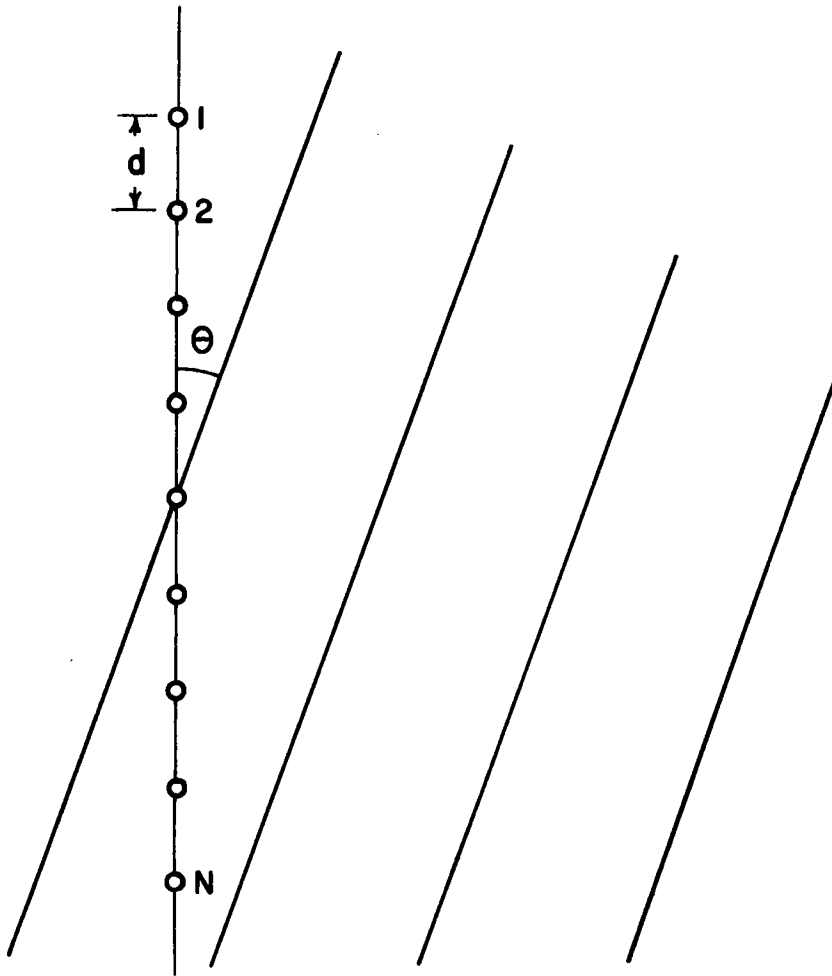
Chapter 3 Beam Patterns and Ambiguity Functions.

Introduction

In the general Introduction we presented the on-axis beam patterns of linear arrays looking at a single plane wave in wavenumber space. These gave us some insight into the high resolution capabilities of the adaptive array. In this chapter we examine the conventional beam pattern of an array looking at hyperbolic waves in velocity-time space. This will provide us with a much better indication of the resolution of the beamforming process which we looked at in a superficial manner in the last chapter.

The general function we need to define this resolution is the parameter ambiguity function. The ambiguity function has been described as the response of a matched filter to a mis-matched signal. In the case of an array processor, it is the normalized response of a steered array to waves other than the primary focus. We consider a uniformly spaced linear array as shown in Figure 3.1. The array may be steered to receive waves from various directions by adding appropriate delays to each element. For plane waves and a linear array, the ambiguity function is given by

Figure 3.1 Plane Wave Incident on a Uniformly Spaced Discrete Array.



$$\phi(k, \theta | k_0, \theta_0) = \frac{1}{N} \sum_{l=-m}^m e^{j(\ell d k \sin \theta - \psi_l(k, \theta_0))} \quad 3.1$$

where the steering function $\psi_l(k, \theta_0)$ is given by

$$\psi_l(k, \theta_0) = \ell d k_0 \sin \theta_0 \quad 3.2$$

and $m = (N-1)/2$, $N =$ number of elements in the array. By modifying the form of the exponent in Equation 3.1, it is easily seen that we can form the ambiguity function for the array response to non-plane waves. In the case of wide angle reflections from horizontal layers, the wave may be specified by the RMS travel time model. We then have the ambiguity function in terms of velocity and depth.

$$\phi(\tau_2, \bar{c}_2 | \tau_1, \bar{c}_1) = \frac{1}{N} \sum_{i=1}^N e^{j2\pi f \left(\sqrt{\tau_2^2 + \frac{x_i^2}{c_2^2}} - \sqrt{\tau_1^2 + \frac{x_i^2}{c_1^2}} \right)} \quad 3.3$$

This is the complex monochromatic ambiguity function. For a case where we had a signal that was zero phase, we could simply weight the complex monochromatic ambiguity function by the frequency spectrum of the signal and integrate over frequency to obtain a wide band ambiguity function. Kline (1976) studied this wideband function and found greatly increased resolution capabilities. With a signal of unknown

phase characteristics, the ambiguity functions (and signals) add incoherently across frequency, and we must resort to integrating the absolute magnitudes of ambiguity and signal over frequency. We continue to weight by the frequency spectrum to account for changes in signal strength. Our wideband ambiguity function becomes

$$\phi_{WB}(\tau_2, \bar{c}_2 | \tau_1, \bar{c}_1) = \frac{1}{B} \int df S(f) \left| \phi(\tau_2, \bar{c}_2 | \tau_1, \bar{c}_1) \right| \quad 3.4$$

$$B = \int df S(f)$$

The velocity-time ambiguity function is not solvable in closed form, and thus requires numerical solutions or approximating functions. Kline (1976) derived approximations for the peak shapes and peak widths of this function for monochromatic and narrow band cases which prove useful when optimizing parameters for beam width or sidelobe structure.

Looking at the monochromatic ambiguity function, we find a large region of ambiguity stretching along a line defined by

$$T_1 \bar{c}_1^2 = T_2 \bar{c}_2^2 = \text{constant} \quad 3.5$$

When focusing on (T_1, C_1) , the array will respond almost equally well to any return falling on the line defined by Equation 3.5. We note that this ambiguity is independent of frequency. The half power points as approximated by Kline (1976) are

$$T_2 \bar{C}_2^2 = \left[\frac{1}{T_1 \bar{C}_1^2} \pm \frac{1.8190}{f L_{eq}^2} \right] \quad 3.6$$

where L_{eq} is the equivalent length of the array. For a discrete element array, the equivalent length is

$$L_{eq} = (N-1)d \quad 3.7$$

Figure 3.2 gives a contour plot of an exact monochromatic ambiguity function calculated for $T_1 = 2.0$ seconds, $C_1 = 2000$ m/s, $f = 20$ Hz, and $N = 12$. The wideband ambiguity function as applicable to our data is the sum of monochromatic ambiguity functions at discrete frequency points obtained by the fast Fourier transform of sampled data. The general form of the ambiguity function is not changed, although the peak is better defined. An example is given in Figure 3.3 for $T_1 = 2.0$ seconds, $C_1 = 2000$ m/s, $f = 20., 24., 28.,$ and $32.$ Hz, and $N = 12$.

Figure 3.2 Monochromatic Ambiguity Function.

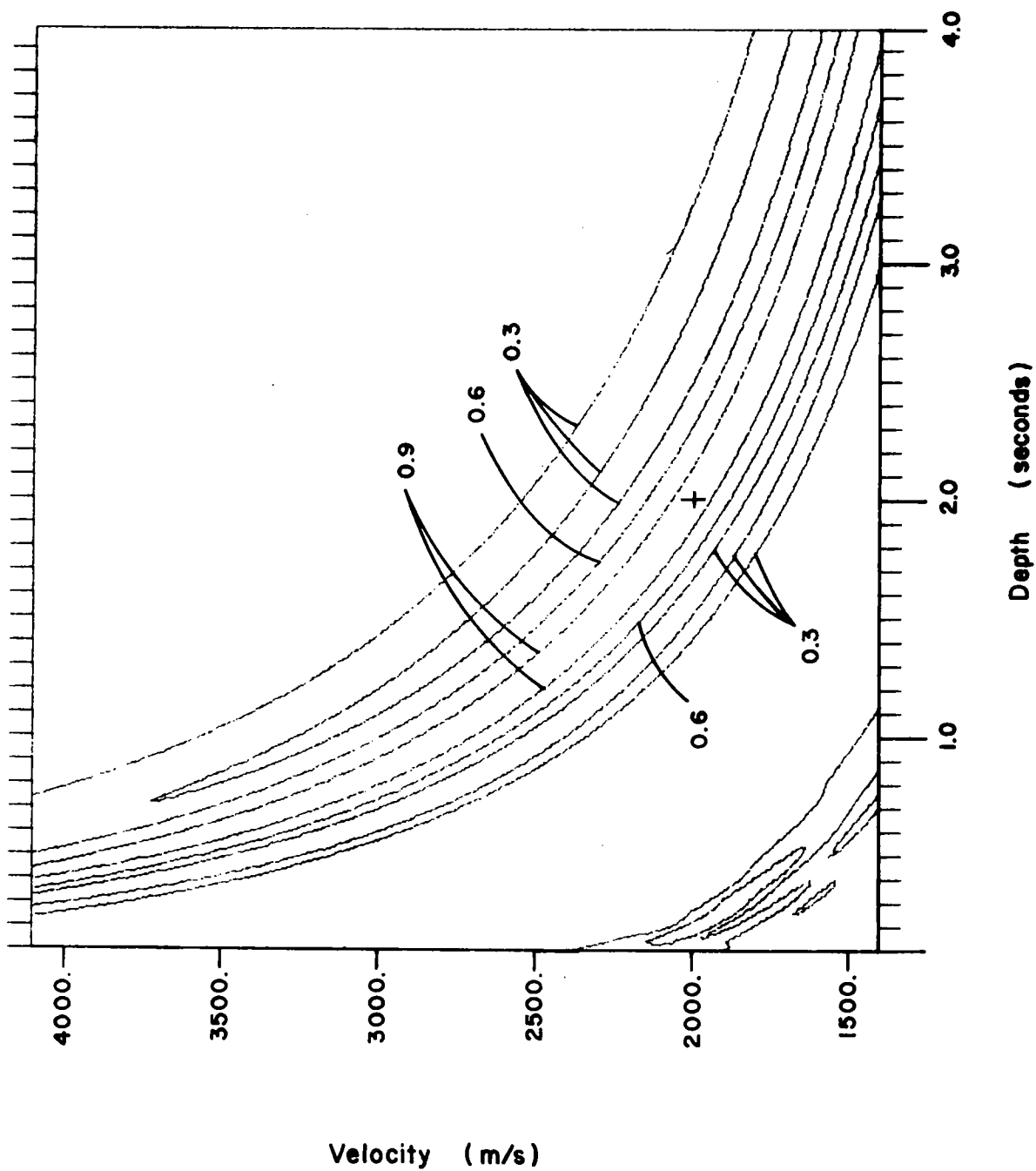
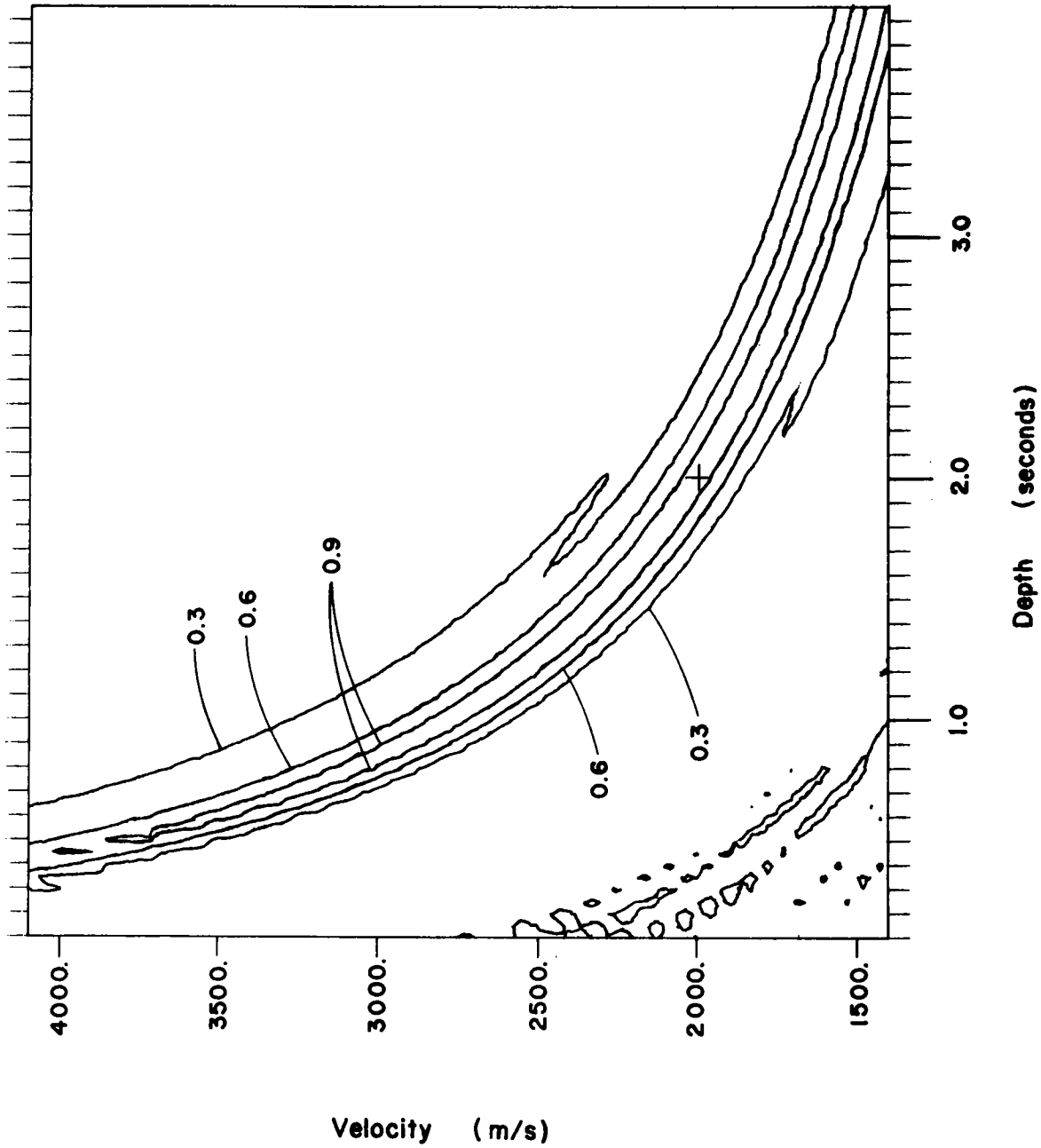


Figure 3.3 Discrete Frequency Ambiguity Function.
Four Frequency Components.



Discussion

We see that the array focusing - the coherent power estimate - allows us to resolve a reflection return to a one dimensional strip or line in velocity-time space. We depend on the time windowing to provide resolution along the length of this strip. The effect of applying the adaptive processor will be primarily to reduce the width of the strip. The time windowing will continue to carry the load of resolution along the length of the strip. Going to a wide band estimator does not produce any significant improvements in the ambiguity function. Higher frequencies give improved resolution, but our primary reason for applying a wideband estimator will be for improved signal-to-noise ratios. In the next chapter we investigate the windowing to remove the ambiguity along the strip, and in Chapter 6 we see how reducing the width of the strip greatly enhances the overall resolution of the velocity/depth estimator.

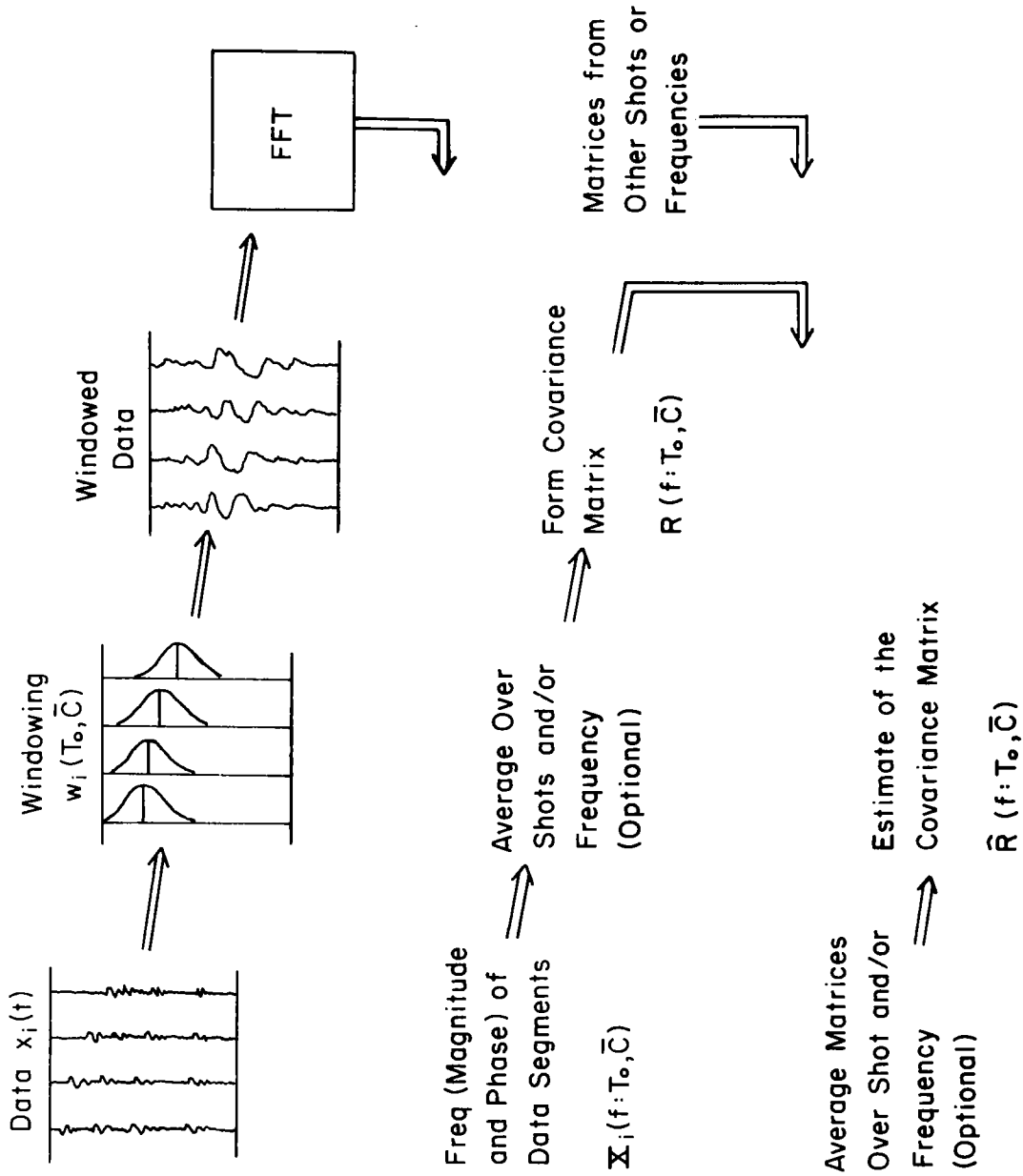
Chapter 4 Estimation of the Cross Spectral Correlation Matrix.

Introduction

Both the MLM and the frequency domain implementation of the conventional semblance criteria for estimating velocity/depth spectra involve determining the cross spectral correlation matrix in one way or another. In applications to stationary homogeneous signal fields this typically involves averaging over transformed segments of the data from each of the channels. In the application to velocity/depth spectra, however, the transient nature of the reflected signals requires a windowing operation, particularly for resolving along the depth, or time coordinate. The details of the cross spectral correlation matrix estimation involving this windowing operation are critical, for the errors and biases introduced propagate directly into the final spectral estimate. The estimation of this matrix has proven to be the most subtle aspect of our experiments in applying the MLM to velocity/depth spectra estimation.

The procedure for estimating the cross spectral correlation matrix using a window is shown schematically in Figure 4.1. At a given frequency the diagonal components of this matrix are measures of the energy at each channel, while the

Figure 4.1 Procedure for Estimation of the Covariance Matrix.



off-diagonal terms are indicative of the coherent energy and its relative phasing from channel to channel. The two most important aspects in the estimation of these components are the smearing, or bias, and the variance. As in any spectral estimation problem there are inevitable tradeoffs between these two quantities; the windowing, however, further complicates this issue. In this chapter we examine some aspects of estimating this matrix - both the smearing introduced by the windowing and the various ways of averaging to improve the stability of it.

4-A Windows and the Bias of Transforms

The spectral correlation matrix is estimated using the direct or FFT method of spectral analysis, so the first step involves analyzing the bias introduced by windowed Fourier transforms. In this section we examine this by first introducing a stochastic model for the reflected signal from which we can calculate bias errors using established methods of spectral analysis. Then we examine the effects of windowing on an airgun source signature which ideally should be representative of the signal reflected from a horizon. Finally, we use estimates of allowable positional errors determined from the results of the stochastic analysis to derive bounds

on perturbations of the moveout parameters T_0 , τ for maintaining a particular level of average bias in the windowed transforms.

We model the reflected signal observed at an array element as a desired signal plus an additive noise, or

$$Y(t) = \mathcal{A}(t - \tau_d) + n(t) \quad 4.1$$

where $\mathcal{A}(t)$ is the reflected signal at the array element which arrives with a total travel time delay or moveout of τ_d .

$n(t)$ is an additive noise which may include both ambient noise and reverberation from other horizons.

As indicated in Figure 4.1, the windowed transform operation consists of multiplying the signal by a window function centered at τ_w and then Fourier transforming, or

$$\hat{J}_w(f) = \int_{-\infty}^{\infty} Y(t) w(t - \tau_w) e^{-j2\pi ft} dt \quad 4.2$$

(We use continuous time notation, although in practice the FFT algorithm is used.) We specify the windows to have a half width duration of M seconds, and some commonly employed

windows are indicated in Figure 4.2.

If there were no windowing and no noise, i.e. $w(t) = 1.$, $n(t) = 0.$, the result of the transformation would be

$$\hat{S}(f) = S(f) e^{-j2\pi f T_d} \quad 4.3$$

which consists of the desired signal transform and a linear phase shift from the travel time delay. Both the windowing and the additive noise term introduce errors in this, so one actually obtains

$$\hat{S}_w(f) = \int_{-\infty}^{\infty} (s(t-T_d) + n(t)) w(t-T_w) e^{-j2\pi f t} dt \quad 4.4$$

It is convenient at this point to define the error, since this is what we wish to quantify. We have

$$E(f) = \int_{-\infty}^{\infty} [s(t-T_d)(w(t-T_w)-1) + n(t)w(t-T_w)] e^{-j2\pi f t} dt \quad 4.5$$

Qualitatively, the duration of the window, M , introduces a tradeoff. A long window leads to low resolution of the depth and higher noise in the transformation; however, it is relatively insensitive to its exact positioning and introduces little bias or smearing. Conversely, a short window

Figure 4.2a Commonly Used Windows in the Time Domain.

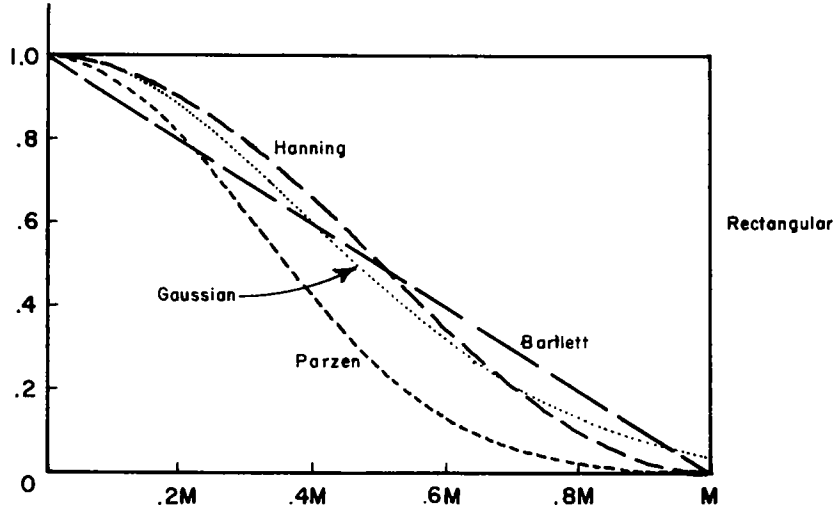
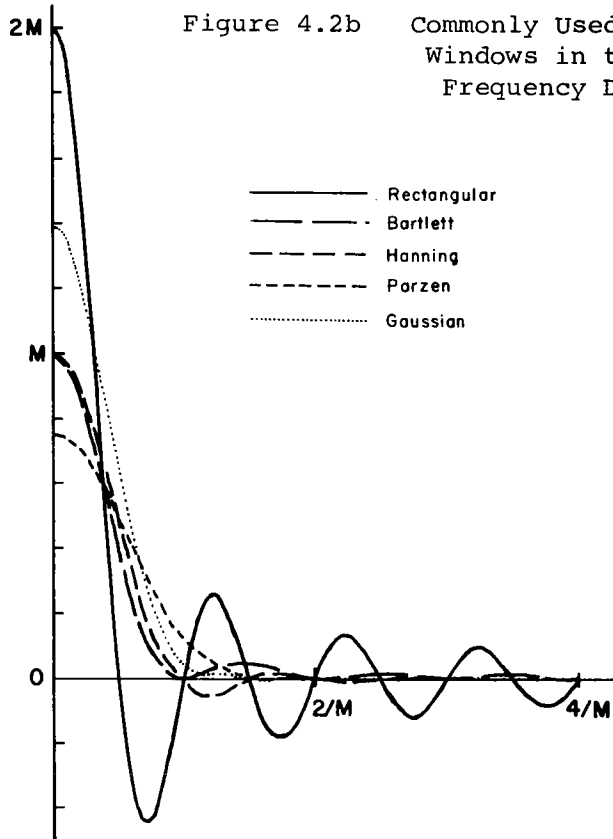


Figure 4.2b Commonly Used Spectral Windows in the Frequency Domain.



leads to higher resolution in depth and lower noise; however, it is very sensitive to its exact positioning and can introduce significant bias, or smearing of the frequency domain signal.

For our stochastic analysis we model the reflected signal as

$$\Delta(t) = \alpha(t) x(t) \quad 4.6$$

where $\alpha(t)$ is an envelope function of approximate duration τ_a (half width) which models the transient, or short duration nature of the reflected signal; $x(t)$ is a wideband stationary process which models the waveform variation of the signal within the duration of the envelope.

If we assure that the signal and the noise are uncorrelated processes, we can determine the mean square error by squaring and averaging Eq. 4.5. If we express all of the correlations in terms of their associated spectra, we obtain

$$\begin{aligned} \overline{|E(f)|^2} &= \int S_x(v) \left| \int a(t-\tau_a) (w(t-\tau_w) - 1) e^{-j2\pi(f-v)t} dt \right|^2 dv \quad 4.7 \\ &+ \int S_n(v) \left| \int w(t-\tau_w) e^{-j2\pi(f-v)t} dt \right|^2 dv \end{aligned}$$

where S_x and S_n are the power density spectra of the processes $x(t)$ and $n(t)$ respectively. We next assume that these spectra are essentially constant across the bandwidths of the window $w(t)$ and the envelope $a(t)$. (This is a common assumption in spectral analysis.) We then can take them outside the integrals, and after using Parseval's theorem we obtain

$$\begin{aligned} \overline{|E(f)|^2} &= S_x(f) \int_{-\infty}^{\infty} [a(t-\tau_a)(w(t-\tau_w)-1)]^2 dt \\ &+ S_n(f) \int_{-\infty}^{\infty} w^2(t) dt \end{aligned} \quad 4.8$$

The details of this derivation are given in Appendix I. The first term describes the error introduced by the duration and position of the window with respect to the desired reflected signal, while the second term describes the effects introduced by the additive noise. We consider each of them separately.

The noise term is easy to analyze. For almost any reasonable window, one can demonstrate that

$$S_n(f) \int_{-\infty}^{\infty} w^2(t) dt \cong S_n(f) K_w M \quad 4.9$$

where K_w is a window factor whose precise value depends

upon the shape of the window, but typically ranges from $.5 < K_w < 2$. The most important observation is that the RMS value of the noise increases as \sqrt{M} , so one wants to avoid excessively long windows for noise as well as resolution considerations.

The signal term is generally the more important one, and it is somewhat more difficult to analyze. First it is convenient to normalize it simply for the purposes of comparison. The mean square value of the desired signal with no windowing is given by

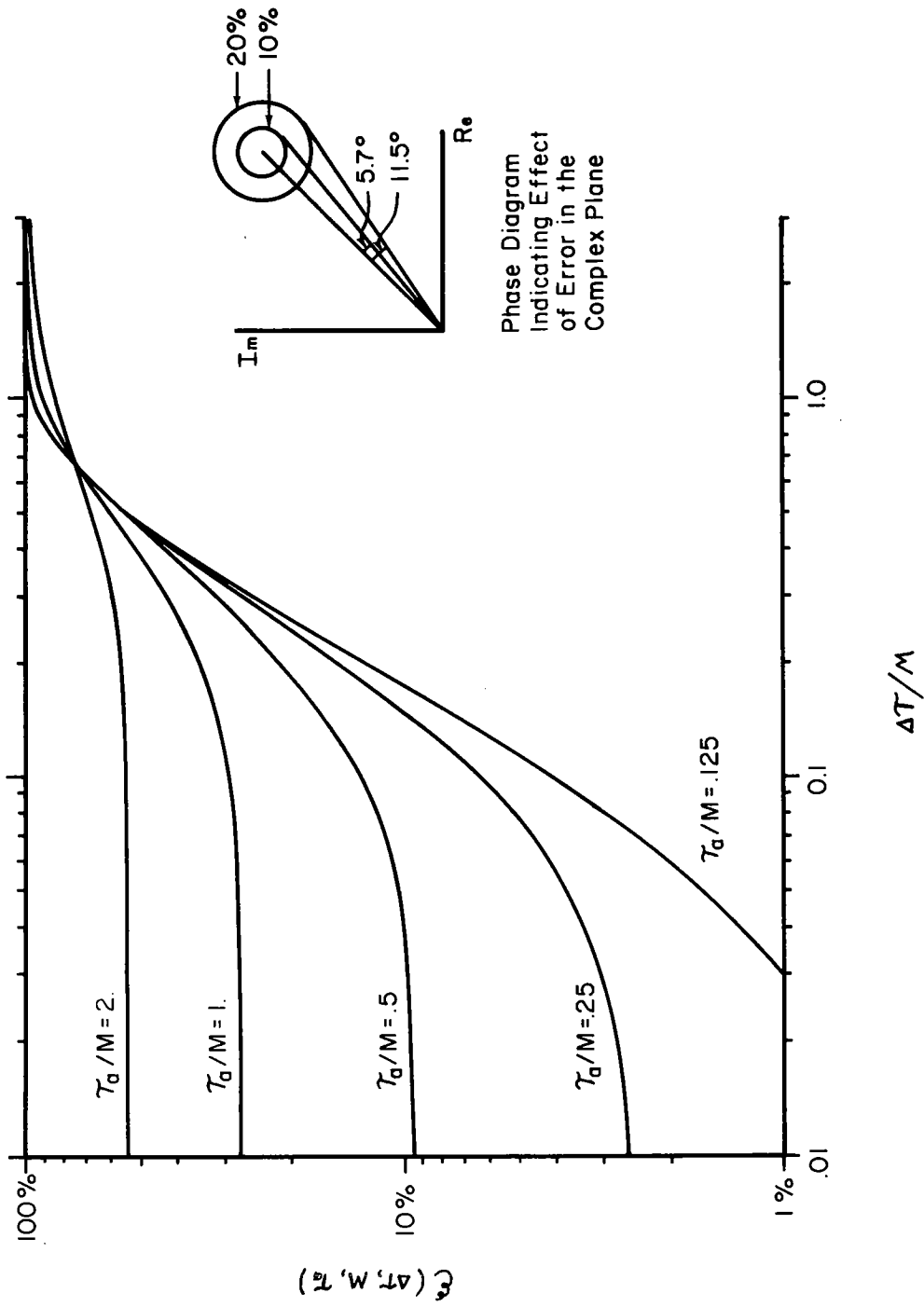
$$\overline{|\mathcal{J}(f) e^{-j2\pi f \tau_d}|^2} \cong S_x(f) \int_{-\infty}^{\infty} a^2(t) dt \quad 4.10$$

The expression which quantifies the relative effects of the mean square bias error due to the windowing is then given by

$$E^2(\Delta T, M, \tau_d) = \frac{\int_{-\infty}^{\infty} [a(t)(w(t-\Delta T)-1)]^2 dt}{\int_{-\infty}^{\infty} a^2(t) dt} \quad 4.11$$

where $\Delta T = \tau_d - \tau_w$ is the difference between the position of the window and the center of the desired signal. The precise shape of this function depends upon the particular window and envelope employed. Figures 4.3 and 4.4 are indicative of the general structure. Figure 4.3 was computed using

Figure 4.3 RMS Error Versus Position Error for Various Ratios of Envelope Duration to Window Duration Gaussian Envelope and Window



Gaussian shaped functions for the window and envelope of the form

$$w(t) = e^{-\pi \left(\frac{t}{M}\right)^2} \quad 4.12a$$

$$a(t) = e^{-\pi \left(\frac{t}{T_a}\right)^2} \quad 4.12b$$

Figure 4.4 was computed using Hanning windows for the shape of both the window and envelope of the form

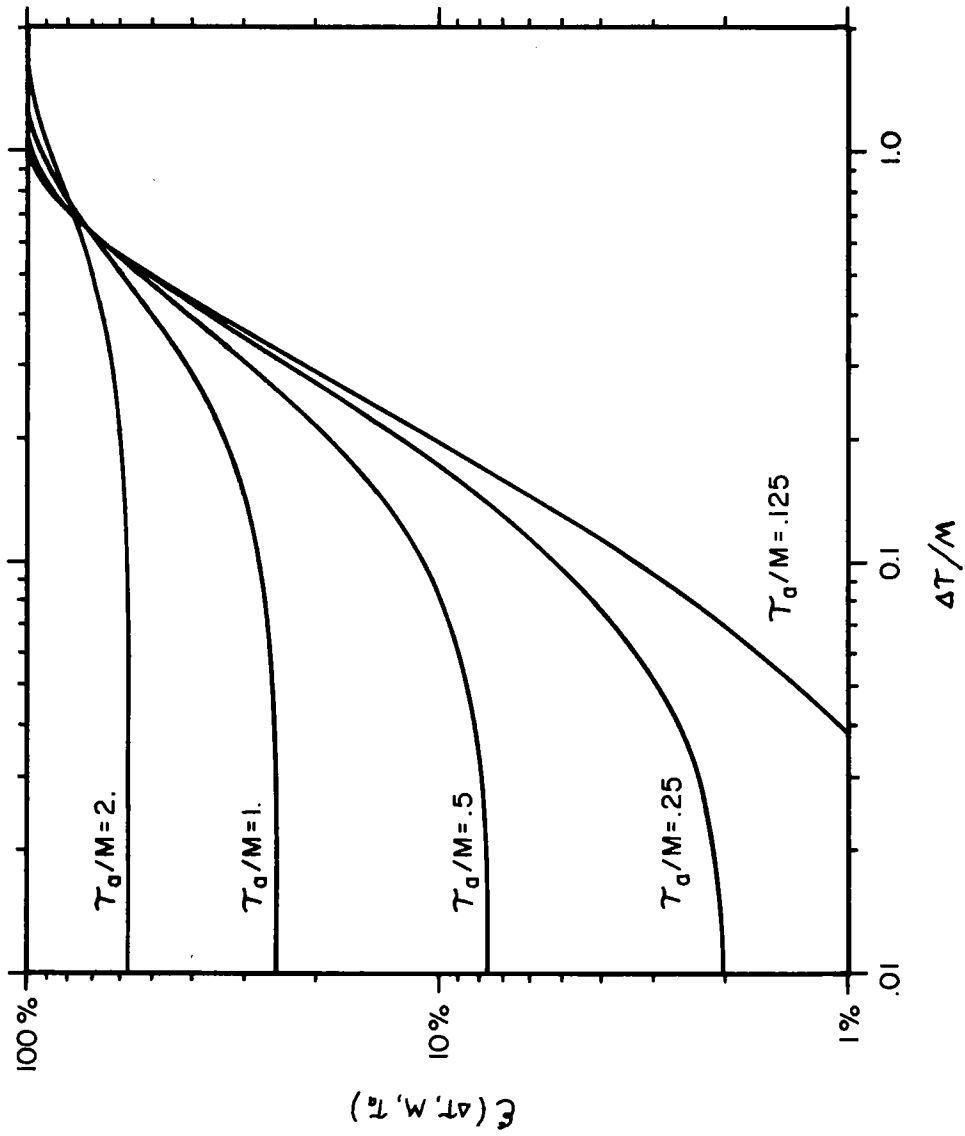
$$w(t) = \frac{1}{2} \left(1 + \cos\left(\frac{\pi t}{M}\right) \right) \quad 4.13a$$

$$a(t) = \frac{1}{2} \left(1 + \cos\left(\frac{\pi t}{T_a}\right) \right) \quad 4.13b$$

Essentially these figures suggest that for less than a conservative 10% error in the average bias of the windowed transform operation, one wants to keep the positional error within ± 0.1 (i.e. 20% of the effective window extent) and use windows with $T_a/M \leq 0.5$, i.e. windows whose duration is at least twice the effective signal duration.

To test the effects of windowing on actual data, several tests were performed upon recorded airgun signatures, which

Figure 4.4 RMS Error Versus Position Error for Various Ratios of Envelope Duration to Window Duration Hanning Envelope and Window



ideally should represent the signal reflected from a horizon. The signature and its unwindowed transform are illustrated in Figure 4.5. One can estimate the energy distribution about a central location by calculating the median signal location and then computing the residual energy outside an interval about that point. This suggests that $\tau_0 \cong 0.12$.

Figure 4.6 illustrates the windowed transform with no positional error using the windows indicated in Figure 4.2 with a value of $M = 0.128$ secs., i.e. not conforming to our previously suggested design guideline of $\tau_a/M \geq 0.5$. One can observe that there is some evident spectral smearing, but the windowed transform is basically accurate. (One needs to compensate visually for the phase jumps at $\pm\pi$ as a shift of 2π in phase is equivalent.) Figure 4.7 is a more sensitive indication of the accuracy of the windowed transform with respect to positional error. Here we have plotted the phase deviation from linearity for the 10 Hz component as the signature is delayed through the window. We can observe that for only two of the windows is there a comparatively narrow range of ± 0.012 sec., or $\Delta\tau/M \cong 0.1$ where the phase deviation is within $\pm 15^\circ$ for an error of $\approx 30\%$. This is essentially in agreement with Figure 4.3 which predicts that for $\tau_a/M = 1$, the error should be constant at 28% for $\Delta\tau/M < 0.1$, and then

Figure 4.5a 300 cu. in. Airgun Signature (including water surface image).

A) Time Signature

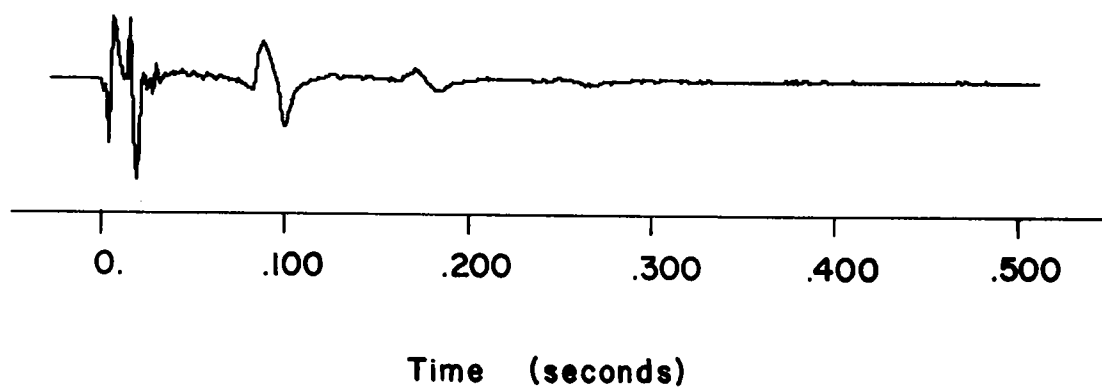
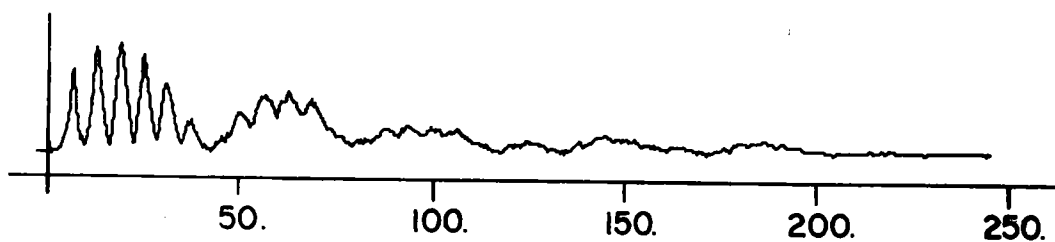


Figure 4.5b and 4.5c Frequency Signature of Airgun.

B) Frequency Magnitude



C) Phase

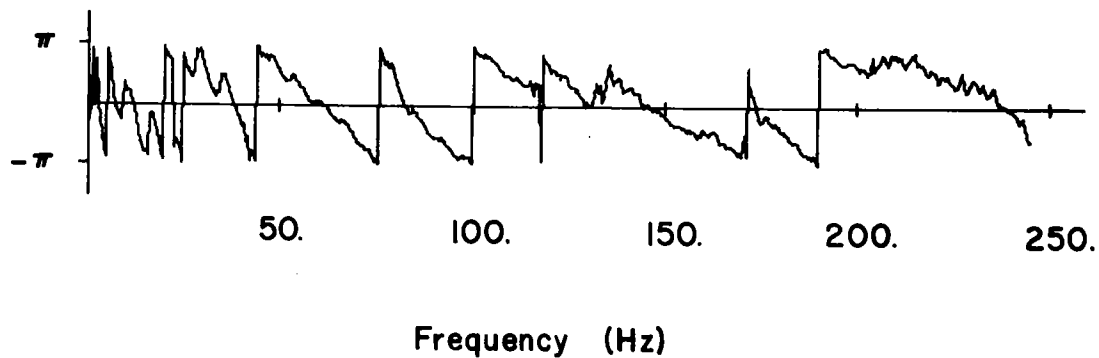


Figure 4.6 Frequency Spectra Estimates of Gun Signature Using Various Lag Windows.

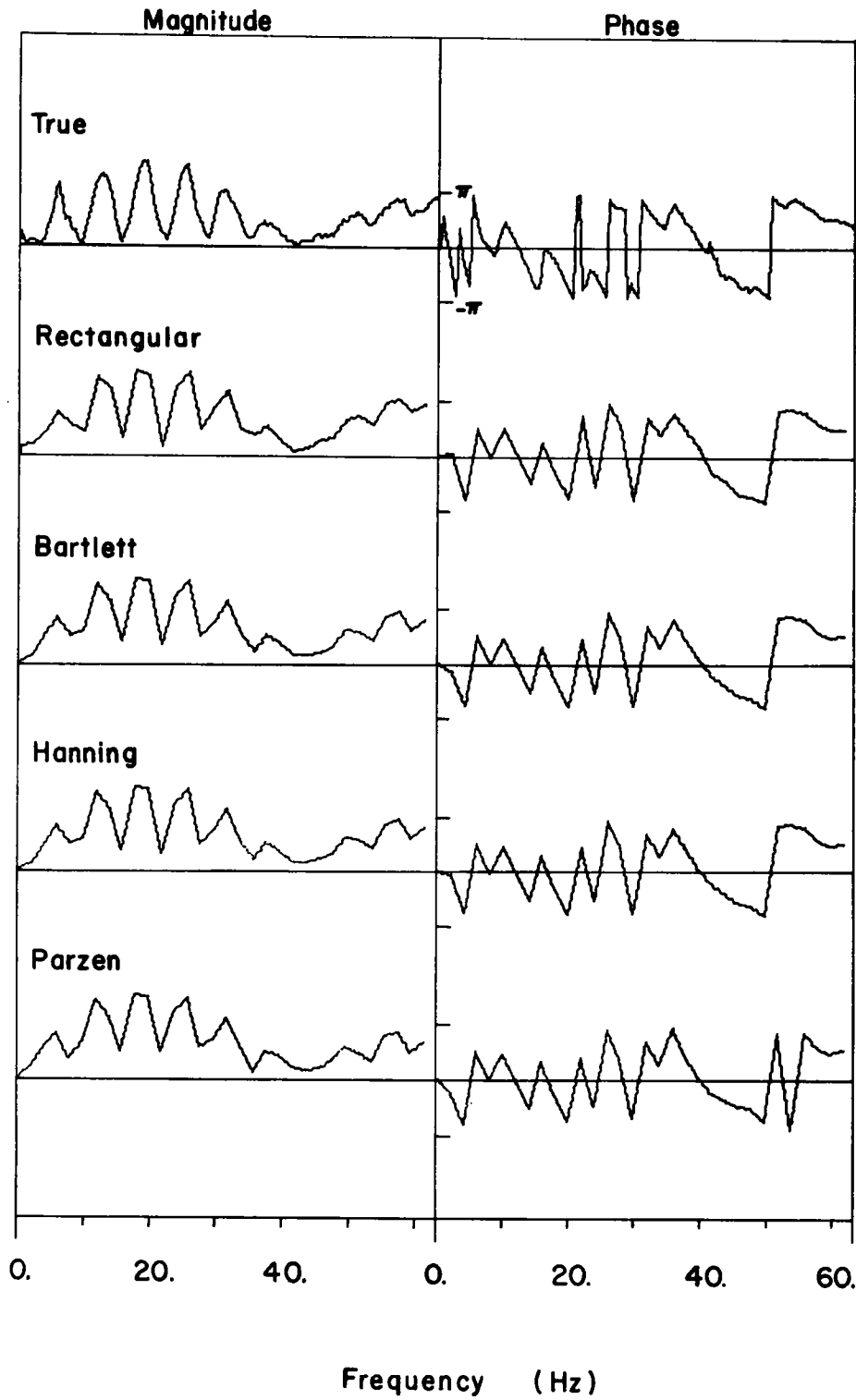
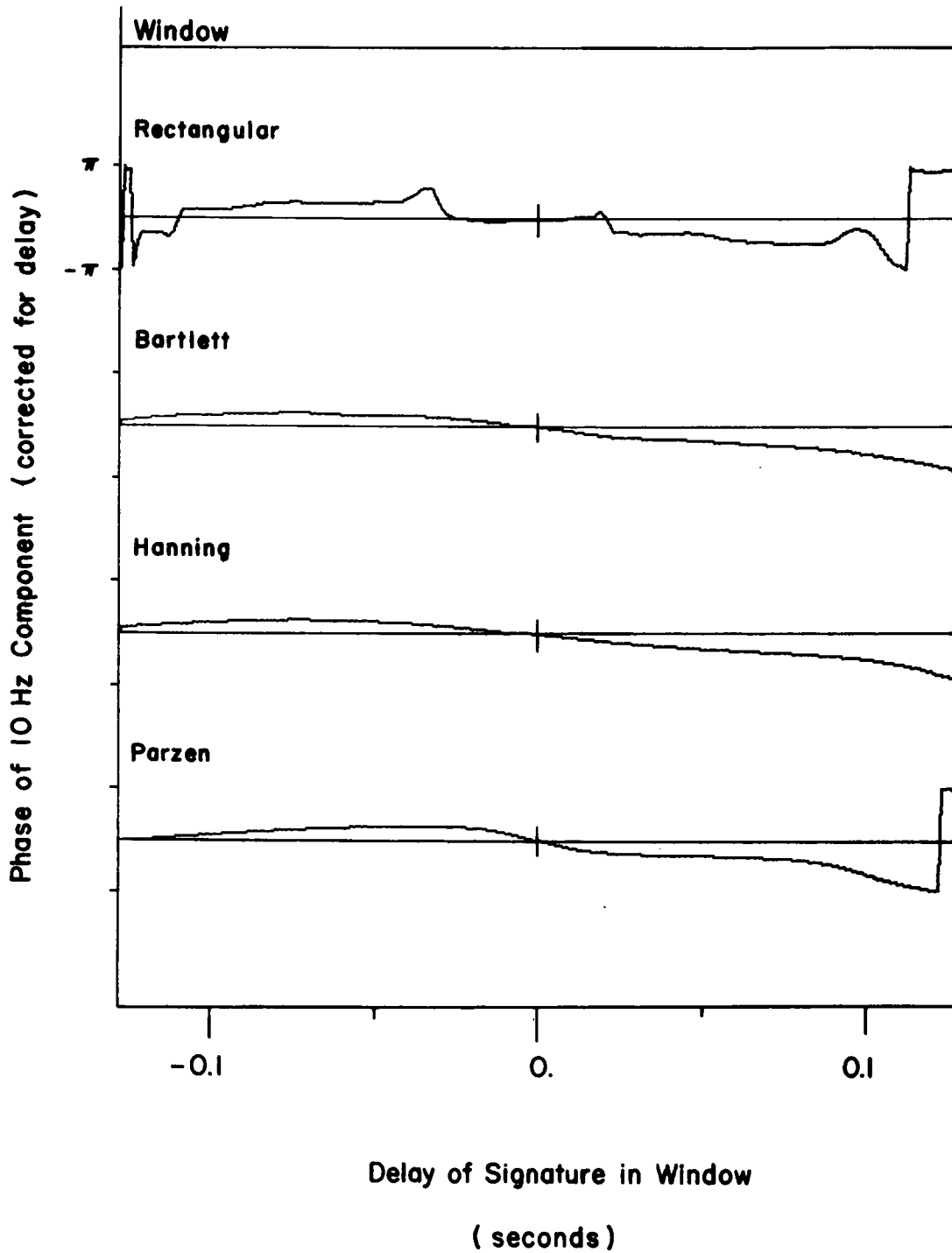


Figure 4.7 Variation From Linear Phase Shift of Gun Signature Moving Through Various Windows.



increase significantly thereafter. Figure 4.4 gives similar results for the Hanning windows.

The final step in our analysis of bias error introduced by windowing is to translate the tolerance in positional error to allowable perturbation in normal incidence time, T_o , and velocity, \bar{C} . Essentially, we have that if changes in these parameters produce large positional errors around a normal moveout curve for the array elements, then we require a dense scanning in estimating the spectral correlation matrix. Obviously this is an added computational burden which one would like to avoid.

We can perform this analysis by taking the total derivative of the normal moveout relationship,

$$T_i(T_o, \bar{C}, X_i) = \sqrt{T_o^2 + (X_i/\bar{C})^2} \quad 4.14a$$

$$\text{or } \Delta T_i = \frac{T_o \Delta T_o - (X_i^2/\bar{C}^3) \Delta \bar{C}}{T_i} \quad 4.14b$$

This can be manipulated into the form

$$\Delta T_i(T_o, \bar{C}, X_i) = \cos \phi_i \Delta T_o - \tan \phi_i \sin \phi_i \frac{T_o}{\bar{C}} \Delta \bar{C} \quad 4.15$$

$$\text{where } \phi_i = \tan^{-1} [X_i/\bar{C}T_o] \quad 4.16$$

The easiest way to employ this relation is to note that the maximum effects of a change in ΔT_o are when $\phi_i \cong 0$. and in $\Delta \bar{C}$ when $\phi_i \cong 90^\circ$. We can use a worst case analysis for a nominal T_o , \bar{C} by considering the situations at $\phi_i = 0$. and $\phi_i = \phi_{max} = \tan^{-1} [X_{max}/\bar{C}T_o]$ where X_{max} is the array element with the most distant offset.

As a simple example we consider a velocity analysis for a 2.5 km. array at $T_o = 3$. secs. and \bar{C} ranging from 1.5 km/sec to 4.5 km/sec. From our previous analysis we allow a positional error of ± 0.025 secs which is divided equally between that caused by ΔT_o and that by $\Delta \bar{C}$. We then have for the allowable normal incidence time change

$$\cos \phi \left| \max \Delta T_o \right| \leq .0125 \text{ secs. ,}$$

$$\text{or} \quad \left| \max \Delta T_o \right| \leq .0125 \text{ secs.} \quad 4.17$$

For the allowable velocity change

$$\tan \phi \sin \phi \frac{T_o}{\bar{C}} \left| \max \Delta \bar{C} \right| \leq .0125 \text{ secs.} \quad 4.18$$

At $\bar{C} = 1.5$ km/sec this implies

$$\phi_{max} = 29^\circ, \quad |max \Delta \bar{C}| \cong .023 \text{ km/sec}, \quad 4.19$$

while at $\bar{C} = 4.5 \text{ km/sec}$ it implies

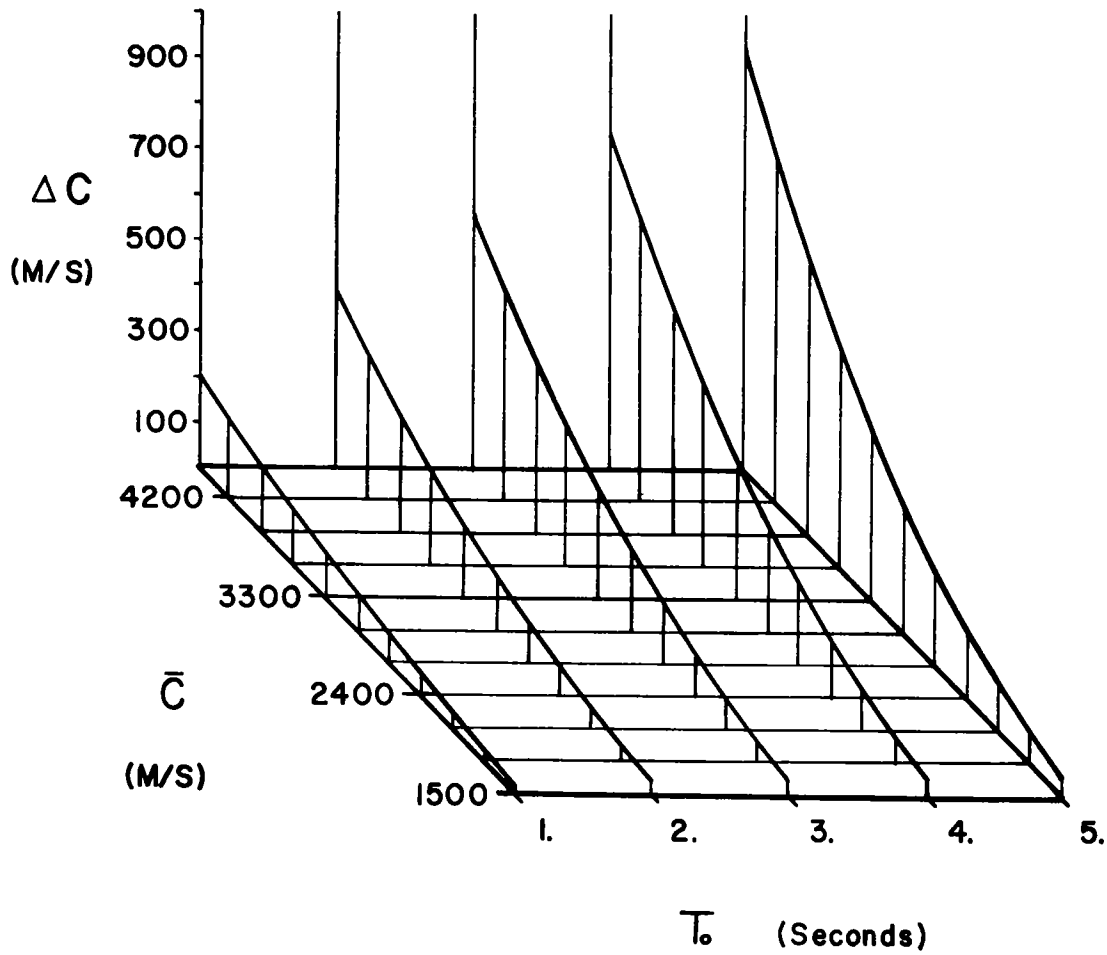
$$\phi_{max} = 10.5^\circ, \quad |max \Delta \bar{C}| \cong .556 \text{ km/sec}. \quad 4.20$$

Obviously the positional errors are more sensitive at the lower velocity, which requires a denser selection of nominal parameters for T_o, \bar{C} . The results for velocity increments for the same 2.5 km array for a range of velocities and depths are plotted in Figure 4.8. Note the large increments that are allowed in the deep, high velocity region.

Discussion

We now can set up the iteration over velocity and depth in an optimum manner. We scan the estimator on increments corresponding to the finest resolution that we can expect in the given dimension. In time the increment is determined by the length of the signature and the length of the data window. In velocity it is dependent on the array spacing and length, on the frequency, and on the estimator form used. The results of this last section offer relief, however, from the necessity of having to form a new covariance matrix for

Figure 4.8 Maximum Velocity Estimate Increments versus Velocity and Depth of the Estimate for a 2.5 km Array.



each increment of the estimator. The estimate can be performed on the same matrix without appreciable degradation over a range specified by Eqs. 4.16 and 4.17, and Figure 4.8.

4-B Averaging and the Stability of the Cross-Spectral Correlation Matrix.

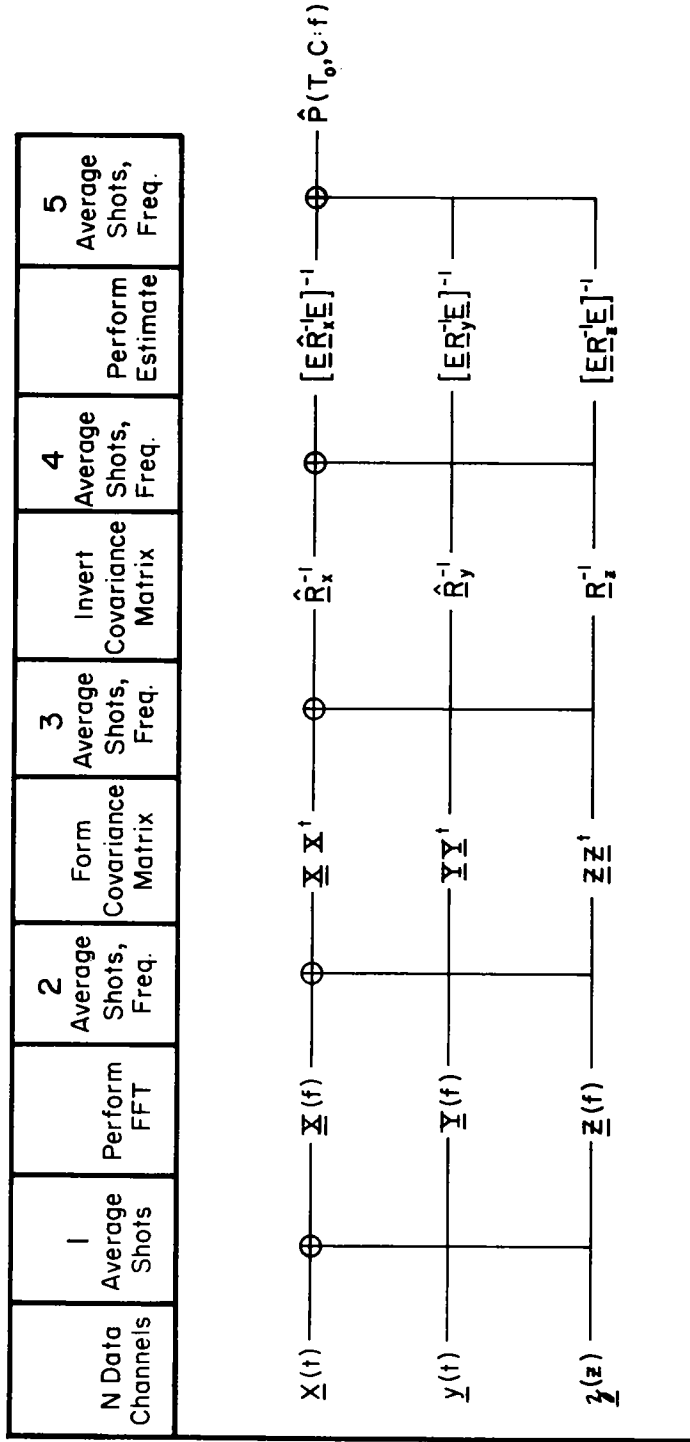
In the previous section we concentrated upon producing an estimate of the cross spectral correlation matrix which had a minimum of bias. In this section we consider the other aspect of this estimate, that of its variance or stability. The stability of the estimate is essentially determined by the deterministic components and the available number of independent degrees of freedom in reducing any random components. The deterministic, or mean, components are indicative of the presence of reflection horizons, while the random ones represent the variation that one observes in the reflections from them. The random components may be caused by variations between the travel paths of adjacent shots, dispersion between different frequencies, or errors caused by random noise. In this section we examine the methods by which one may increase the stability of the estimate. We reserve until the following chapter a discussion of the statistics and probability models for the estimators. The probabilistic models for describing a non-linear estimator with

many controlling parameters tend to become intractable. By first considering how one goes about stabilizing the estimate, we gain some insight into the description of the statistics of the complete estimator which we examine in Chapter 5.

The primary mechanism for increasing the stability of a spectral estimate is one of averaging over blocks of data. Within the constraints of our windowing requirements there are two domains over which one can average to reduce the variance of the estimate - across shots and across frequency. This averaging of the data may be performed at several positions before, within, and after the application of the estimation procedure, each with slightly differing results. These positions are indicated in Figure 4.9. The two averaging domains are sufficiently different from each other that each bears a separate set of comments.

The possibility of averaging over successive shots is suggested by the similarity of signals produced by closely spaced shots. The estimate is improved only if the signals being processed are coherent in some respect across the shots being averaged, and the noise is uncorrelated. The effectiveness of this is then a function of the horizontal homogeneity of the medium and the distance between shot points, as well

Figure 4.9 Averaging Over Shotpoint and Frequency in Velocity-Depth Estimates



Available Coherent Shotpoints

as the control of the array geometry and the stability of the airgun signatures. For a horizontal planar structure and closely spaced shot points, the signal may be coherent over many shots and extensive averaging is possible.

There are two respects by means of which a signal may be coherent over a shot sequence. In the first the waveform may repeat from shot to shot, and here a linear averaging of signals, or their transforms (since the transformation is a linear operation) is appropriate. This is indicated in the first two averaging columns of Figure 4.9.

Alternatively, the signal may vary from shot to shot, but the correlation and relative phasing may be stable. Here a quadratic averaging of the cross products used in estimating the cross spectral correlation matrix is appropriate. This is illustrated in the third averaging column of the figure.

In estimating the matrix one can average across frequency if the signals are broadband, and the relative phasing is not severely distorted across the frequency band used. The same concepts that appear in the analysis of conventional planar arrays also appear here. (See Skolnik, 1962). The basic calculation that is performed is to compute the bandwidth of the array about a nominal center frequency. For the case of a simple linear array in a field consisting of a single

plane wave, we have a normalized response given by

$$\rho(f_0, c_0, \theta_0 | f_1, c_1, \theta_1) = \frac{1}{N} \sum_{\ell} \left(e^{j\ell d \frac{2\pi f_0}{c_0} \sin \theta_0} e^{-j\psi_{\ell}(f_1, c_1, \theta_1)} \right) \quad 4.21$$

where the steering function is given by

$$\psi_{\ell}(f_1, c_1, \theta_1) = \ell d \frac{2\pi f_1}{c_1} \sin \theta_1 \quad 4.22$$

This is the plane wave ambiguity function. (see Eq.s 3.1 and 3.2.) For a correctly steered array, we have

$$f_1 = f_0$$

$$c_1 = c_0$$

$$\theta_1 = \theta_0$$

4.23

Now, if we let f_0 vary while keeping f_1 fixed, we have

$$\rho(f_0, c_0, \theta_0 | f_1, c_0, \theta_0) = \frac{1}{N} \sum_{\ell} e^{j\ell \left(\frac{d 2\pi}{c_0} \sin \theta_0 \right) (f_0 - f_1)} \quad 4.24$$

The response to waves of other frequencies is dependent on the propagation velocity and the angle of incidence, as well as on the frequency shift. For the case of the bandwidth of the array in velocity/depth estimation, the response to other frequencies is given by

$$p(f_0, T_0, \bar{C} | f, T_0, \bar{C}) = \frac{1}{N} \sum_{\ell} e^{j2\pi T(T_0, \bar{C}, \Sigma_{\ell})(f_0 - f)} \quad 4.25$$

Because of the complexity of the geometry here, it is difficult to state anything very general. The array bandwidth depends on the depth and velocity of focus, as well as on the array geometry. For the adaptive processor, the increased resolution will decrease the array bandwidth significantly, although this is even more difficult to quantify.

These comments, however, do not hold for averaging across frequency in column 5 of Figure 4.9; averaging the final estimate. Averaging at this point produces a wideband estimate as described in Chapters 2 and 3. Here there is no longer phase information and the estimates average coherently as long as the information in the two frequency bands is consistent.

We have found that in regions with a reasonable amount of horizontal homogeneity, the velocity/depth spectra are quite consistent across adjacent or closely spaced shots. (See Chapter 6) Averaging across shots in any of the positions is of some benefit. We have had mixed results, however, in averaging across the frequency domain. In all of the positions except column 5 the smearing has been noticeable. In column 5 we have found that it is often useful to maintain the separate estimates over frequency. It appears that

the reflection process can be frequency selective, with horizons which are evident in a CDP profile appearing only in some of the velocity/depth estimates versus frequency. It may be possible to use this frequency selectivity constructively, either for the design of filters in subsequent stacking operations or as a diagnostic tool in interpreting the character of the reflection horizons.

Summary

The estimation of the covariance matrix from the data is a critical step in forming the velocity/depth spectrum. Two important aspects of this estimation are the time windowing prior to transforming and the averaging of the data. The optimum window shape and length is dependent on the reflected signature. Once the window is determined from a tradeoff of time resolution and frequency smearing, the bias due to positional errors is easily calculated. Defining limits for this bias, we can then perform the velocity/depth spectral power estimate over a small range of depths and velocities using the same estimate of the covariance matrix. Numerically, this can be a time saver. In practice we have found this to work quite well for a range of velocities, but not for the time increments, which depend on the window increments for

resolution. Averaging of the data reduces the random components, but must be done with discretion. It is very seldom that the return signals do not vary to some extent from shot to shot, even in the best of conditions. Nature never quite follows our assumption of flat, laterally homogeneous layers of sediments, and we rapidly begin to lose information if we average very many data sets. Again experience with real data provides the final answer, and we have had some of our best results without averaging over shots, and summing over frequency only in the final stage of the estimator. After examining the statistics of the estimators in the next chapter, we investigate the results of applying the estimators to real data in Chapter 6.

Chapter 5 Statistics of the Estimators.

Introduction

In this chapter we examine the statistical distributions of both the conventional and MLM velocity/depth spectral estimators. We calculate the bias and variance of both forms of the estimator for Gaussian input data. Simplified results are presented for the special case of independent (between channels and between observations) noise. With the aid of a matrix whitening process we solve the estimator forms and their statistics for the case of a singular (rank 1) estimate of the covariance matrix. The moments for the MLM estimate operating on a singular covariance matrix are shown to be a form of confluent hypergeometric function. These are calculated and compared with the conventional moments using the same covariance matrix estimate. The MLM is shown to improve the velocity/depth spectral estimate, even when employing a singular covariance matrix.

Throughout this chapter we characterize the data (the output from the FFT operation) as a complex valued signal plus complex Gaussian noise. The signal is considered as unknown but constant, and the noise is multi-variate normal with zero mean and a covariance matrix Σ . The data from

observation "k" is denoted by

$$\underline{Y}_k = \underline{S} + \underline{N}_k \quad 5.1$$

where \underline{S} is the vector of signals and \underline{N}_k is a noise vector. This is a common assumption in geophysical data and permits us to calculate and compare the statistics of the two forms of the estimators.

Conventional Estimator Statistics

We begin by considering the statistics of the conventional estimate. We use matrix notation to simplify our calculations. The data may be considered an $N \times L$ matrix formed from L observations of vectors composed of the N data channels.

$$\begin{array}{cccc} \underline{Y}_1 & \underline{Y}_2 & \dots & \underline{Y}_L \\ \left[\begin{array}{cccc} Y_{11} & Y_{12} & \dots & Y_{1L} \\ Y_{21} & Y_{22} & & \\ \vdots & & & \\ Y_{N1} & & & Y_{NL} \end{array} \right] & = & \underline{U}(f) & 5.2 \end{array}$$

The estimated covariance matrix is formed by

$$\hat{R}(f) = \underline{U}(f) \underline{U}(f)^\dagger \quad 5.3a$$

where the ij^{th} component of \hat{R} is

$$\hat{R}_{ij} = \sum_{k=1}^L \Upsilon_{ik} \Upsilon_{jk}^* \quad 5.3b$$

Referring to section 4-B, the averaging inherent in this form of the estimated matrix is the quadratic averaging in column 3 of Figure 4.9. This is the form generally used for the estimate of the covariance matrix of a process (Anderson 1958, Goodman 1963).

We write the data as a signal plus Gaussian noise,

$$\Upsilon_{ik} = S_i + n_{ik} \quad 5.4$$

where Υ_k is distributed as $N(\underline{S}, \underline{\Sigma})$, $\underline{S} = [s_i]$ is the unknown but constant signal, and $\underline{\Sigma}$ is the actual covariance matrix of the noise process. It has been shown (Goodman 1963, Rao 1965, and others) that the estimated covariance matrix \hat{R} has a non-central complex Wishart distribution. This is a multivariate generalization of the non-central complex chi-square distribution.

It can be shown that for a Wishart distributed matrix \hat{R} and a column vector of constants \underline{E} , the quantity

$$P_c = \frac{1}{N} \left[\underline{E}^+ \hat{R} \underline{E} \right]$$

is distributed as a first order Wishart with L degrees of freedom, which is equivalent to $\chi^2_{(L)}$ (Rao, 1965). Specifically, the distribution is

$$\sigma_E^2 \chi^2(L, \lambda) \quad 5.5a$$

where $\sigma_E^2 = \frac{1}{N} \underline{E}^+ \underline{\Sigma} \underline{E}$ 5.5b

and λ is a non-centrality parameter given by

$$\lambda = \frac{\left| \frac{L}{N} \underline{E}^+ \underline{S} \right|^2}{\sigma_E^2} \quad 5.5c$$

If we look at the on-axis response ($E_i S_i = \delta$) and consider the noise to be uniform and independent ($\underline{\Sigma} = \sigma_Y^2 \underline{I}$), then we have, for a simplified case,

$$\sigma_E^2 = \frac{\sigma_Y^2}{N} \quad 5.6a$$

$$\lambda = \frac{NL^2 \delta^2}{\sigma_Y^2} \quad 5.6b$$

The characteristics and moments of the non-central chi-square

are well known. The mean is

$$E[P_c] = \sigma_E^2 (L + \lambda) \quad 5.7a$$

and the variance is

$$\sigma_{P_c}^2 = (\sigma_E^2)^2 (2 + 4\lambda) \quad 5.7b$$

For our simplified case we have

$$E[P_c] = \sigma_Y^2 \left(\frac{L}{N} + \frac{L^2 \delta^2}{\sigma_Y^2} \right) \quad 5.8a$$

$$\sigma_{P_c}^2 = \sigma_Y^4 \left(\frac{2L}{N^2} + \frac{4L^2 \delta^2}{N \sigma_Y^2} \right) \quad 5.8b$$

MLM Estimator Statistics

We begin our investigation of the statistics of the MLM with results derived by Capon and Goodman (1970). Using a relation given by Rao (1965), we can derive Capon and Goodman's result in a simple fashion. Rao (1965) gives the following result for a matrix \hat{R} distributed as $W(L, \Sigma)$.

The quantity

$$\frac{\underline{E}^{\dagger} \underline{\Sigma}^{-1} \underline{E}}{\underline{E}^{\dagger} \underline{\hat{R}}^{-1} \underline{E}}$$

where \underline{E} is any fixed vector, is distributed as $\chi^2_{(L-N+1)}$.

The numerator is a variance term which remains constant.

We rewrite this result to give

$$P_{MLM} = \frac{1}{\underline{E}^T \underline{R}^{-1} \underline{E}}$$

is distributed as

$$\left[\frac{1}{\underline{E}^T \underline{\Sigma}^{-1} \underline{E}} \right] \chi^2_{(L-N+1)}, \quad L \geq N \quad 5.9$$

This result, as well as the existence of the Wishart distribution density function, depends on $L \geq N$. The expressions for the mean and variance are

$$E[P_{MLM}] = \left[\underline{E}^T \underline{\Sigma}^{-1} \underline{E} \right]^{-1} (L-N+1+\lambda) \quad 5.10a$$

$$\sigma_{P_{MLM}}^2 = \left[\underline{E}^T \underline{\Sigma}^{-1} \underline{E} \right]^{-2} (2(L-N+1) + 4\lambda) \quad 5.10b$$

where λ is the non-centrality parameter given in Eq. 5.5c.

We again simplify for the case of $\underline{\Sigma} = \sigma_Y^2 \underline{I}$ and $E_i S_i = \delta$. The results are

$$E[P_{MLM}] = \sigma_Y^2 \left(\frac{L-N+1}{N} + \frac{L^2 \delta^2}{\sigma_Y^2} \right) \quad 5.11a$$

and

$$\sigma_{P_{MLM}}^2 = \sigma_Y^4 \left[2 \left(\frac{L-N+1}{N^2} \right) + 4 \frac{L^2 \delta^2}{N \sigma_Y^2} \right] \quad 5.11b$$

Comparing Eq.s 5.8 and 5.11, we see that both the expected value due to the noise power and the variance are reduced by the MLM. This verifies the concept that the MLM is a higher resolution estimator and does not respond as greatly to incoherent signals.

We note in applying these results that the requirement that L be greater than N is a problem. In most of our applications we have used only one or several shots or observations in forming the covariance matrix. In order to examine the statistics of these cases, we propose another approach which is presented in the next section.

MLM for a Singular Covariance Matrix

The general results of Capon and Goodman (1970) are not valid for the case where $L < N$, which is a region we are most interested in. The rank of the estimated covariance matrix $\hat{\underline{R}}$ is L , and $\hat{\underline{R}}^{-1}$ does not exist when $L < N$. We have found that by adding a small real quantity to the diagonal elements of $\hat{\underline{R}}$, we eliminate the singularity of the inversion

and can invert the modified matrix even when its original rank was unity. This operation is commonly done in spectral analysis techniques and is described as whitening the matrix. The effect of whitening is much the same as the quadratic averaging of many observations, each of which contain some white noise. The diagonal terms (which are all zero phase) are enhanced relative to the off-diagonal terms (which have non-zero phases that vary with the noise components). We note that the diagonal terms are spectral components and the off-diagonal terms are cross-spectral components. White noise contributes to the level of a spectral estimate without affecting the cross-spectral level. We also note here that the linear averaging in columns 1 and 2 of Figure 4.9 reduce the noise by increasing the number of observations, but do not contribute to increasing the rank of the matrix. The estimated matrix following the linear averaging of the terms is of rank 1. The comments in the next section on the single observation case are also applicable to this case if we consider a reduced input variance.

Some insight into the singular covariance matrix may be gained from factoring the matrix into its eigenvectors and eigenvalues.

$$\hat{\underline{R}} = \underline{W} \underline{\Lambda} \underline{W}^\dagger \quad 5.12$$

$\underline{\Lambda}$ is a diagonal matrix whose diagonal terms are λ_i , and \underline{W} is a matrix of column eigenvectors. The eigenvectors are orthogonal so that $\underline{W}^\dagger \underline{W} = \underline{I}$. $\hat{\underline{R}}$ is hermitian, which implies that the λ_i are real and non-negative. The inverse of $\hat{\underline{R}}$ is given by

$$\hat{\underline{R}}^{-1} = \underline{W} \underline{\Lambda}^{-1} \underline{W}^\dagger \quad 5.13$$

$\underline{\Lambda}^{-1}$ is a diagonal matrix whose terms are $(1/\lambda_i)$. When one or more of the λ_i are zero, $\hat{\underline{R}}$ is singular and the inverse is ill-defined.

If we now consider the modified covariance matrix

$$\hat{\underline{R}}' = \hat{\underline{R}} + \beta \underline{I} \quad 5.14a$$

we get a modified eigenvalue matrix.

$$\hat{\underline{R}}' = \underline{W} \underline{\Lambda} \underline{W}^\dagger + \beta \underline{I} \quad 5.14b$$

or
$$\hat{\underline{R}}' = \underline{W} (\underline{\Lambda} + \beta \underline{I}) \underline{W}^\dagger \quad 5.14c$$

The eigenvalues of the modified matrix are

$$\lambda_i' = \lambda_i + \beta \quad 5.15$$

and the eigenvalues of the inverse are

$$\frac{1}{\lambda_i'} = \frac{1}{\lambda_i + \beta} \quad 5.16$$

These are always finite for $\beta > 0$ and the inverse is no longer ill-defined.

The stability of the inversion operation is determined by a quantity known as the condition number, \mathcal{K} (Householder 1964). The condition number of the covariance matrix is the ratio of its largest to its smallest eigenvalue.

$$\mathcal{K} = \frac{\max_i \lambda_i}{\min_j \lambda_j} \quad 5.17$$

For \mathcal{K} approaching one, the inverse operation is a well posed problem and the solution involves very stable calculations.

For \mathcal{K} increasing, the computation of the inverse becomes more and more unstable, and the matrix approaches a singular condition. By whitening the matrix, we are limiting the value of \mathcal{K} . The largest eigenvalue is bounded by

$$\frac{\text{Tr}(\hat{R})}{N} \leq \lambda_{i_{\max}} \leq \text{Tr}(\hat{R}) \quad 5.18$$

The minimum eigenvalue in the modified matrix is greater than or equal to β . Letting β be a function of $\text{Tr}(\hat{R})$, we control \mathcal{K} and the stability of the inversion operation. The optimum maximum value of \mathcal{K} is determined by the numerical stability and accuracy of the computational device used for the calculations. For computers with a 7 significant figure accuracy, a value of about 10^4 is suggested. The tradeoff we make for stabilizing the matrix inversion is one of distorting the matrix, and ultimately distorting the final estimate. Our results which follow indicate that this distortion is toward the conventional form of the estimator; hence we have a valid, if slightly less than optimum, estimate. This bias toward the conventional estimate is intuitively correct in that as we increase the level of white noise in the signal field, the weighting coefficients approach uniform and the optimum beam pattern approaches the conventional. We conclude that, with the whitening, it is possible to employ the MLM estimator on a singular covariance matrix. The estimate suffers from not having reduced the random components, but the adaptive procedure should still produce a higher resolution estimate than the conventional.

Single Observation MLM Estimator - Exact Solution

A simple case that we can solve exactly and generally is for the inversion of the whitened covariance matrix from one observation of the data set. The estimated covariance matrix becomes

$$\hat{R} = \underline{Y} \underline{Y}^\dagger + \beta \underline{I} \quad 5.19$$

where β is the power of the added white noise. Generally we let β be in the range of 10^{-4} to 10^{-2} times the trace of $\underline{Y} \underline{Y}^\dagger$. From Graybill (1969) we have

$$\hat{R}^{-1} = \frac{1}{\beta} \underline{I} - \frac{\underline{Y} \underline{Y}^\dagger}{\beta^2 + \beta \sum_{i=1}^N \underline{Y}_i \underline{Y}_i^*} \quad 5.20$$

Solving for both estimators in terms of the vector components, we obtain

$$P_c = \frac{\beta}{N} + \frac{1}{N^2} \sum_{i=1}^N \sum_{j=1}^N E_i^* \underline{Y}_i \underline{Y}_j^* E_j \quad 5.21$$

$$P_{MLM} = \frac{\beta^2 + \beta \sum_{i=1}^N \underline{Y}_i \underline{Y}_i^*}{N\beta + N \sum_{i=1}^N \underline{Y}_i \underline{Y}_i^* - \sum_{i=1}^N \sum_{j \neq i}^N E_i^* \underline{Y}_i \underline{Y}_j^* E_j} \quad 5.22$$

We make the following substitutions

$$\Psi = \frac{\left| \sum_{i=1}^N A_i \right|^2}{N^2} \quad 5.23a$$

$$\Theta = \frac{\sum_{i=1}^N |A_i - \bar{A}|^2}{N} \quad 5.23b$$

where $A_i = E_i^* Y_i$ 5.23c

and $\bar{A} = \frac{1}{N} \sum_{i=1}^N A_i$ 5.23d

We note that Ψ is the square of the sample mean of the steered data and Θ is the sample variance. Substituting these into Eqs. 5.21 and 5.22, we obtain

$$P_c = \frac{\beta}{N} + \Psi \quad 5.24$$

$$P_{MLM} = \frac{\beta}{N} + \frac{\Psi}{1 + \frac{N}{\beta} \Theta} \quad 5.25$$

These results are derived in Appendix II. We use these expressions for the estimators in the remainder of this discussion.

For β increasing, we note that the MLM estimate asymptotically approaches the conventional estimate. The two

estimates also converge for the case when the variance of the steered samples approaches zero. This corresponds to the correctly steered estimate of a signal without noise.

Statistics of Single Observation Estimators.

In order to determine the statistics of the single observation case, we again consider multi-variate non-zero mean Gaussian data as the input to the estimators.

$$\underline{Y} \sim N(\underline{S}, \underline{\Sigma}) \quad 5.26a$$

$$\underline{A} \sim N\left(\underline{[S_i E_i^*]} \quad \underline{[E_i^* \sigma_{ij} E_j]}\right) \quad 5.26b$$

Constraining the noise to be identically distributed and independent, and the phase corrected signals to be identical for each channel, we have

$$\underline{A} \sim N(\delta \underline{1}, \sigma_r^2 \underline{I}) \quad 5.27$$

Deriving the distributions of ψ and Θ is straight forward, and we take our results from Papoulis (1965). ψ is a first order non-central chi-square process. The probability density function is

$$f_{\psi} = \frac{1}{\frac{\sigma_Y}{\sqrt{N}} \sqrt{2\pi\psi}} e^{-\frac{(\psi + \delta^2)}{2\sigma_Y^2/N}} \left[\frac{e^{\frac{\delta\sqrt{\psi}}{\sigma_Y^2/N}} + e^{-\frac{\delta\sqrt{\psi}}{\sigma_Y^2/N}}}{2} \right] U(\psi) \quad 5.28$$

Θ is central chi-square with density function

$$f_{\Theta} = \frac{1}{2^{\frac{N-1}{2}} \left(\frac{\sigma_Y^2}{N}\right)^{\frac{N-1}{2}} \Gamma\left(\frac{N-1}{2}\right)} \Theta^{\frac{N-3}{2}} e^{-\frac{N\Theta}{2\sigma_Y^2}} U(\Theta) \quad 5.29$$

We also have that ψ and Θ are independent. Changing variables

$$\xi = 1 + \frac{N}{\beta} \Theta \quad 5.30$$

$$\Theta = \frac{\beta}{N} (\xi - 1) \quad 5.31$$

we obtain

$$f_{\xi} = \left(\frac{\beta}{2\sigma_Y^2}\right)^{\frac{N-1}{2}} \frac{e^{\frac{\beta}{2\sigma_Y^2}}}{\Gamma\left(\frac{N-1}{2}\right)} (\xi - 1)^{\frac{N-3}{2}} e^{-\frac{\beta\xi}{2\sigma_Y^2}} U(\xi - 1) \quad 5.32$$

and

$$P_{MLM} = \frac{\beta}{N} + \frac{\psi}{\xi} \quad 5.33$$

Since ψ and ξ are independent, we can solve for the distribution of the quotient $Z = \left(\frac{\psi}{\xi}\right)$ in a straight forward, but algebraically complicated manner (see Appendix III).

$$f_z = \Omega z^{-\frac{1}{2}} \int_1^{\infty} f^{\frac{1}{2}} (f-1) e^{-f \left(\frac{\beta + Nz}{2\sigma_Y^2} \right)} \cosh \left[\frac{N\delta \sqrt{zf}}{\sigma_Y^2} \right] df U(z)$$

$$\Omega = \left(\frac{\beta}{2} \right)^{\frac{N-1}{2}} \frac{e^{\frac{\beta - N\delta^2}{2\sigma_Y^2}}}{\sigma_Y^N \sqrt{\frac{2\pi}{N}} \Gamma\left(\frac{N-1}{2}\right)} \quad 5.34$$

This expression is not reducible in terms of closed form functions. Because ψ and f are independent, we can solve for the mean and variance of the estimator most simply by returning to the expressions for the distribution functions of ψ and f . Calculating the first and second moments of ψ and $\frac{1}{f}$, we have

$$E[\psi] = \frac{\sigma_Y^2}{N} + \gamma^2 \quad 5.35a$$

$$E[\psi^2] = 3 \frac{\sigma_Y^4}{N^2} + 6 \gamma^2 \frac{\sigma_Y^2}{N} + \gamma^4 \quad 5.35b$$

$$E\left[\frac{1}{f}\right] = \left(\frac{\beta}{2\sigma_Y^2}\right)^{\frac{N-1}{2}} \mathcal{U}\left(\frac{N-1}{2}, \frac{N-1}{2}, \frac{\beta}{2\sigma_Y^2}\right) \quad 5.35c$$

$$E\left[\frac{1}{f^2}\right] = \left(\frac{\beta}{2\sigma_Y^2}\right)^{\frac{N-1}{2}} \mathcal{U}\left(\frac{N-1}{2}, \frac{N-3}{2}, \frac{\beta}{2\sigma_Y^2}\right) \quad 5.35d$$

$\mathcal{U}(a, b, x)$ is the second form of Kummer's function, a type of confluent hypergeometric function. (Abramowitz and Stegun, 1965). It is convenient when looking at the mean to drop

the constant β/N and consider only the mean of ψ/ξ for the MLM estimator and the mean of ψ for the conventional. The mean of the MLM estimator is given by

$$E[P_{MLM}] = E[\psi] E\left[\frac{1}{\xi}\right] \quad 5.36$$

The variance of the estimator is given by

$$VAR[P_{MLM}] = E[\psi^2] E\left[\frac{1}{\xi^2}\right] - E^2[\psi] E^2\left[\frac{1}{\xi}\right] \quad 5.37$$

Using the relation

$$U(a, b, z) = \frac{\pi}{\sin \pi b} \left\{ \frac{M(a, b, z)}{\Gamma(1+a-b)\Gamma(b)} - z^{1-b} \frac{M(1+a-b, 2-b, z)}{\Gamma(a)\Gamma(2-b)} \right\} \quad 5.38$$

we solve for the moments of $\left(\frac{1}{\xi}\right)$ with $N = 6$.

$$E\left[\frac{1}{\xi}\right] = \frac{4}{3} \sqrt{\pi} e^Q Q^{5/2} + \frac{2}{3} Q \left[1 - 2Q M\left(1, \frac{1}{2}, Q\right) \right] \quad 5.39a$$

$$E\left[\frac{1}{\xi^2}\right] = \frac{4}{3} Q^2 \left(\frac{3}{2} + Q\right) M\left(1, \frac{1}{2}, Q\right) - \frac{2}{3} Q^2 - \frac{2}{3} Q^{5/2} \sqrt{\pi} (3+2Q) e^Q \quad 5.39b$$

$$Q = \frac{\beta}{2\sigma_\gamma^2} \quad 5.39c$$

$M(a,b,x)$ is the first form of Kummer's function, which may be determined from tabulated values or calculated from the series definition (see Abramowitz and Stegun, 1965).

The expected values of the MLM estimator versus the noise variance are plotted in Figure 5.1. As the noise in the data increases - as the signal structure deviates from the form decreed by the steering vectors, the output of the estimator drops off sharply. This is an indicator of the increased resolution that we find with the adaptive estimator, and how the resolution is controlled by the level of β . As β is decreased, the estimator permits smaller and smaller deviations from the desired signal structure in order to maintain the same level of output (i.e., the resolution is increased).

The variance of the single observation MLM estimator is plotted in Figure 5.2 along with the variance of the corresponding conventional estimator. Since the adaptive estimator is dependent on the signal field, we have plotted the variance versus the variance of the input data for several values of signal strength and for different values of additive white noise. For small values of σ_y^2 the variance of P_{MLM} is highly dependent on the strength of the signal. As the noise variance increases, the dependency on the level of

FIGURE 5.1 Expected Values of Estimators-
Single Observation Estimate.

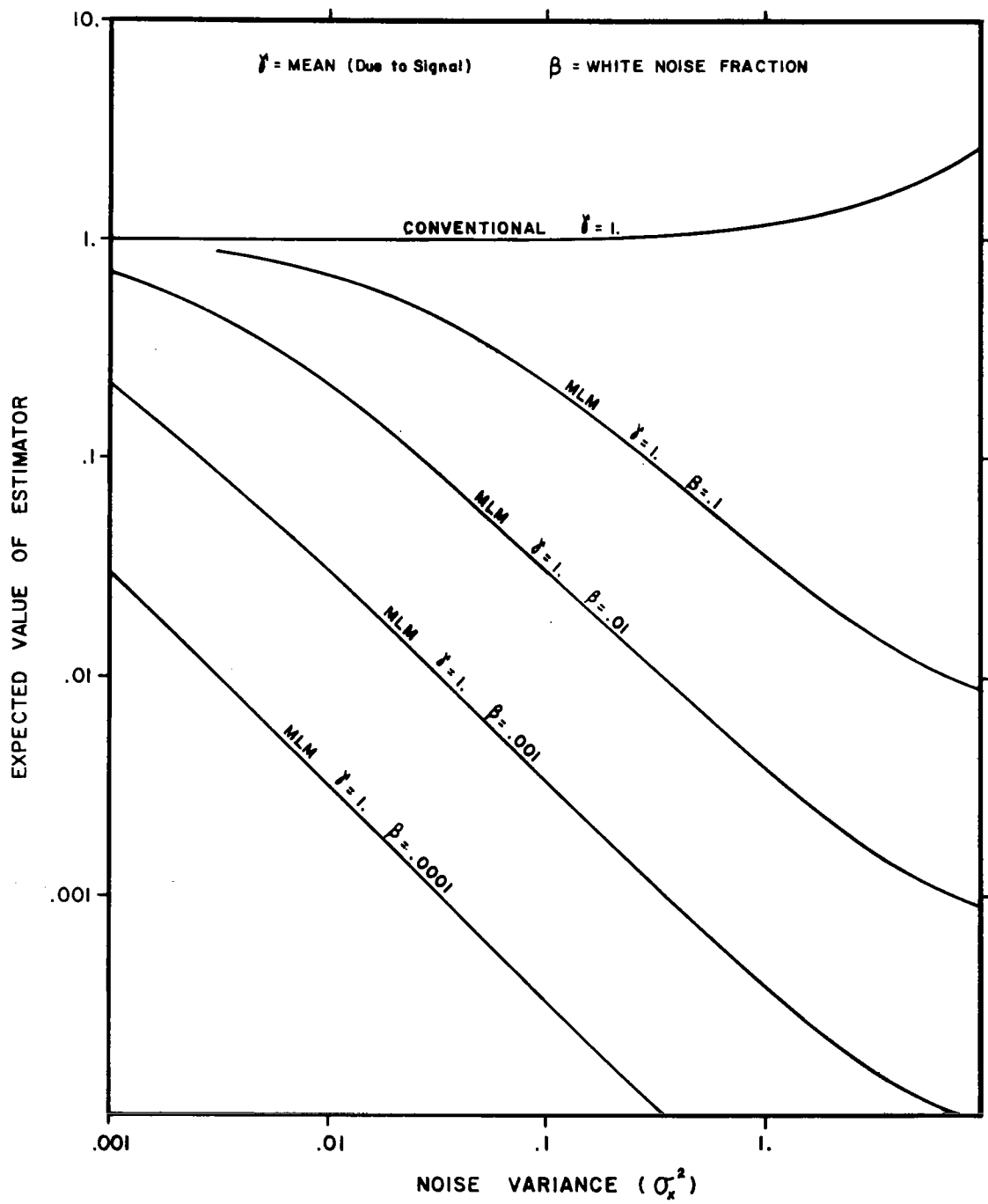
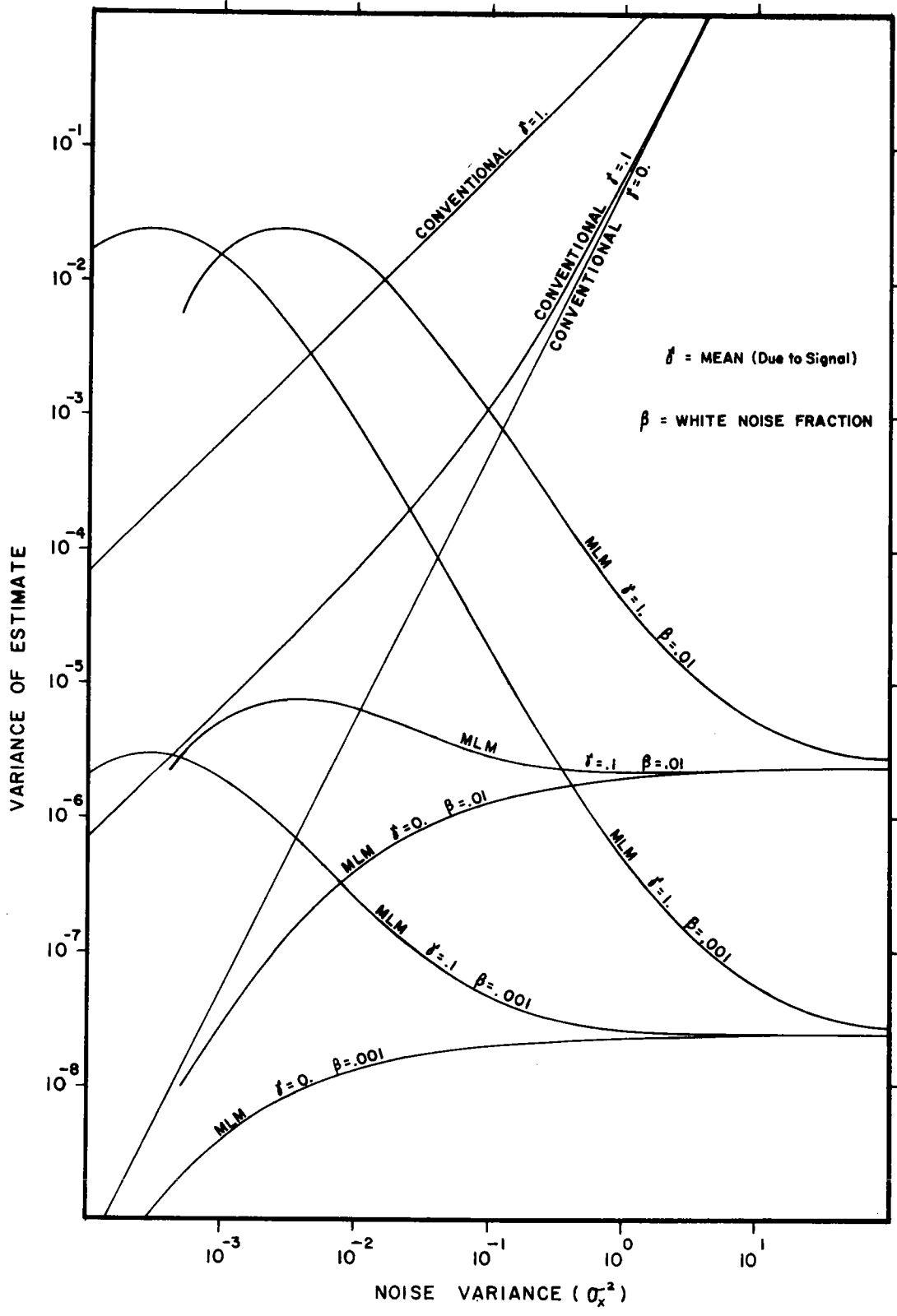


FIGURE 5.2 VARIANCE OF ESTIMATORS - Single Observation Estimate



additive white noise becomes the dominant factor. For comparison purposes we also have plotted the variance of the conventional estimator for the same signal levels.

Summary

In our probabilistic models we have over simplified the actual processes, and the accuracy of the models suffers accordingly. Without these simplifications, however, the problem becomes intractable. There are too many dimensions to allow reasonable interpretations to be made. Our most vulnerable simplifications are the restriction on the noise to be independent and the restriction to looking only at correctly steered signals. The noise in seismic reflection data is generally highly colored and propagating. As we scan the steering vectors versus T_0 and \bar{C} , what was the desired signal in one instance is a strong part of the noise field in the next. But the simplifications do allow us to identify some of the major characteristics of the estimator and make some simple comparisons. The results from the singular matrix case are applicable in a more general sense if we consider unwanted signals as non-random components which reduce the degrees of freedom of the matrix. Off-axis signals increase the sample variance of the steered data

and increase the value of Θ in Eq. 5.27. The resulting estimator shows a much higher resolution in depth and velocity than does the conventional estimator, which is one of the strong points of the adaptive processor.

As we saw in the beginning of this chapter, the multi-observation matrix provides its own whitening while reducing the random components within the data. Considering the constraints used to develop the estimator, this whitening should be optimum; i.e., the white noise level, which we have seen to be an indicator of the resolution, is a direct function of the noise variance of the data. Noisier data calls for a broader resolution. The single observation MLM estimator is sub-optimum in two senses. First, there is no way for it to distinguish between signal and noise - there is no averaging to reduce the random components. Second, the white noise level is externally adjusted and is not directly related to the noise variance of the data. In spite of these short comings, the MLM single observation estimate is a large improvement over the conventional single observation estimate. The single observation MLM estimator still has a greatly increased resolution and a reduced variance. We simply need to be judicious in our estimate of the noise level of the data and our choice of the parameter β .

If we consider noise as errors in the data, then there is a tradeoff between the mean square value of the errors which we assume to be present in the data and the resolution that we call for. We cannot afford a high resolution if there are significant random or systematic errors present.

For the MLM estimators in general, we find that we have an increased resolution and a reduced variance. For the single observation, and any case where the random components have not been completely averaged out, the resolution and variance are gained at the expense of an increased bias. This bias, however, which is a decreased signal level, is a direct contribution to the increased resolution of the estimate. If used cautiously, it is to be desired rather than avoided.

Chapter 6 Experimental Results and Conclusions

Introduction

The experimental development of the MLM estimator in our study has been through a step by step procedure. We began by doing studies of the estimator response to an ideal covariance matrix as in Figure 2.9. Following this investigation we created synthetic tapes in which we could control the characteristics of the reflectors and in which we could be certain that the data matched the travel time model. Studies with this data brought out the requirements for careful windowing and demonstrated the increased velocity resolution. Studies with real data have substantiated the results and conclusions of the synthetic data studies, and have also identified some interesting points that were not accounted for in the synthetic data. These include the ability to resolve overlapping signals and multiples, and the strong frequency dependence of certain returns.

Figures 6.1 and 6.2 give typical results from the ideal covariance matrix studies. Figure 6.1 is the conventional estimate and 6.2 is the MLM estimate of a four reflector case. The reflectors are indicated on the plots by a \dagger . These spectra were calculated entirely from a single covariance

FIGURE 6.1 Ideal Covariance Matrix Spectrum. Conventional Estimate at 25 Hz. Six Channels.

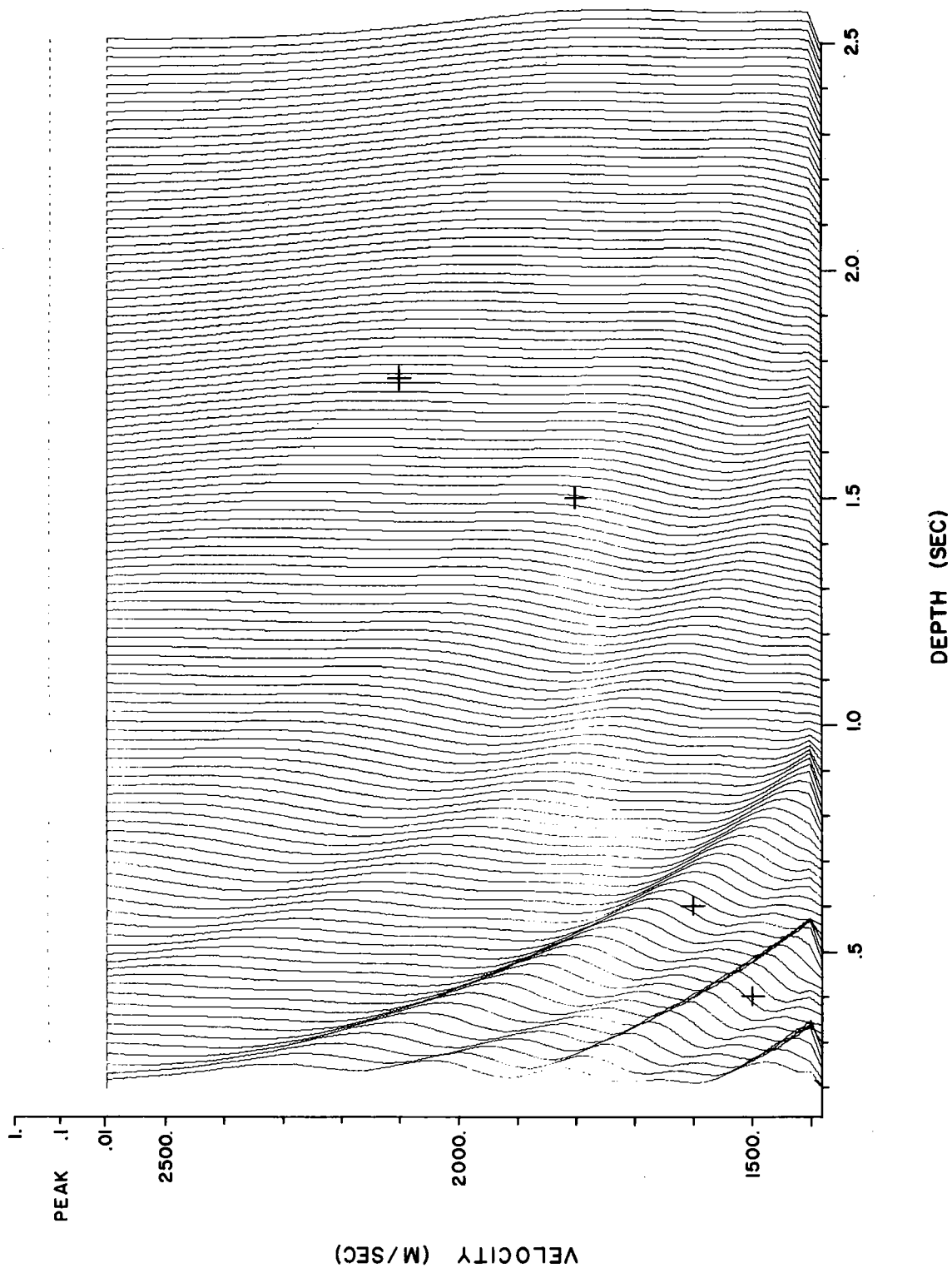
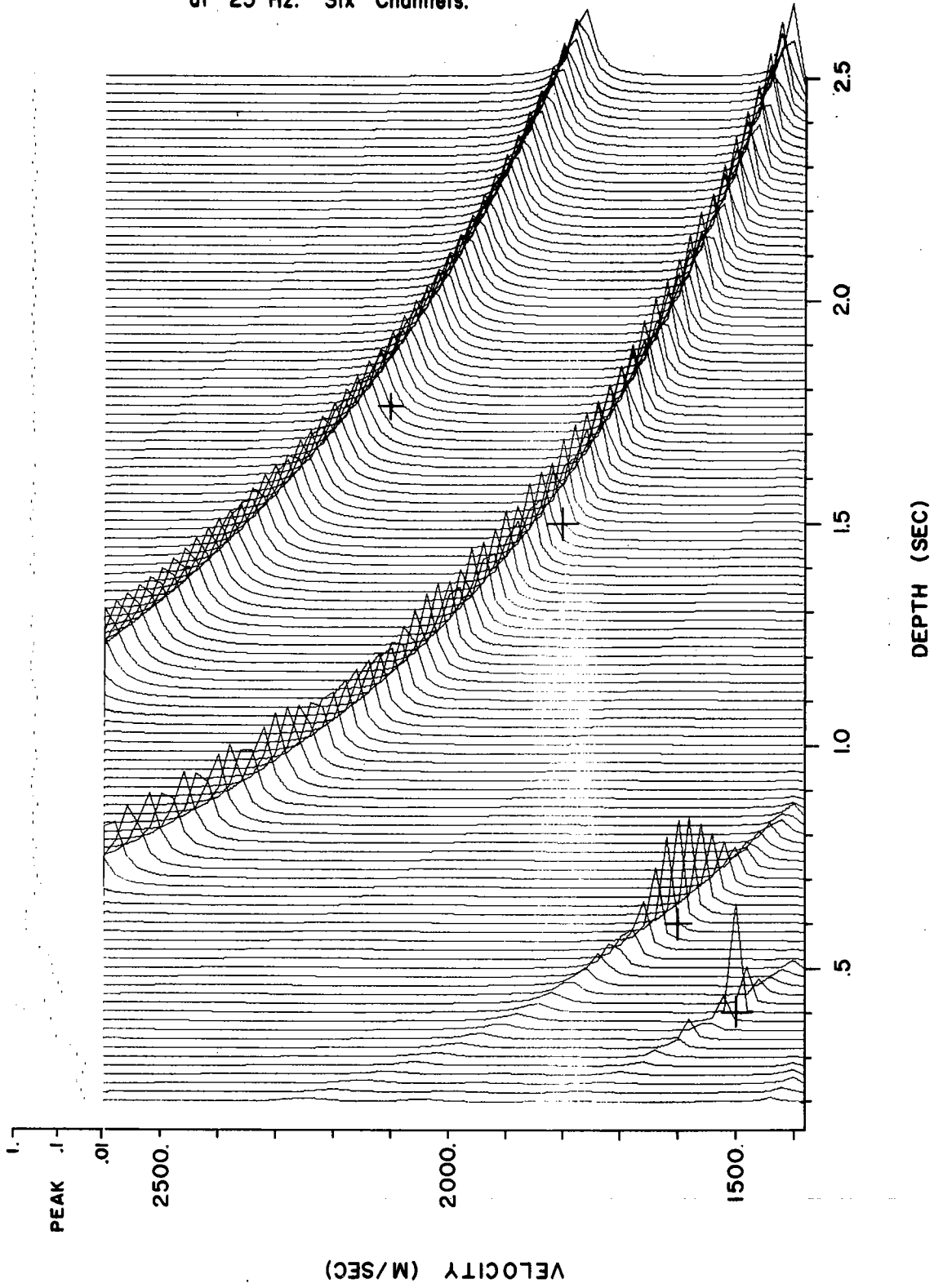


FIGURE 6.2 Ideal Covariance Matrix Spectrum. Adaptive Estimate at 25 Hz. Six Channels.



matrix containing all the reflectors. The ambiguous strip and the higher resolution at shallow depths that we predicted from the ambiguity functions are evident. The effect of holographic focusing is indicated by the resolution in both depth and velocity of the shallowest reflector. In comparing the relative resolution of the two estimators, the MLM processor appears to extend the focusing range of the array, as well as providing a higher resolution in the normal range of the conventional processor.

The next step in the development of our study was to estimate the covariance matrix from ideal data. A common ground point gather from a 12 channel synthetic tape is given in Figure 6.3. There are 8 reflectors whose parameters are given in Table 6.1. This data does not contain any noise wavefronts other than those introduced by a filtered random noise generator applied to each channel. Nor does it contain multiples or refracted arrivals. All the delay times follow the RMS travel time model. The reflection signatures are damped sinusoids. The conventional and MLM spectra of this

Figure 6.3 12 Channel Synthetic Data. 1800 Meter Array.

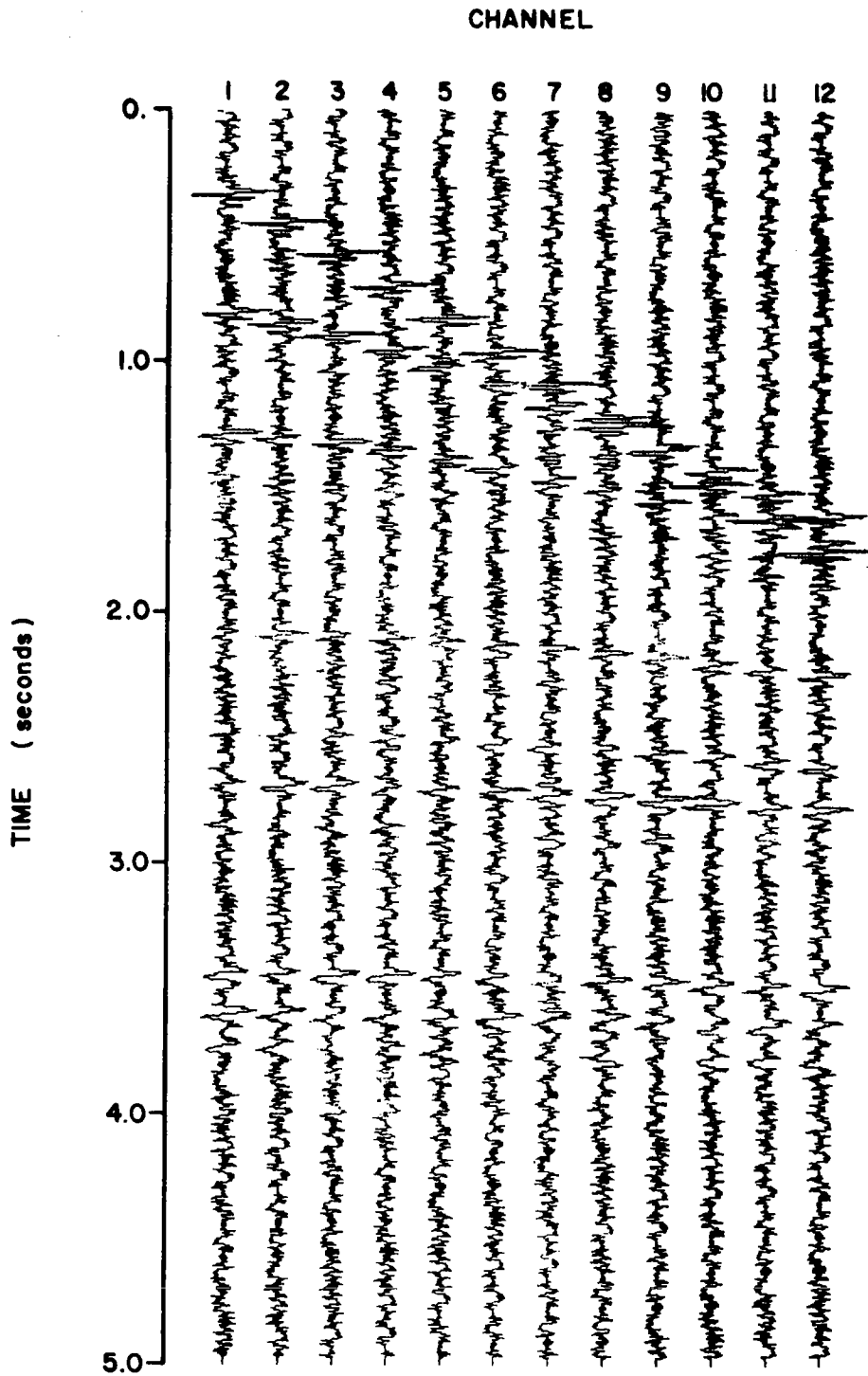


Table 6.1 Reflectors in Synthetic Data Tape.

T_o (sec)	\bar{C} (m/s)	Primary Frequency (Hz)
.20	1490.	34.
.80	1840.	30.
1.30	2260.	27.
2.10	3050.	24.
2.50	3230.	22.
2.70	3490.	20.
3.45	4120.	18.
3.60	4430.	15.

data are given in Figures 6.4 and 6.5.¹ These estimates are summed over frequency and include the frequency band from 19 to 35 Hz. An interesting point of comparison is the flatness of the background in the adaptive estimate; the absence of much of the fine structure that is present in the conventional estimate. The noise is white Gaussian and we are observing the reduced variance predicted in Chapter 5. The resolution along the time axis is comparable for both estimates, as we would expect from Figures 2.8 and 2.9. There is a notable increase in the velocity resolution in the MLM estimate, particularly for the deeper reflectors. The spectra for 6 channels of this same data (the even numbered channels, giving the same array length) are given in Figures 6.6 and 6.7. The results of the adaptive procedure applied to the 6 channel array are not quite as good as in the 12 channel estimate, but continue to be greatly improved over the conventional estimate.

Following the synthetic data studies, we turned our

¹ We note that most of our spectra plots are contoured at 6 dB intervals. These were plotted before we normalized the gain factors between the conventional and adaptive estimation programs, so we can only say that the levels are arbitrary. All the contours above an arbitrary level are shaded to aid in interpretation. The shading contour was chosen in each case to highlight the peaks.

Figure 6.4 Conventional Velocity/Depth Spectrum of
12 Channel Synthetic Data. 19-35 Hz.
6 dB contour levels.

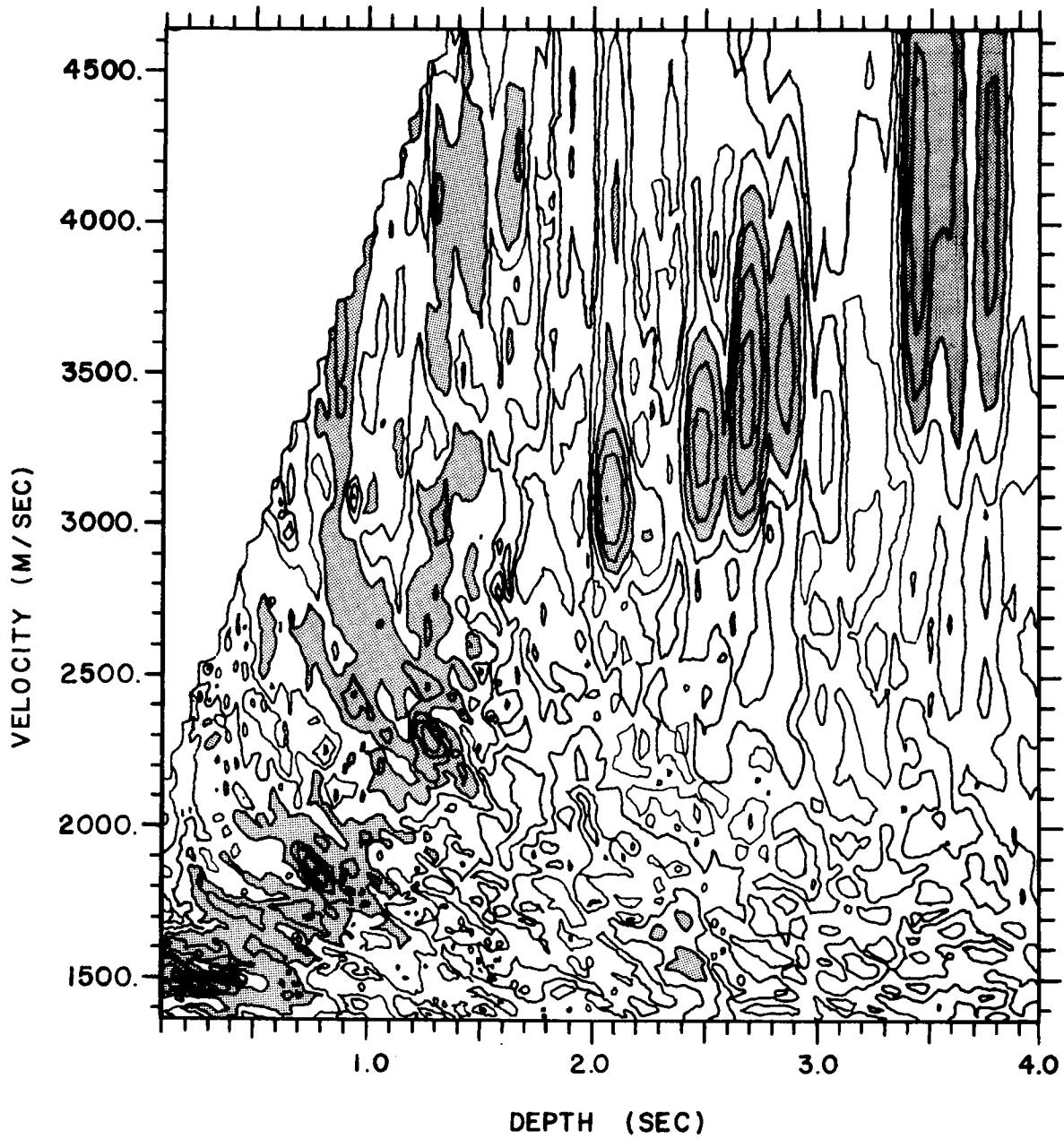


Figure 6.5 Data Adaptive Velocity/Depth Spectrum of
12 Channel Synthetic Data. 19-35 Hz.
6 dB contour levels.

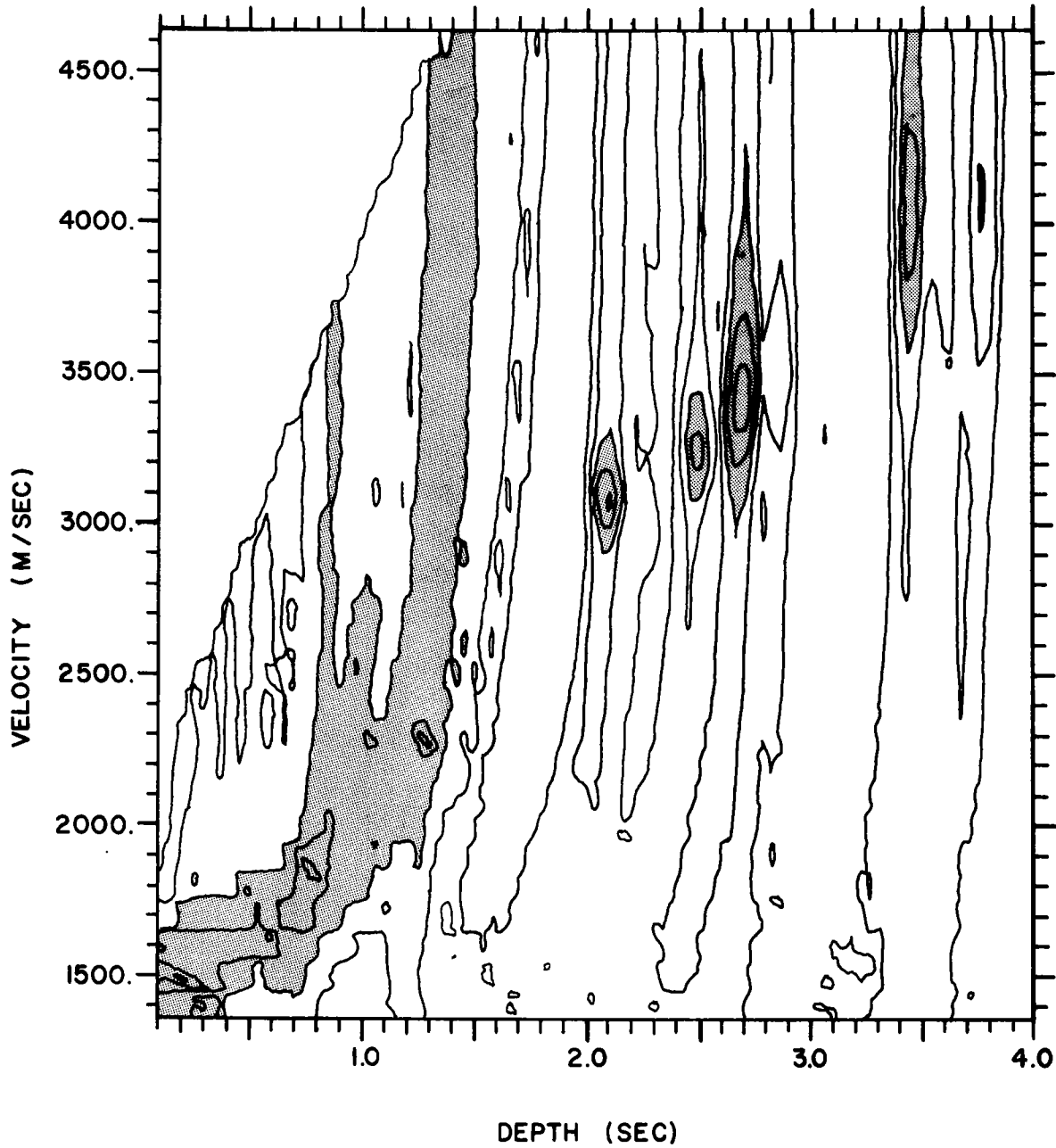


Figure 6.6 Conventional Velocity/Depth Spectrum of
6 Channel Synthetic Data. 19-35 Hz.
6 dB contour levels.

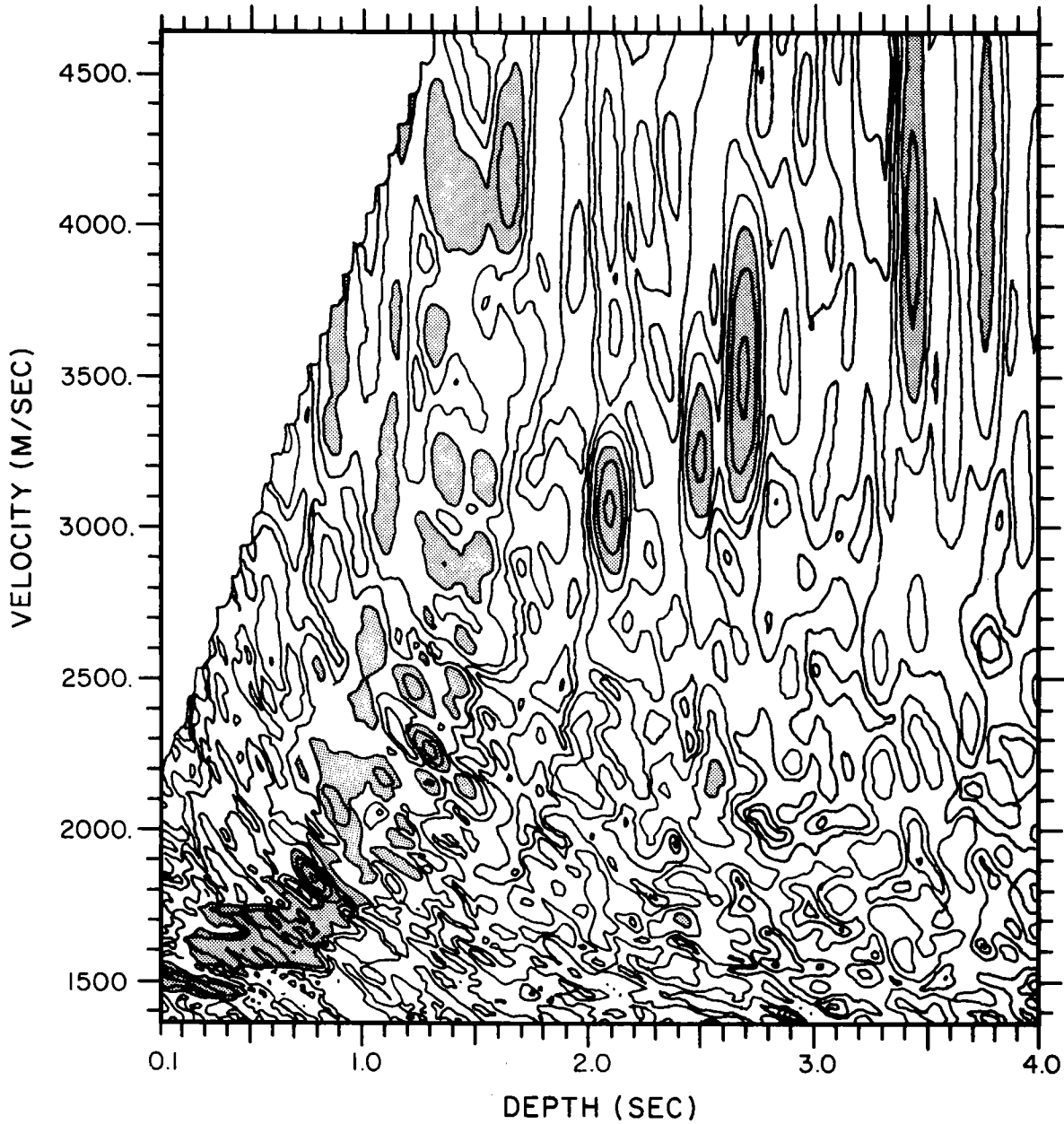
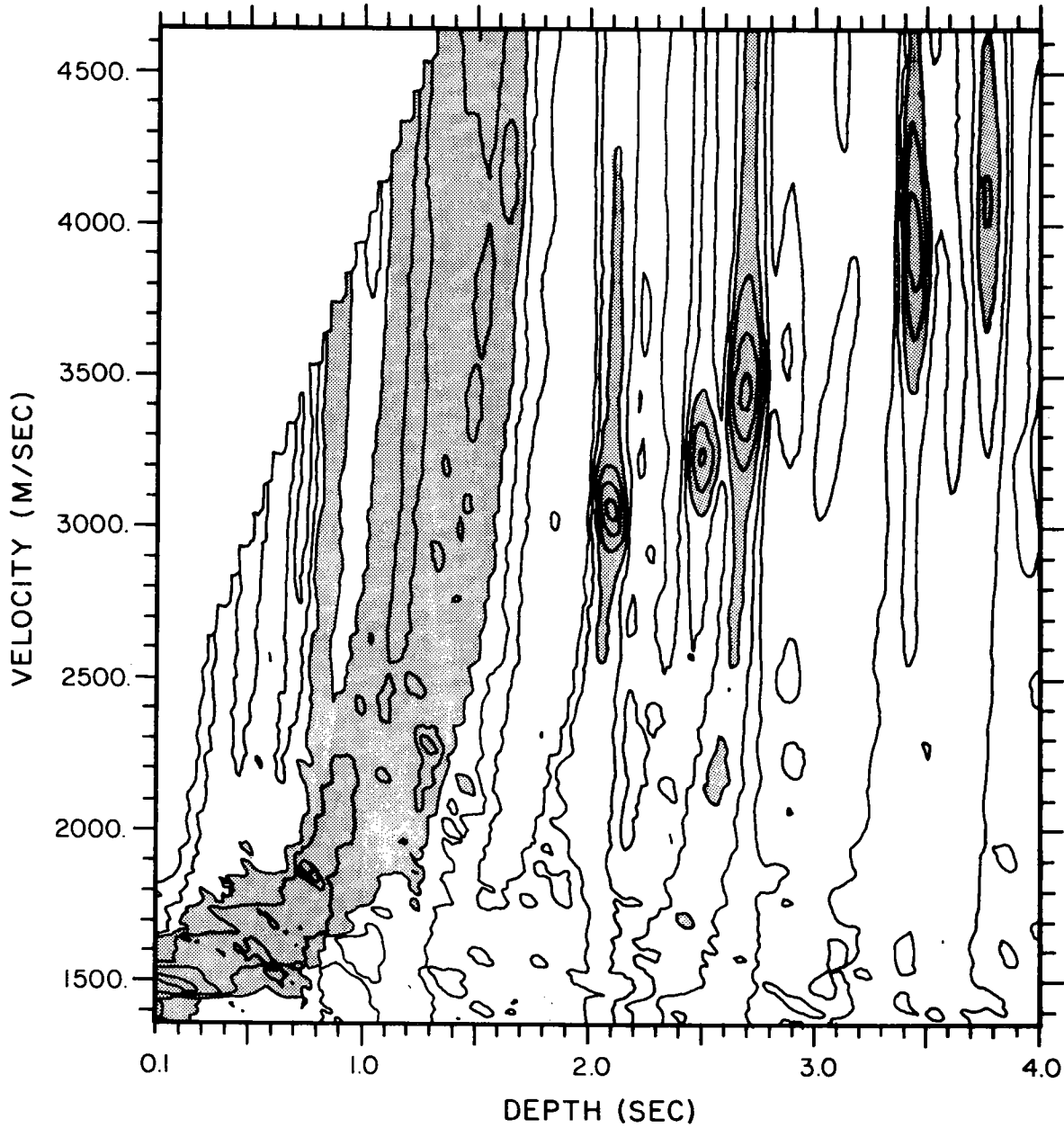


Figure 6.7 Data Adaptive Velocity/Depth Spectrum of
6 Channel Synthetic Data. 19-35 Hz.
6 dB contour levels.



attention to actual field data. The data is from the WHOI multi-channel system employing six channels at 150 meter spacings. The shot points are spaced at 37.5 meter intervals, so we would expect a fairly high correlation between adjacent gathers. The next four figures give the conventional and adaptive spectra of two consecutive common ground point gathers. Figures 6.8 and 6.9 give the conventional estimates, and Figures 6.10 and 6.11 give the adaptive estimates. We see the same reduction in sidelobe energy and flatness of spectrum that we observed in the synthetic data. Note the reflector at 0.85 seconds and 1800. meters per second that is virtually lost in the energy from the shallow refracted and direct arrivals in the conventional spectra. The higher resolution of the MLM allows it to discriminate between the direct and refracted returns and those returns fitting the RMS travel time model. Comparing the reflector at 1.7 seconds and 2400 meters per second in Figures 6.9 and 6.11, the adaptive estimate distinguishes between the reflector and a slower multiple, while the conventional estimate smears them together. Finally, the general stationarity of the data between adjacent gathers is an indication that we can further improve the estimate by averaging the covariance matrices.

Figure 6.8 Conventional Velocity/Depth Spectrum of
6 Channel Georges Bank Data. 19-35 Hz.
Shotpoint 300. 6 dB contour levels.

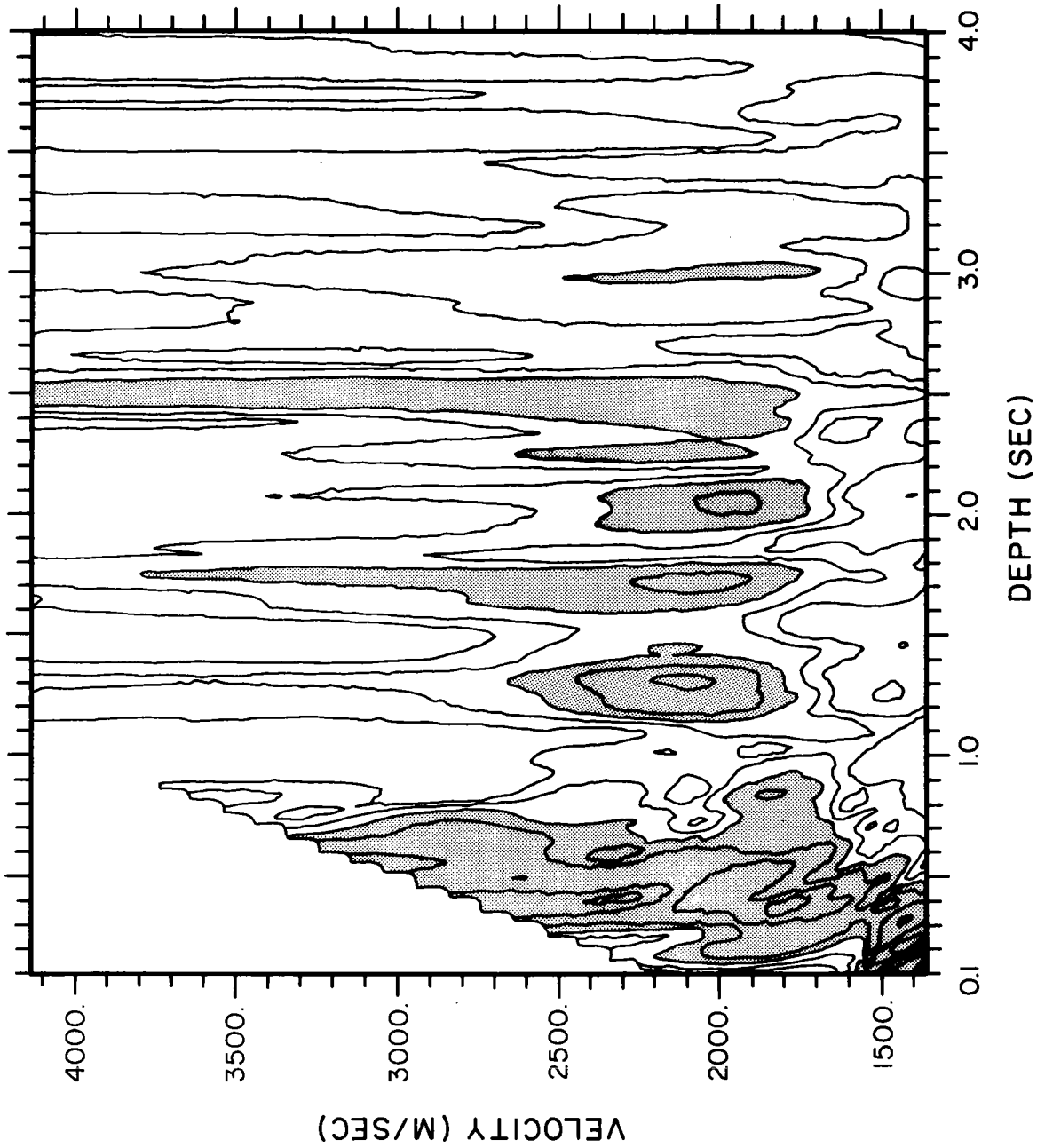


Figure 6.9 Conventional Velocity/Depth Spectrum of
6 Channel Georges Bank Data. 19-35 Hz.
Shotpoint 301. 6 dB contour levels.

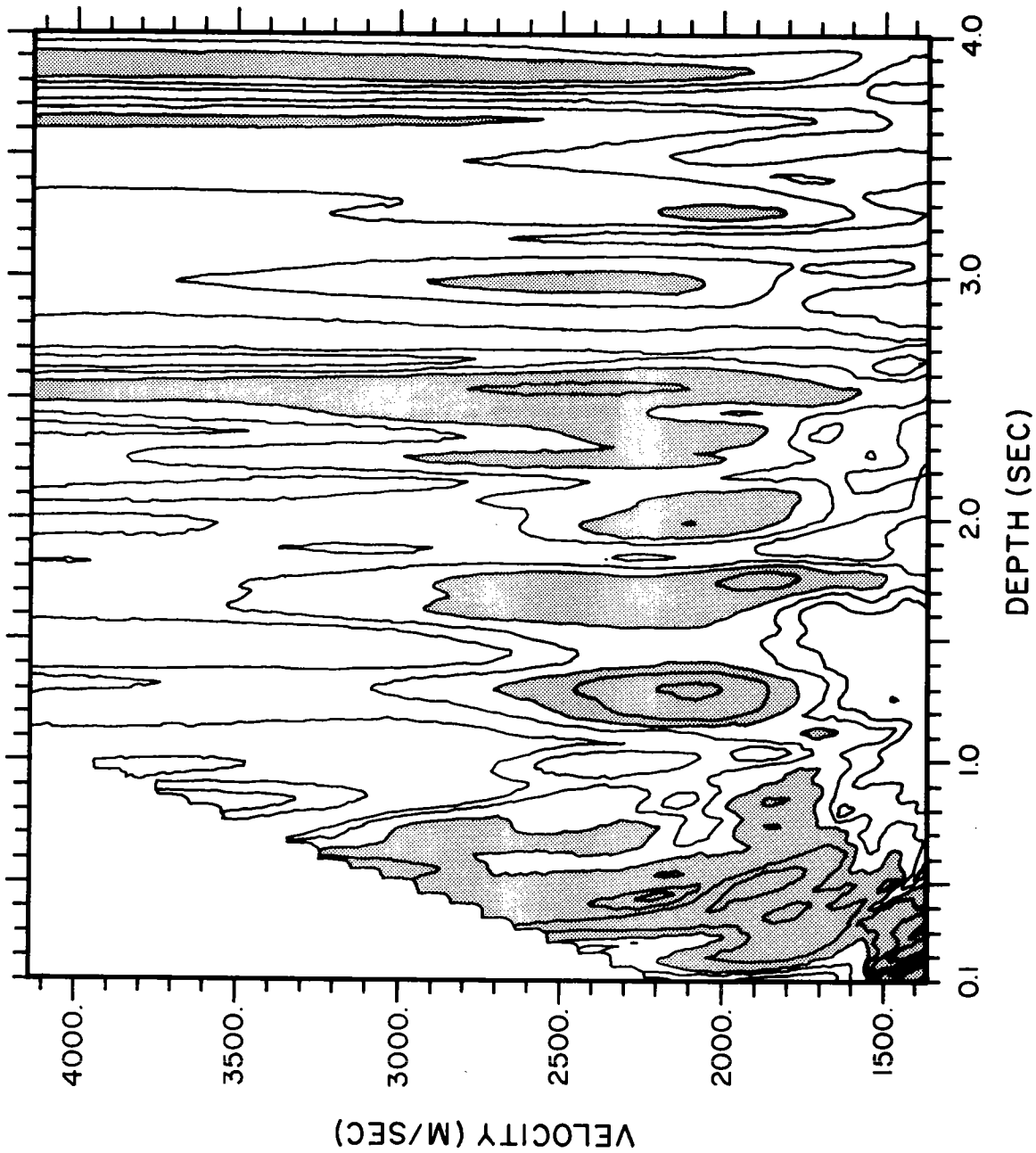


Figure 6.10 Data Adaptive Velocity/Depth Spectrum of
6 Channel Georges Bank Data. 19-35 Hz.
Shotpoint 300. 6 dB contour levels.

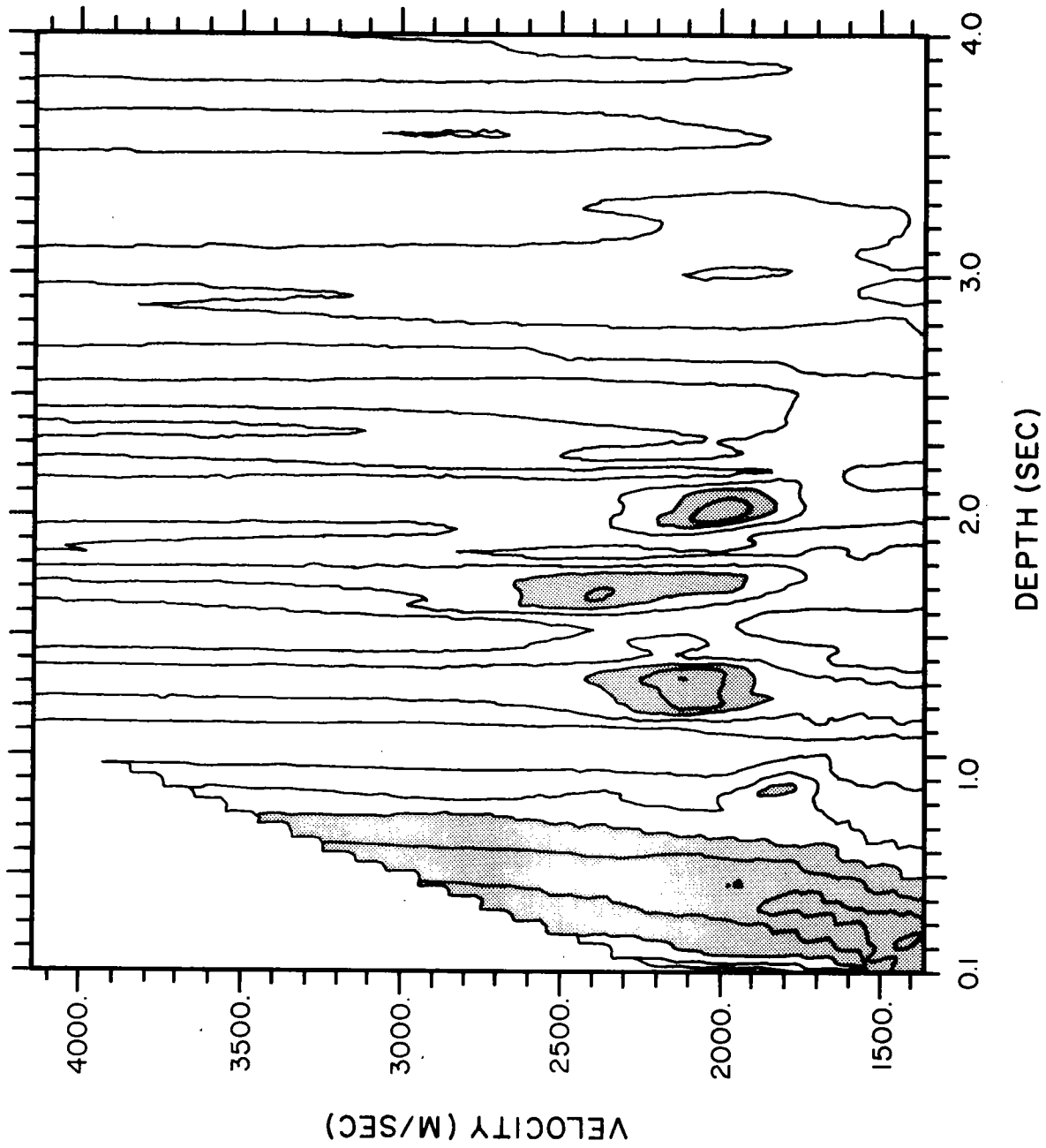
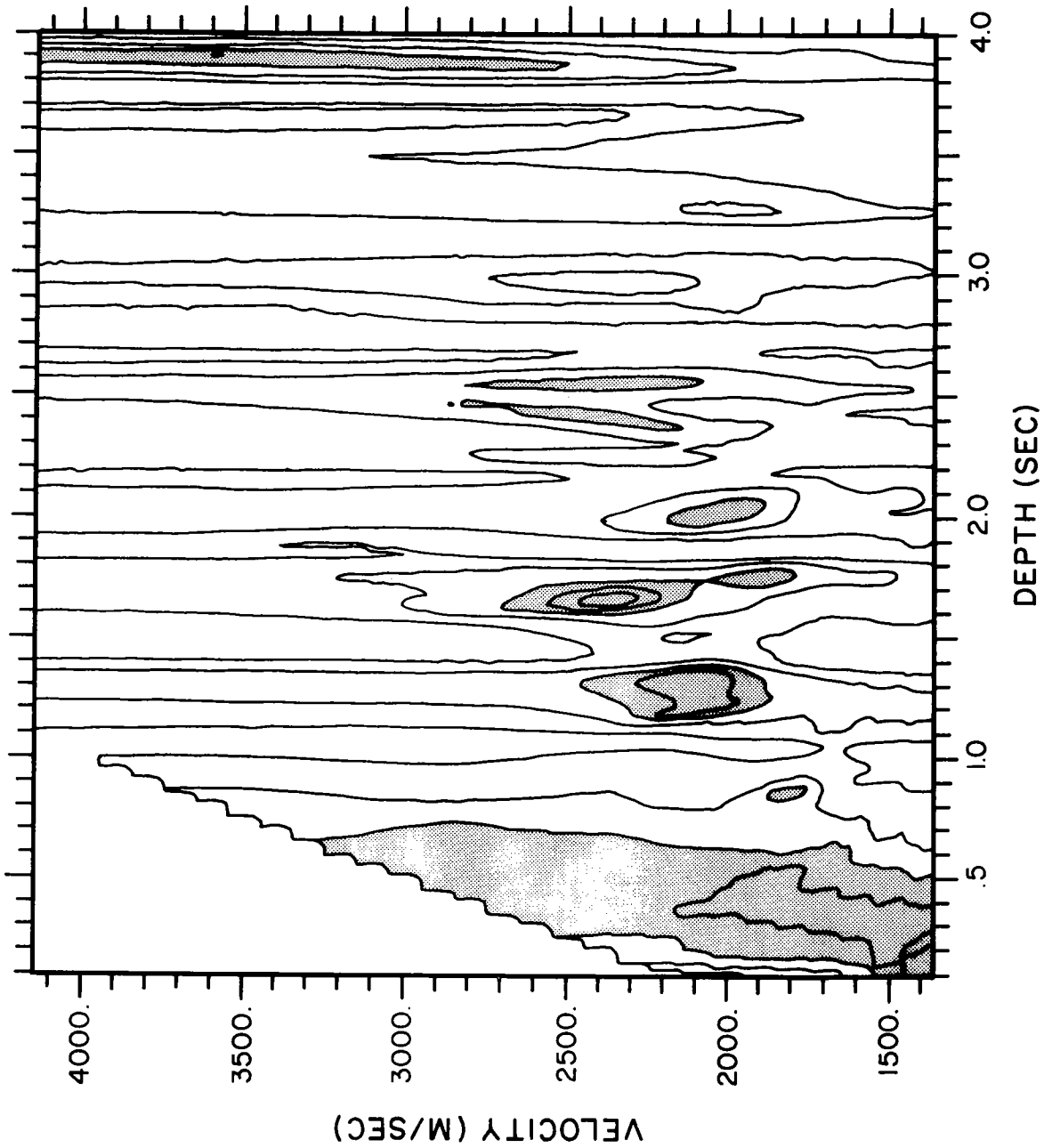


Figure 6.11 Data Adaptive Velocity/Depth Spectrum of
6 Channel Georges Bank Data. 19-35 Hz.
Shotpoint 301. 6 dB contour levels.



Another example of the improvements gained by use of the adaptive estimator is given in Figures 6.12 and 6.13. This is another WHOI 6 channel data set from Georges Bank. We again observe the same relative improvements of the MLM over the conventional estimate. Note that Figure 6.13 is plotted at 3 dB increments to bring out the structure of the spectrum. The energy from the direct and shallow refracted arrivals in the conventional estimate is greatly attenuated in the MLM spectrum. Two reflectors at 1.45 and 2.25 seconds and 2700 meters per second are greatly enhanced relative to slower velocity returns in the adaptive estimate. The velocity resolution of the reflector at 3.35 seconds and 3100 meters per second is significantly better in the adaptive estimate.

This same data also gives us a good example of the information partitioning as a function of frequency. The spectra in the previous six figures (6.8 - 6.13) have all been averaged over a 19 to 35 Hz frequency band. If we look at the estimates for each frequency component for shotpoint 1020 (Figure 6.13), we find that the different travel paths are highly frequency selective. Monochromatic MLM estimates for this shotpoint are given in Figures 6.14 through 6.18. Most of the multiple energy is in the higher frequencies of the band, and most of the penetrating primary energy is in the

Figure 6.12 Conventional velocity/depth spectrum of 6 channel Georges Bank data. 19-35 Hz. Shotpoint 1020. 6 dB contour levels.

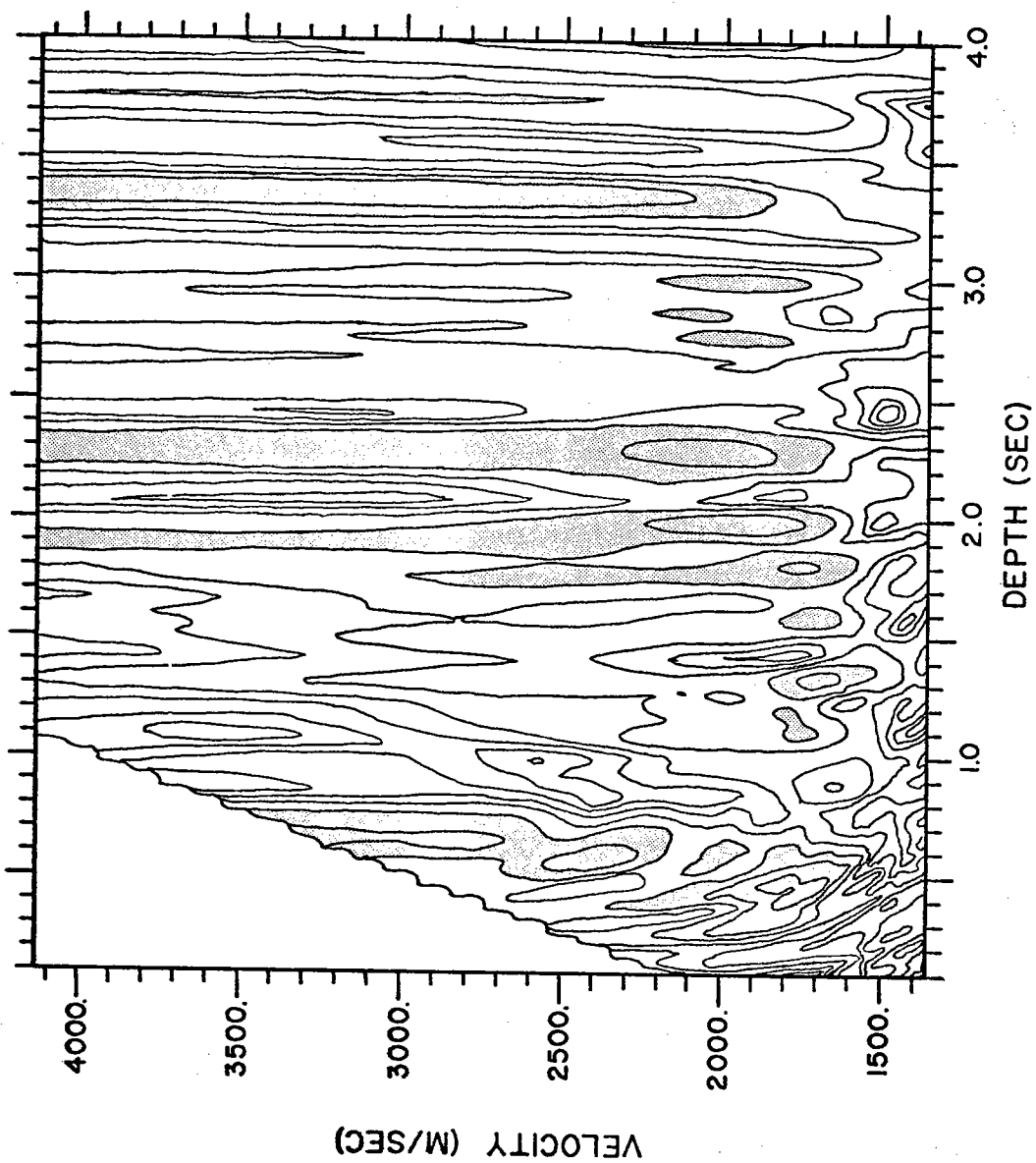


Figure 6.13 Data Adaptive velocity/depth spectrum of 6 channel Georges Bank data. 19-35 Hz. Shotpoint 1020. 3 dB contour levels.

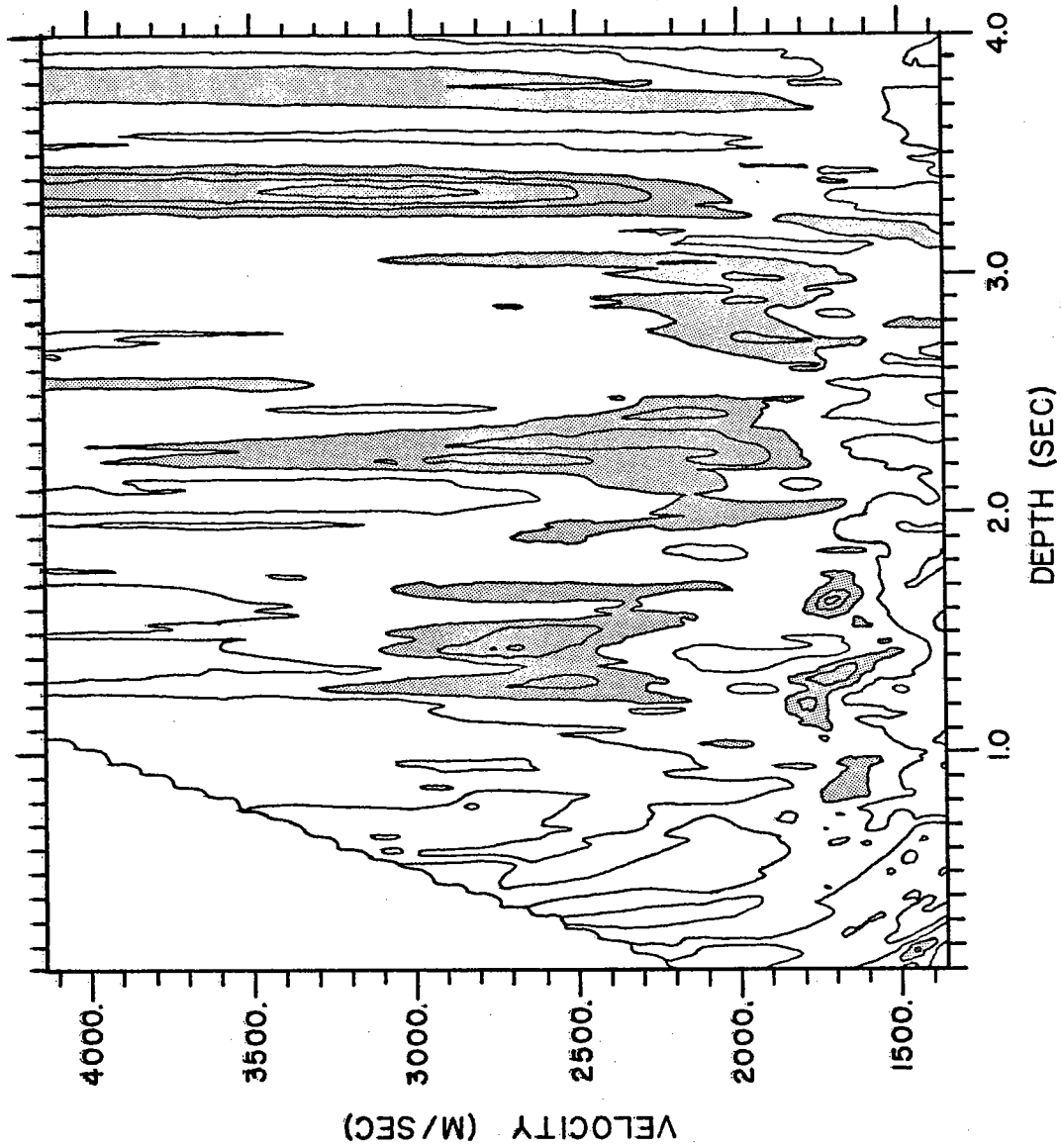


Figure 6.14 Adaptive Velocity/Depth Spectrum of 6 Channel Data. Frequency Breakdown of Shotpoint 1020. 19 HZ. 6 dB contour levels.

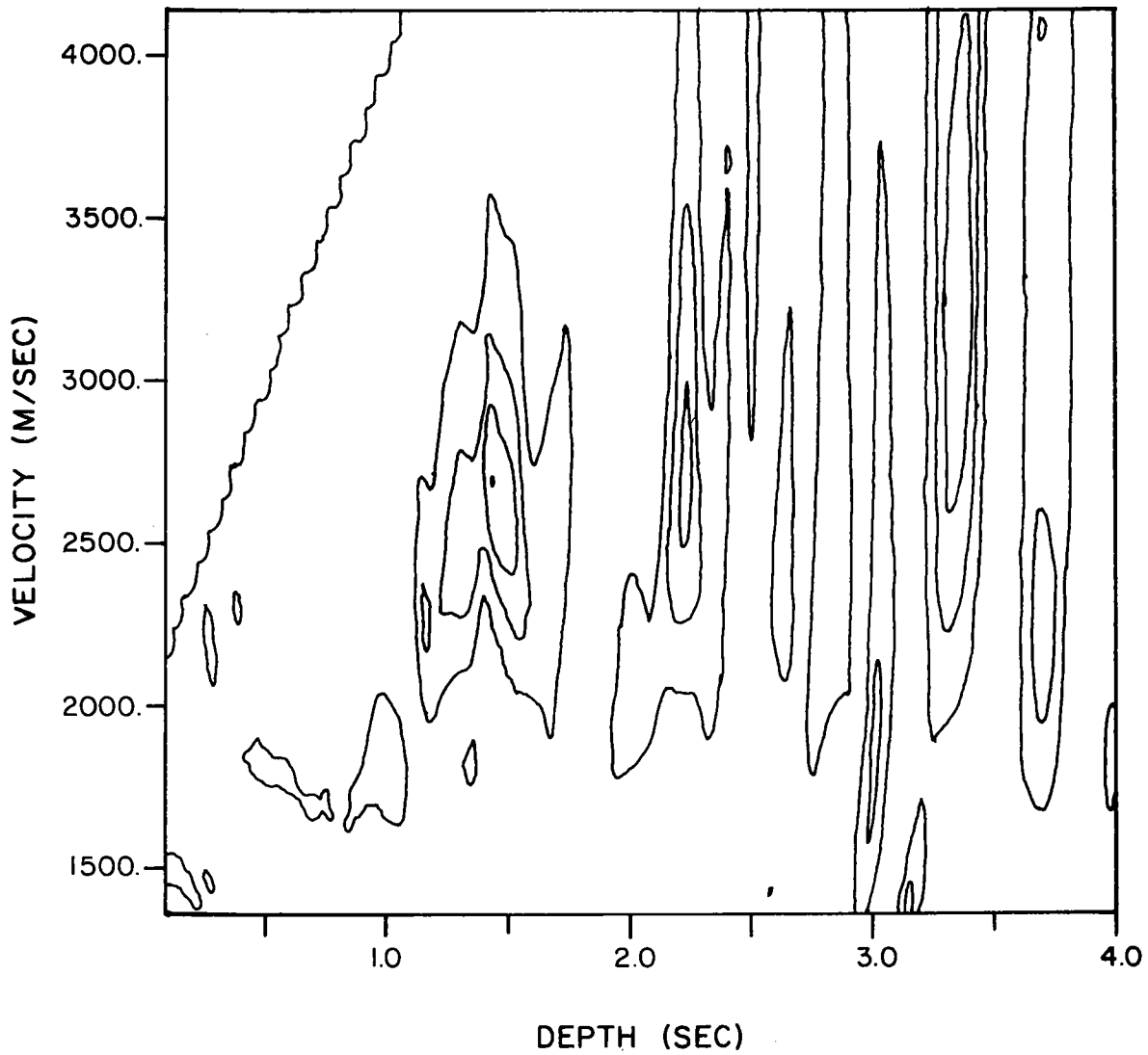


Figure 6.15 Adaptive Velocity/Depth Spectrum of 6 Channel Data. Frequency Breakdown of Shotpoint 1020. 23 Hz. 6 dB contour levels.

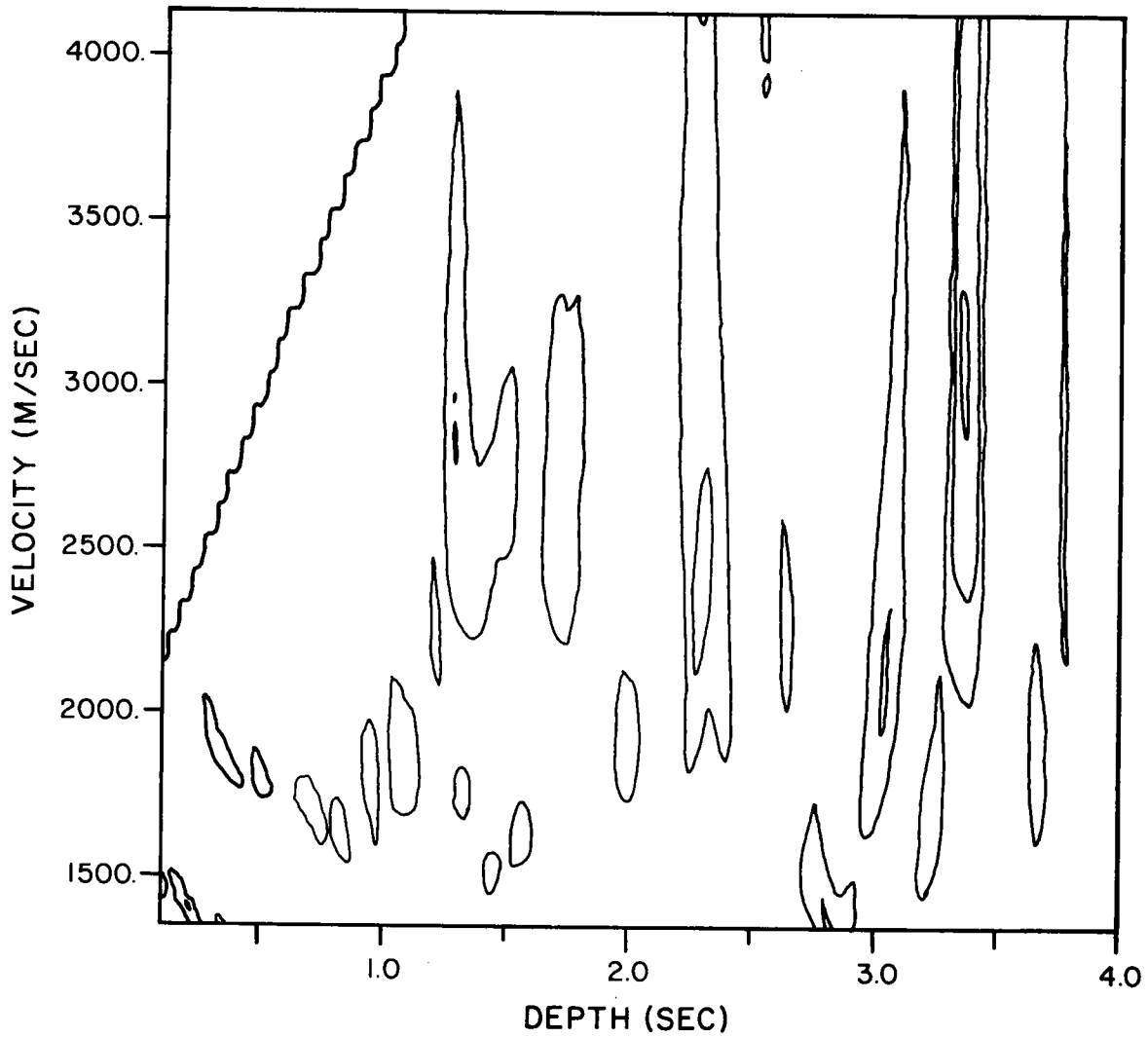


Figure 6.16 Adaptive Velocity/Depth Spectrum of 6 Channel Data. Frequency Breakdown of Shotpoint 1020. 27. Hz. 6 dB contour levels.

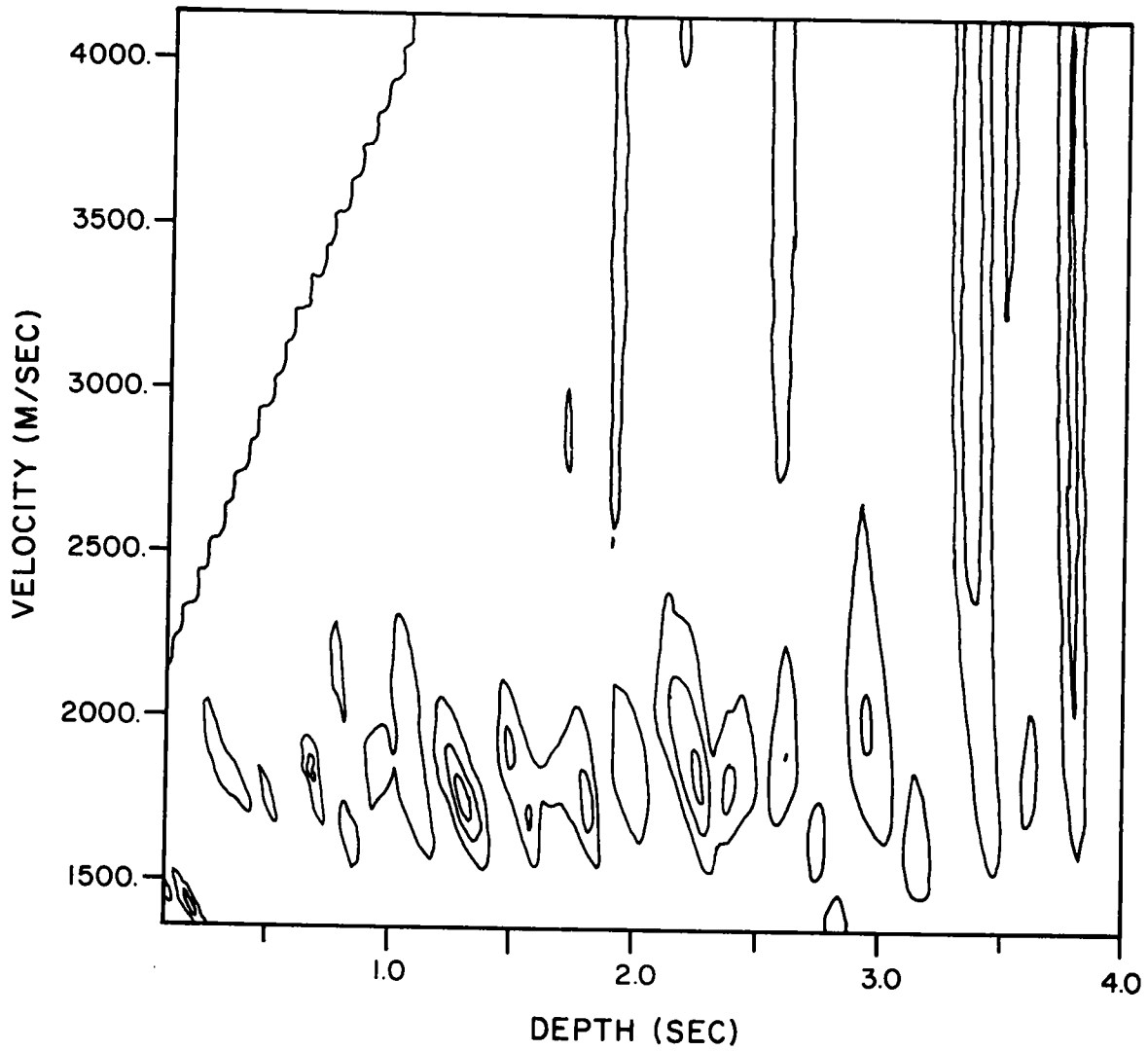


Figure 6.17 Adaptive Velocity/Depth Spectrum of 6 Channel Data. Frequency Breakdown of Shotpoint 1020. 31 Hz. 6 dB contour levels.

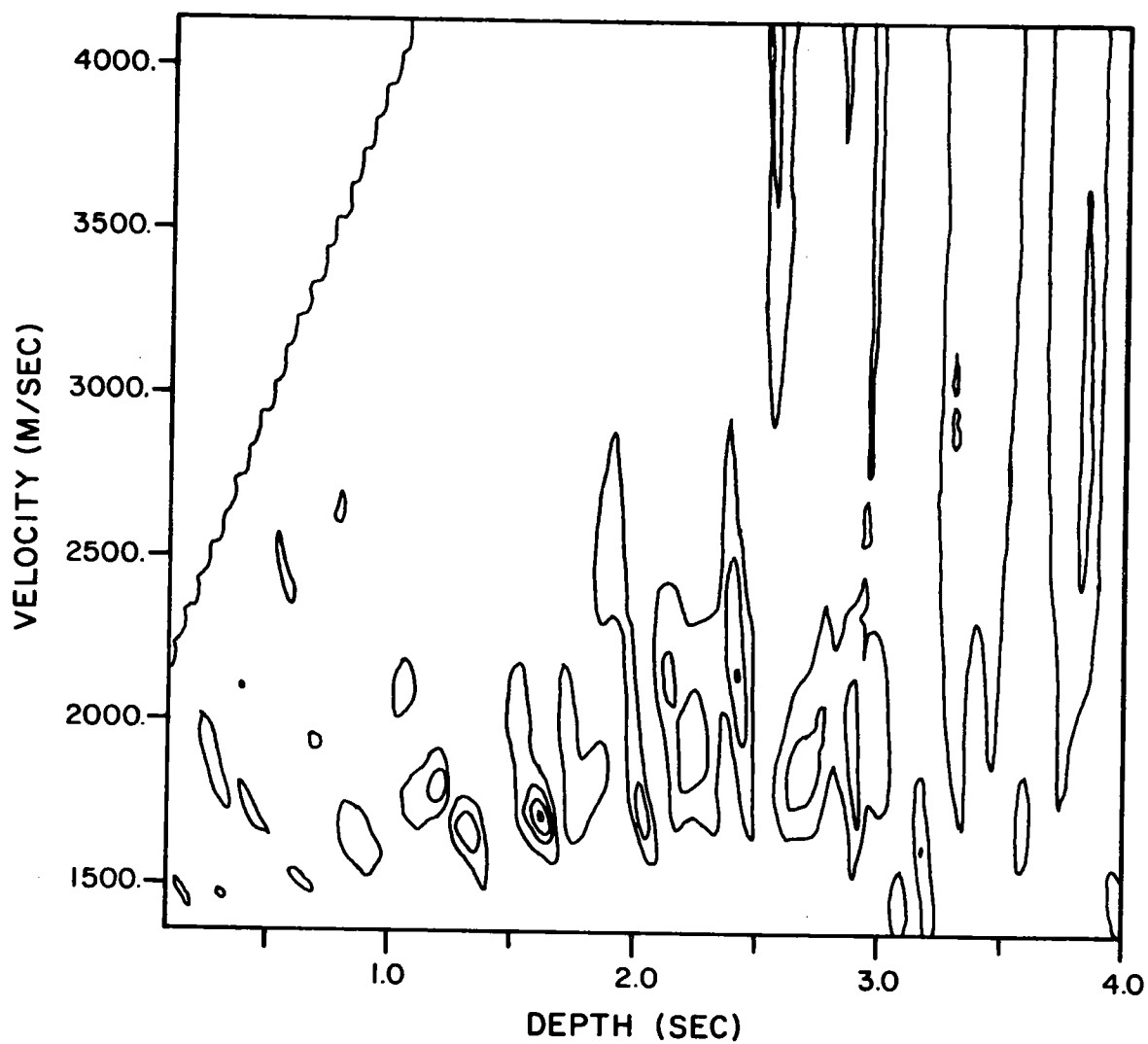
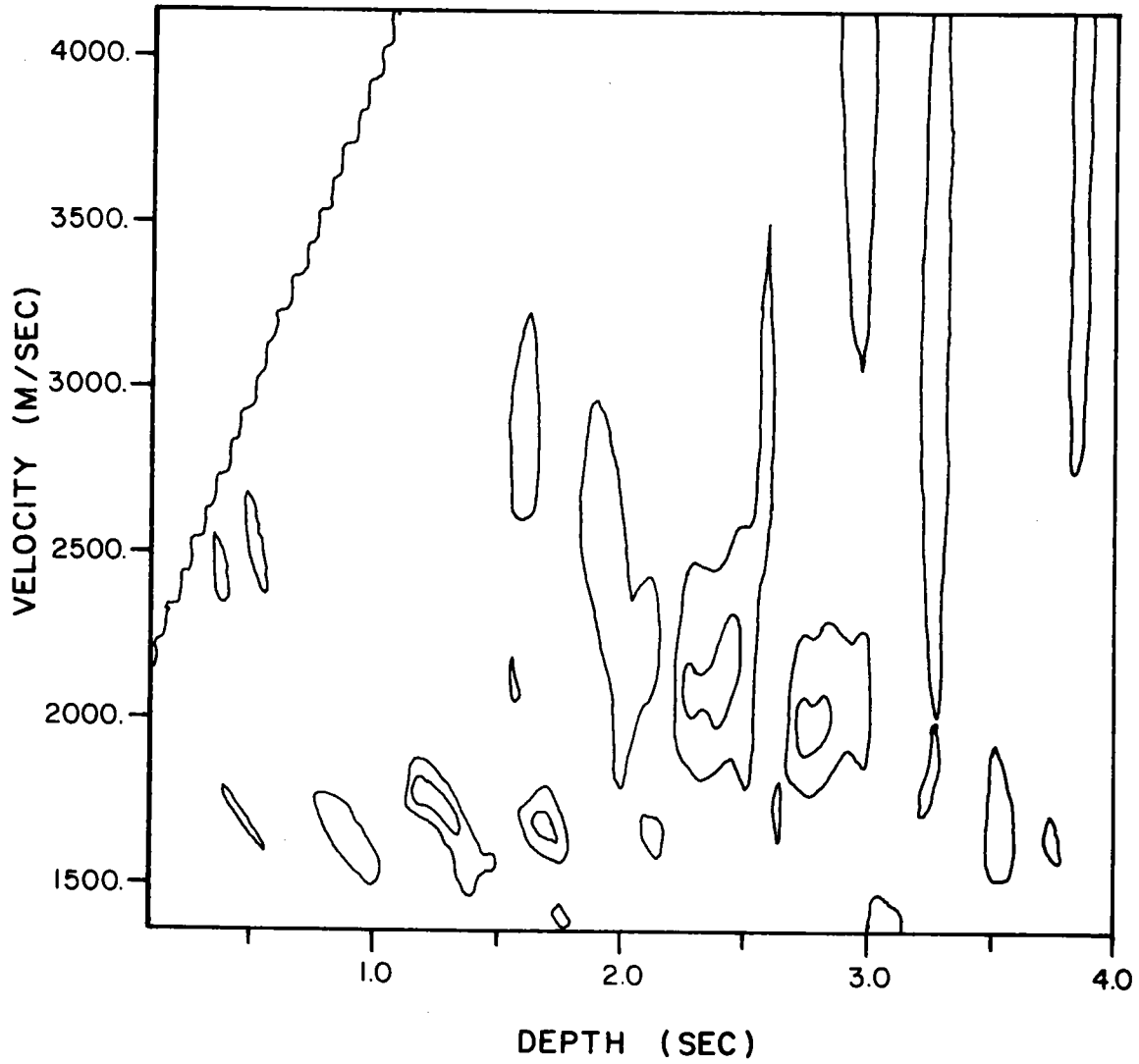


Figure 6.18 Adaptive Velocity/Depth Spectrum of 6 Channel Data. Frequency Breakdown of Shotpoint 1020. 35 Hz. 6 dB contour levels.



lower frequencies. This is indicative of the filtering done by the travel path medium, and points out the usefulness of working in the frequency domain for both the conventional and adaptive spectra estimates.

We can also use this data to demonstrate the effects of averaging over shots. The estimated spectra (MLM) for shotpoints 1021 and 1022 are given in Figures 6.19 and 6.20. A spectral estimate using shotpoints 1020 - 1022 in forming the covariance matrix is given in Figure 6.21. Some of the reflectors (1.25 seconds) are improved, while some (2.3 and 3.35 seconds) are degraded over the better of the single observation estimates.

Conclusions

We have seen how the Maximum Likelihood Method, when applied to velocity/depth spectra estimation, gives improved resolution of reflector parameters. The resolution in depth is determined by the windowing of the data, which is identical for both the conventional and MLM processors. The resolution in velocity is determined primarily by the coherent power estimate, and here the MLM introduces significant improvements. The improvement is dependent on the additive noise field, but is substantial for the synthetic and field data that we

Figure 6.19 Data Adaptive Velocity/Depth Spectrum of
6 Channel Georges Bank Data. 19-35 Hz.
Shotpoint 1021. 6 dB contour levels.

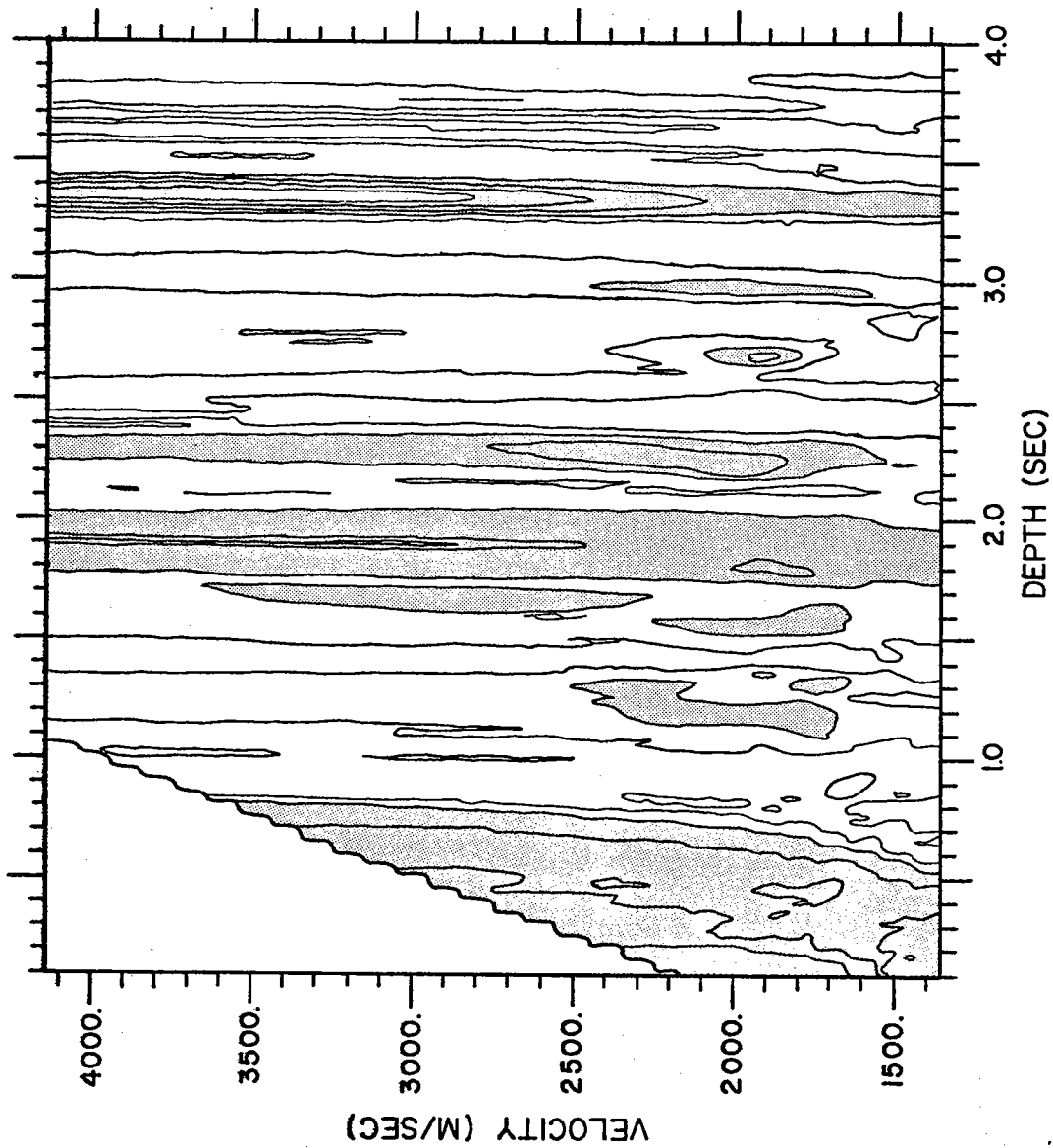


Figure 6.20 Data Adaptive Velocity/Depth Spectrum of
6 Channel Georges Bank Data. 19-35 Hz.
Shotpoint 1022. 6 dB contour levels.

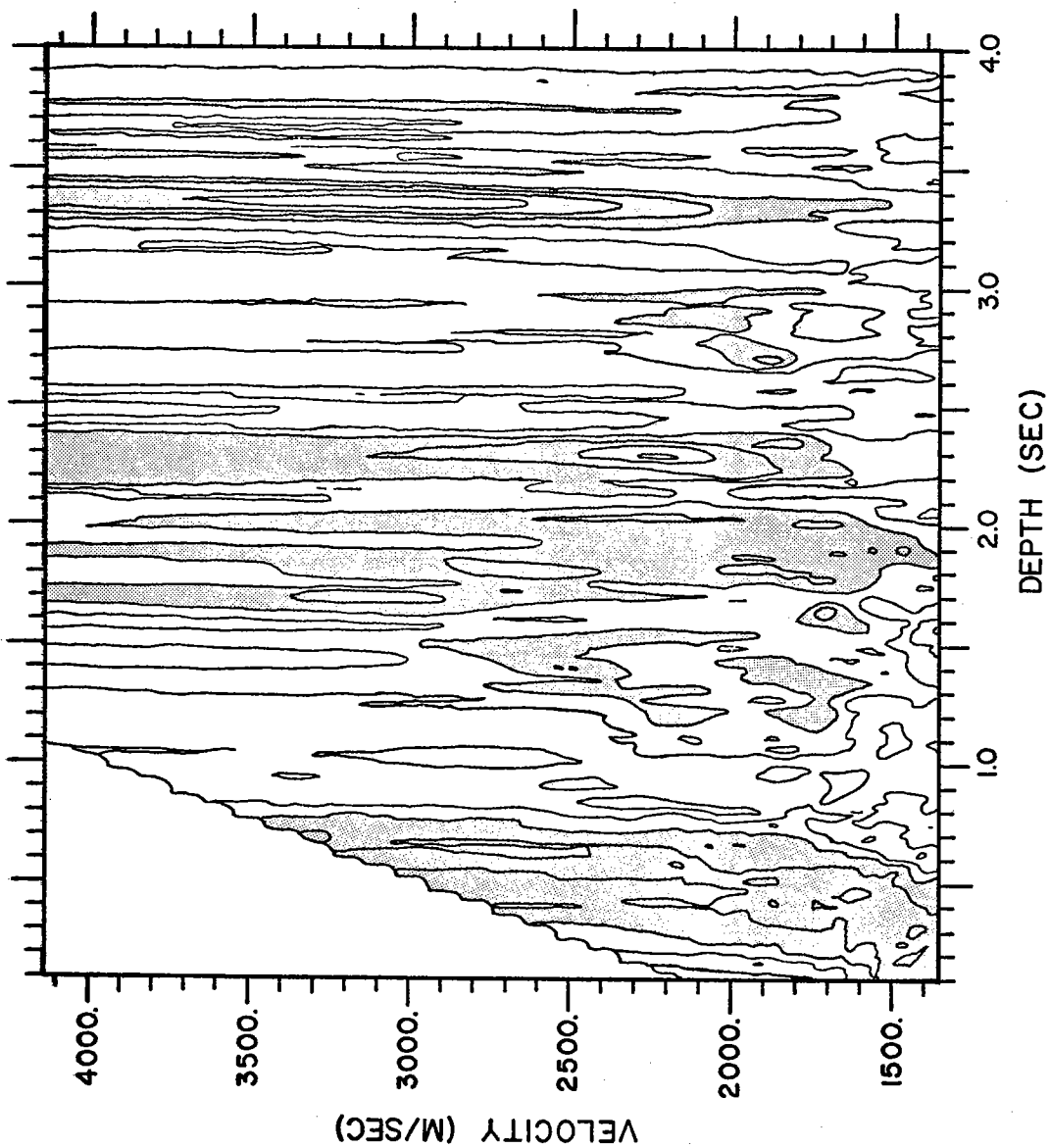
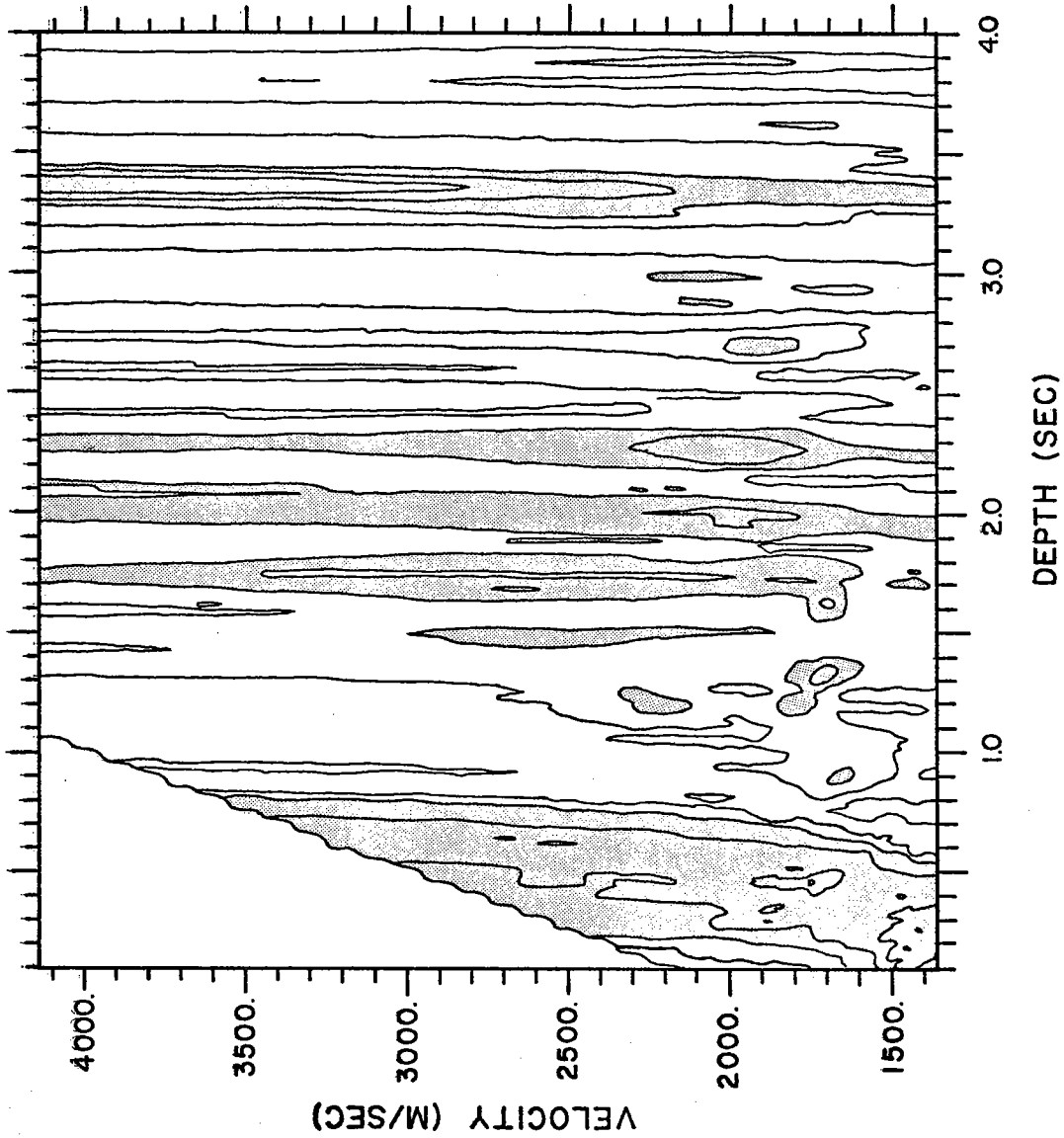


Figure 6.21 Data Adaptive Velocity/Depth Spectrum of
6 Channel Georges Bank Data. 19-35 Hz.
Shotpoints 1020-1022. 6 dB contour levels.



examined. The increased velocity resolution is of particular significance for deep returns where the array is approaching the limit of its near field geometry. Here the MLM can extend the practical operating range of the array.

We have identified two aspects of applying the estimator which are critical to its successful implementation. The windowing is an important, although subtle, aspect of the estimation procedure. Its dual role of transform window and arrival time detector creates a tradeoff between time and frequency resolution. The expected form of the signature and its frequency spectrum must be considered in resolving this tradeoff. In addition to the windowing, another critical area is the averaging of data. Here again we find tradeoffs, this time between the stability of the estimate and the ability to resolve reflectors that may be present in only one or few shots and/or frequencies.

In examining the statistics of the estimates, we have extended previous results to include our application, as well as derived the statistics for a new case; the single observation MLM estimate. A by-product of this is a new expression for the MLM estimator which promises to be a much faster algorithm to implement (Eq. 5.25). The MLM has a reduced

variance which is obtained at the expense of an increased bias. This bias can be controlled somewhat through the matrix whitening parameter. It is a direct consequence of the higher resolution of the adaptive estimator, and is not a severe problem if the whitening parameter is adjusted to suit the data.

In concluding, the advantages of applying the MLM estimator are primarily in the resolution of velocity, both when distinguishing between multiples and primaries and at the limit of the array's operating range. The method allows the use of shorter and sparser arrays to obtain results equivalent to a conventional analysis, and hence reduces operating and processing costs. On the other hand, it resolves reflectors that would not be resolvable with the conventional analysis for a given data set.

Appendix I Development of a simplified expression for the mean square error of the Fourier transform due to windowing of the time series.

The error is given by Equation 4.5

$$E(f) = \int_{-\infty}^{\infty} \left[\Delta(t-\tau_d) \{w(t-\tau_w) - 1\} + n(t) w(t-\tau_w) \right] e^{j2\pi ft} dt \quad 4.5$$

If we square this and take the expected value, we have

$$\begin{aligned} \overline{|E(f)|^2} = & \int_{-\infty}^{\infty} \int_{-\infty}^{\infty} \left\{ E[\Delta(t_1-\tau_d) \Delta(t_2-\tau_d)] \{w(t_1-\tau_w) - 1\} \{w(t_2-\tau_w) - 1\} \right. \\ & \left. + E[n(t_1) n(t_2)] w(t_1-\tau_w) w(t_2-\tau_w) \right\} e^{j2\pi f(t_1-t_2)} dt_1 dt_2, \end{aligned} \quad \text{AI.1}$$

noting that the cross terms drop out because we have assumed $\Delta(t)$ and $n(t)$ independent. We can rewrite the expected value terms as autocorrelation functions.

$$E[\Delta(t_1-\tau_d) \Delta(t_2-\tau_d)] = a(t_1-\tau_d) R_x(t_1-t_2) a(t_2-\tau_d) \quad \text{AI.2a}$$

$$E[n(t_1) n(t_2)] = R_n(t_1-t_2) \quad \text{AI.2b}$$

We can write the autocorrelation function as the inverse transform of the frequency spectrum.

$$R(t_1 - t_2) = \int S(\nu) e^{j2\pi\nu(t_1 - t_2)} d\nu$$

AI.3

Substituting this into Equation AI.1, we have

$$\begin{aligned} \overline{|E(f)|^2} &= \int d\nu S_x(\nu) \int dt_1 \int dt_2 a(t_1 - \tau_d) a(t_2 - \tau_d) * \\ &\quad \{w(t_1 - \tau_w) - 1\} \{w(t_2 - \tau_w) - 1\} e^{-j2\pi(f - \nu)(t_1 - t_2)} \\ &\quad + \int d\nu S_n(\nu) \int dt_1 \int dt_2 w(t_1 - \tau_w) w(t_2 - \tau_w) e^{-j2\pi(f - \nu)(t_1 - t_2)} \end{aligned}$$

AI.4

The integrations in t_1 and t_2 factor and are complex conjugates of each other.

$$\begin{aligned} \overline{|E(f)|^2} &= \int d\nu S_x(\nu) \left| \int dt a(t - \tau_d) \{w(t - \tau_w) - 1\} e^{j2\pi(f - \nu)t} \right|^2 \\ &\quad + \int d\nu S_n(\nu) \left| \int dt w(t - \tau_w) e^{-j2\pi(f - \nu)t} \right|^2 \end{aligned}$$

AI.5

If we now assume that S_x and S_n are approximately constant for $(f - \nu)$ small; i.e., within the bandwidths of the squared quantities, we can take them out of the integral and we get

$$\begin{aligned} \overline{|E(f)|^2} &= S_x(f) \int d\nu \left| \int dt a(t-\tau_a) \{w(t-\tau_w)-1\} e^{-j2\pi(f-\nu)t} \right|^2 \\ &+ S_n(f) \int d\nu \left| \int dt w(t-\tau_w) e^{-j2\pi(f-\nu)t} \right|^2 \end{aligned} \quad \text{AI.6}$$

Letting

$$g(t) = a(t-\tau_a) \{w(t-\tau_w)-1\} \quad \text{AI.7a}$$

and

$$h(t) = w(t-\tau_w) \quad \text{AI.7b}$$

we have

$$G(f-\nu) = \int g(t) e^{-j2\pi(f-\nu)t} dt \quad \text{AI.8a}$$

and

$$H(f-\nu) = \int h(t) e^{-j2\pi(f-\nu)t} dt \quad \text{AI.8b}$$

Substituting this into Equation AI.6, we then have

$$\overline{|E(f)|^2} = S_x(f) \int d\nu |G(f-\nu)|^2 + S_n \int d\nu |H(f-\nu)|^2$$

AI.9

From Parseval's theorem we have

$$\int d\nu \left| G(f-\nu) \right|^2 = \int d\nu \left| G(\nu) \right|^2 = \int dt \left| g(t) \right|^2 \quad \text{AI.10a}$$

$$\int d\nu \left| H(f-\nu) \right|^2 = \int d\nu \left| H(\nu) \right|^2 = \int dt \left| h(t) \right|^2 \quad \text{AI.10b}$$

Substituting AI.10 into AI.9, we finally obtain

$$\begin{aligned} \overline{|E(f)|^2} &= S_x(f) \int dt \left(a(t-\tau_d) \{ w(t-\tau_w) - 1 \} \right)^2 \\ &\quad + S_n(f) \int dt \left(w(t-\tau_w) \right)^2 \\ \overline{|E(f)|^2} &= S_x(f) \int dt \left[a(t) \{ w(t-\Delta\tau) - 1 \} \right]^2 \\ &\quad + S_n(f) \int dt w^2(t) \quad \text{AI.11} \end{aligned}$$

Appendix II Derivation of simplified expressions for estimators using one observation of the data set.

The two estimators are

$$P_c = \frac{1}{N^2} [\underline{E}^t \hat{R} \underline{E}] \quad \text{AII.1}$$

and

$$P_{MLM} = [\underline{E}^t \hat{R}^{-1} \underline{E}]^{-1} \quad \text{AII.2}$$

with

$$\hat{R} = \underline{Y} \underline{Y}^t + \beta \underline{I} \quad \text{AII.3}$$

and

$$\underline{E}^t \underline{E} = N \quad \text{AII.4}$$

We have

$$\hat{R}^{-1} = \frac{1}{\beta} \underline{I} - \frac{\underline{Y} \underline{Y}^t}{\beta^2 + \beta \sum_{i=1}^N \underline{Y}_i \underline{Y}_i} \quad \text{AII.5}$$

Multiplying out the conventional estimator and gathering the terms in summations, we have

$$\begin{aligned} P_c &= \frac{1}{N^2} \sum_{i=1}^N E_i^* \beta E_i + \frac{1}{N^2} \sum_{i=1}^N \sum_{j=1}^N E_i^* \underline{Y}_i \underline{Y}_j^* E_j \\ &= \frac{\beta}{N} + \frac{1}{N^2} \sum_{i=1}^N \sum_{j=1}^N E_i^* \underline{Y}_i \underline{Y}_j^* E_j \end{aligned} \quad \text{AII.6}$$

The MLM estimator becomes

$$\begin{aligned}
 P_{MLM} &= \left[\frac{1}{\beta} E^t I E - \frac{E^t Y Y^t E}{\beta^2 + \beta \sum_{i=1}^N Y_i Y_i^*} \right]^{-1} \\
 &= \left[\frac{N}{\beta} - \frac{\sum_{i=1}^N \sum_{j=1}^N E_i^* Y_i Y_j^* E_j}{\beta^2 + \beta \sum_{i=1}^N Y_i Y_i^*} \right]^{-1} \\
 &= \left[\frac{N\beta + N \sum_{i=1}^N Y_i Y_i^* - \sum_{i=1}^N \sum_{j=1}^N E_i^* Y_i Y_j^* E_j}{\beta^2 + \beta \sum_{i=1}^N Y_i Y_i^*} \right]^{-1} \\
 P_{MLM} &= \frac{\beta^2 + \beta \sum_{i=1}^N Y_i Y_i^*}{N\beta + N \sum_{i=1}^N Y_i Y_i^* - \sum_{i=1}^N \sum_{j=1}^N E_i^* Y_i Y_j^* E_j}
 \end{aligned}$$

AII-7

Since $E_i E_i^* = 1$, we can make the substitutions

$$A_i = E_i^* Y_i \quad \text{AII.8a}$$

$$A_i A_i^* = Y_i Y_i^* \quad \text{AII.8b}$$

This gives us

$$P_c = \frac{\beta}{N} + \frac{1}{N^2} \sum_{i=1}^N \sum_{j=1}^N A_i A_j^* \quad \text{AII.9}$$

$$P_{MLM} = \frac{\beta^2 + \beta \sum_{i=1}^N A_i A_i^*}{N\beta + N \sum_{i=1}^N A_i A_i^* - \sum_{i=1}^N \sum_{j=1}^N A_i A_j^*} \quad \text{AII.10}$$

We can further simplify P_{MLM} with the following two identities.

$$\sum A_i A_i^* = \sum |A_i|^2 \quad \text{AII.11a}$$

and

$$\sum \sum A_i A_j^* = \left| \sum A_i \right|^2 \quad \text{AII.11b}$$

We also make use of a simple theorem.

Theorem I

$$\sum x_i^2 = \sum (x_i - \bar{x})^2 + \frac{1}{N} \left(\sum x_i \right)^2 \quad \text{AII.12a}$$

$$\text{where } \bar{x} = \frac{1}{N} \sum x_i \quad \text{AII.12b}$$

Proof:

$$\begin{aligned} \sum_i^N (x_i - \bar{x})^2 &= \sum_i^N (x_i^2 - 2\bar{x}x_i + \bar{x}^2) \\ &= \sum_i^N x_i^2 - 2\bar{x} \sum x_i + N\bar{x}^2 \end{aligned}$$

$$\sum (x_i - \bar{x})^2 = \sum x_i^2 - \frac{1}{N} \left(\sum x_i \right)^2 \quad \text{Q.E.D.}$$

Applying the identities, we have

$$P_{MLM} = \frac{\beta + \sum_{i=1}^N |A_i|^2}{N + \frac{N}{\beta} \sum_{i=1}^N |A_i|^2 - \frac{1}{\beta} \left| \sum_{i=1}^N A_i \right|^2} \quad \text{AII.13}$$

Applying Theorem I to this result, we then obtain

$$P_{MLM} = \frac{\beta + \sum |A_i - \bar{A}|^2 + \frac{1}{N} \left| \sum A_i \right|^2}{N \left(1 + \frac{1}{\beta} \sum |A_i - \bar{A}|^2 \right)}$$

$$P_{MLM} = \frac{\frac{\beta}{N} + \frac{\frac{1}{N} \left| \sum_{i=1}^N A_i \right|^2}{N + \frac{N}{\beta} \left| A_i - \bar{A} \right|^2}}{\quad} \quad \text{AII.14}$$

We define two new variables

$$\Theta = \frac{1}{N} \sum |A_i - \bar{A}|^2 \quad \text{AII.15a}$$

$$\Psi = \left| \frac{\sum A_i}{N} \right|^2 \quad \text{AII.15b}$$

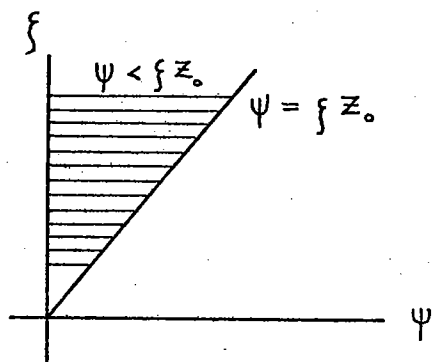
Substituting into the two estimator forms, we finally obtain

$$P_c = \frac{\beta}{N} + \psi \quad \text{AII.16}$$

$$P_{MLM} = \frac{\beta}{N} + \frac{\psi}{1 + \frac{N}{\beta} \Theta} \quad \text{AII.17}$$

Appendix III Derivation of the probability density function of $z = (\psi/\xi)$.

Both ψ and ξ are constrained to be positive. We are therefore limited to the first quadrant in the ψ - ξ plane. We first calculate the cumulative distribution function $F_z(z < z_0)$.



$$\psi = \xi z$$

$$F_z(z < z_0) = \int_1^{\infty} d\xi \int_0^{\xi z_0} d\psi f_{\xi, \psi}(\xi, \psi) \quad \text{AIII.1}$$

Differentiating with respect to z_0 , we obtain the density function

$$f_z = \frac{d}{dz_0} F_z \Big|_{z_0=z} = \int_1^{\infty} d\xi \xi f_{\xi, \psi}(\xi, \xi z) \quad \text{AIII.2}$$

The joint density function $f_{\xi, \psi}$ is simply the product of f_{ξ} and f_{ψ} .

$$f_{\xi, \psi} = \left(\frac{\beta}{2\sigma_Y^2}\right)^{\frac{N-1}{2}} \frac{e^{\frac{\beta - N\delta^2}{2\sigma_Y^2}}}{2\sqrt{\frac{2\pi}{N}} \Gamma\left(\frac{N-1}{2}\right)} \Psi^{-\frac{1}{2}} (\xi-1)^{\frac{N-3}{2}} e^{-\frac{\beta\xi + N\psi}{2\sigma_Y^2}} \\ \times \left[e^{\frac{N\delta\sqrt{\psi}}{\sigma_Y^2}} + e^{-\frac{N\delta\sqrt{\psi}}{\sigma_Y^2}} \right] U(\xi-1) U(\psi)$$

AIII.3

Substituting this into Eq. AIII.2, we then obtain an integral expression for the density function.

$$f_z(z) = \Omega z^{-\frac{1}{2}} \int_1^{\infty} \xi^{\frac{1}{2}} (\xi-1)^{\frac{N-3}{2}} e^{-\xi\left(\frac{\beta + Nz}{2\sigma_Y^2}\right)} \cosh\left(\frac{N\delta\sqrt{z\xi}}{\sigma_Y^2}\right) d\xi$$

AIII.4

$$\Omega = \left(\frac{\beta}{2\sigma_Y^2}\right)^{\frac{N-1}{2}} \frac{e^{\frac{\beta - N\delta^2}{2\sigma_Y^2}}}{\sqrt{\frac{2\pi}{N}} \Gamma\left(\frac{N-1}{2}\right)}$$

This does not appear to be solvable in closed form. For the case of $\delta=0$ it reduces to a form of confluent hypergeometric function.

Glossary of Notations and Symbols

Notations

- \cdot^* Complex conjugate.
- \cdot^\dagger Complex conjugate transpose.
- \cdot^T Transpose.
- \sim Is distributed as.
- $\underline{\cdot}$ Vector or matrix quantity.
- $\hat{\cdot}$ Estimated quantity.
- $\underline{[x_i]}$ Vector or Matrix with elements x_i .

Symbols

$a(t)$	Envelope for stochastic signal model.
\underline{A}	Array element gains for adaptive processor (2). Steered data vector (5).
A_i	Coefficients for series expansion of travel time (1).
β	Matrix whitening parameter - quantity added to diagonal elements
γ	Uniform signal magnitude for simplified statistics.
$\Gamma(\cdot)$	Complete gamma function.
C, C_i	Seismic velocity within (i^{th}) layer.
\bar{C}	RMS velocity.
d	Array spacing (3).
D	Depth of first layer (1).
ΔT	Difference in position of window and position of center of desired signal (4).
E_i	Steering phase for i^{th} channel.
$\underline{E}, \underline{E}(f), \underline{E}(T, \bar{C}; f)$	Steering vector of phase shifts used to focus the array.
$E(f)$	Error in transform due to windowing and to noise (4).
$E[\cdot]$	Expected value of (\cdot)
$\mathcal{E}(\Delta T, M, \tau_a)$	RMS bias error of transform due to windowing.
f_{Θ}	Probability density function for Θ .
f_{Ψ}	Probability density function for Ψ .

ξ	Reducing coefficient in adaptive estimator (5).
Θ	Sample variance of steered data (5).
\underline{I}	Identity matrix.
\underline{k}	Wavenumber vector.
K_w	Window factor.
χ	Matrix condition number.
L	Number of observations used in forming the covariance matrix.
λ	Ray parameter (1). Non-centrality parameter (5).
λ_i	Eigenvalues of \underline{R} .
$\underline{\Lambda}$	Eigenvalue matrix of \underline{R} .
M	Half width of data window.
$M(a,b,x)$	First form of Kummer's function.
$n(t)$	Noise in data.
n_{ij}	Noise from i^{th} channel and j^{th} observation.
N	Number of channels.
\underline{N}_k	Noise vector from k^{th} observation.
$N(\underline{S}, \underline{\Sigma})$	Multi-variate complex Gaussian-normal distribution.
$P_c(t_0, \bar{c}; f), P_c(f), P_c$	Conventional velocity/depth estimator.
$P_{MLM}(t_0, \bar{c}; f), P_{MLM}(f), P_{MLM}$	Maximum Likelihood Method velocity/depth estimator.

ϕ_i	Angle with vertical of wave vector in i^{th} layer (1).
$\Phi(k, \theta k_0, \theta_0)$	Monochromatic plane wave ambiguity function (3).
$\Phi(T_2, C_2 T_1, C_1)$	Monochromatic velocity/time ambiguity function.
$\Phi_{\text{WB}}(T_2, C_2 T_1, C_1)$	Wideband velocity/time ambiguity function.
$\chi^2(L, \lambda), \chi^2(L), \chi^2$	Chi-squared distribution function.
$\Psi_p(k_0, \theta_0)$	Plane wave steering function.
Ψ	Square of the sample mean of steered data (5).
$\underline{R}(f)$	Covariance matrix of data field.
$\hat{R}(T, C; f), \hat{R}(f)$	Estimated local covariance matrix for data windowed by T, C.
$\rho(f_0, T_0, \bar{C} f_i, T_i, \bar{C})$	Normalized response of velocity depth array (conventional) to frequency bandwidth.
$\mathcal{A}(t)$	Reflected signal in data.
$\mathcal{J}(f)$	Fourier transform of signal $\mathcal{A}(t)$.
S_j	Signal from channel j.
\underline{S}	Vector of signals in the data.
$S(f)$	Frequency spectrum of seismic source signal (3).
$S_x(f)$	Frequency spectrum of process $x(t)$.
$S_n(f)$	Frequency spectrum of process $n(t)$.
$S_{\text{MLM}}(k)$	MLM wavenumber estimator.
σ_{ij}	Covariance of noise process $n(t)$, channels i and j.
σ_E^2	Distribution scaling factor.

σ_P^2	Variance of conventional estimator.
$\sigma_{P_{MLM}}^2$	Variance of MLM estimator.
σ_Y^2	Uniform noise variance of data for simplified statistics.
$\underline{\Sigma}$	Covariance matrix of noise process \underline{N} .
t_i	Travel time (one-way) through i^{th} layer (1).
t_{o_i}	Travel time thickness of i^{th} layer (1).
T, T_j	Two-way acoustic travel time from source to (j^{th}) receiver.
T_o	Normal incidence two-way travel time.
$\text{Tr}(\cdot)$	Trace of (\cdot).
τ_a	Half width of signal envelope $a(t)$.
τ_d	Delay of signal
τ_w	Delay of data window $w(t)$.
$U(\cdot)$	Unit step function.
$\underline{U}(f)$	Data matrix.
${}^qU(a,b,x)$	Second form of Kummer's function.
$w(t)$	Data window function.
$W(L, \underline{\Sigma})$	Wishart distribution function.
\underline{W}	Eigenvector matrix of \underline{R} .
$x(t)$	Wideband stationary process of stochastic signal model.
$\underline{X}, \underline{X}_j$	Source to (j^{th}) receiver distance.
$Y(t), Y_i(t)$	Data from channel i .

$\underline{Y}_i(f), \underline{Y}_{ij}$

Frequency domain representation of signal from channel i (observation j).

 $\underline{Y}(f), \underline{Y}_j$

Vector of channels of frequency domain representations (observation j).

 $\underline{Y}(T, C; f)$

Frequency domain representation of data in windows positioned according to T, C .

 \underline{Z}

Non-constant part of adaptive estimator.

 $\underline{\mathbb{1}}$

Unitary vector (all ones).

REFERENCES

- Abramowitz, Milton; and Stegun, Irene A., Handbook of Mathematical Functions, Dover Publications, New York,
- Anderson, T. W., An Introduction to Multivariate Statistical Analysis, John Wiley and Sons, Inc., New York, 1958.
- Baggeroer, A. B., "High Resolution Velocity/Depth Spectra Estimation for Seismic Profiling", paper presented at 1974 I.E.E.E. Conference on Engineering in the Ocean Environment, Ocean'74 Proceedings, Vol. II, p. 201., 1974.
- Baggeroer, A. B.; and Leverette, S. J., "Estimation of Velocity/Depth Spectra Using the Maximum Likelihood Method", Paper presented at the 1975 Annual Meeting of the S.E.G., Denver, Colorado, October, 1975.
- Burg, J. P., "Maximum Entropy Spectral Analysis", Paper presented at the 37th Annual International S.E.G. Meeting, Oklahoma City, Oklahoma, October 31, 1967.
- Capon, J.; Greenfield, R. J.; Kolker, R. J., "Multidimensional Maximum Likelihood Processing of a Large Aperture Seismic Array", Proceedings of the I.E.E.E., Vol. 55, No. 2, p. 192-211, February, 1967.

- Capon, J., "High-Resolution Frequency-Wavenumber Spectrum Analysis", Proceedings of the I.E.E.E., Vol. 57, No. 8, p. 1408-1448, August 1969.
- Capon, J.; Goodman, N. R., "Probability Distributions for Estimators of the Frequency Wavenumber Spectrum", Proceedings of the I.E.E.E., Vol. 58, p. 1785-1786, October 1970.
- Dix, C. H., "Seismic Velocities from Surface Measurements", Geophysics, Vol. XX, No. 1, p. 68-86, January 1955.
- Dürbaum, H., "Zur Bestimmung von Wellengeschwindigkeiten aus reflexionsseismischen Messungen", Geophysical Prospecting, Vol. 2, p. 151-167, 1954.
- Edelblute, D. J.; Fisk, J. M.; Kinnison, G. L., "Criteria for Optimum-Signal-Detection Theory for Arrays", Journal of the Acoustical Society of America, Vol. 41, No. 1, p. 199-205, 1967.
- Gabriel, William F., "Adaptive Arrays - An Introduction", Proceedings of the I.E.E.E., Vol. 64, No. 2, p. 239-272, February 1976.
- Goodman, N. R., "Statistical Analysis Based on a Certain Multivariate Complex Gaussian Distribution", Ann. Math. Stat. Vol. 34, p. 152-177, March 1963.

- Graybill, F. A., Introduction to Matrices with Applications in Statistics, Wadsworth Publishing Company, Inc., Belmont, California, 1969.
- Green, C. H., "Velocity Determinations by Means of Reflection Profiles", Geophysics, Vol III, No. 4, p. 295-305, October 1938.
- Green, P. E. Jr.; Frosch, R. A.; Romney, C. F., "Principles of an Experimental Large Aperture Seismic Array (LASA)", Proceedings of the I.E.E.E., Vol. 53, p. 1821-1833, December 1965.
- Kline, R. B., "Performance of Adaptive Arrays in the Fresnel Region", Masters Thesis, Mass. Inst. of Tech., dept. of Electrical Engineering, May 11, 1976.
- Kramer, F. S.; Peterson, R. A.; Walter, W. C., editors, Seismic Energy Sources - 1968 Handbook, Bendix United Geophysical Corporation, October 1968.
- Lacoss, R. T., "Data Adaptive Spectral Analysis Methods", Geophysics, Vol. 36, No. 4, p. 661-675, August 1971.
- LePichon, Xavier; Ewing, J.; Houtz, R. E., "Deep-Sea Sediment Velocity Determination Made While Reflection Profiling", Journal of Geophysical Research, Vol. 73, No. 8, p. 2597-2614, April 15, 1968.

- Makhoul, John, "Linear Prediction: A Tutorial Review",
Proceedings of the I.E.E.E., Vol. 63, No. 4, p. 561-580,
April 1975.
- Papoulis, Athanasios, Probability, Random Variables, and
Stochastic Processes, McGraw-Hill, New York, 1965.
- Parzen, E., "Multiple Time Series Modeling", Tech. Rep. 12
on contract NONR-223-(80), Stanford University, 1968.
- Parzen, E., "Multiple Time Series Modeling" in Multivariate
Analysis, Vol. 2, P. R. Krichnaiak, editor, Academic
Press, New York, 1969.
- Pusey, L., "An Innovations Approach to Spectral Estimation and
Wave Propagation", Ph.D. Thesis, M.I.T., 1975.
- Rao, C. Radhakrishna, Linear Statistical Inference and its
Applications, John Wiley & Sons, Inc., New York, 1965.
- Skolnik, Merril I., Introduction to Radar Systems, McGraw-Hill,
New York, 1962.
- Taner, M. Turhan; Koehler, Fulton, "Velocity Spectra - Digital
Computer Derivation and Applications of Velocity
Functions", Geophysics, Vol. 34, No. 6, p. 859-881,
December 1969.
- Van Trees, H. L., Detection, Estimation, and Modulation
Theory, Part I, John Wiley & Sons, Inc., New York, 1968.

Biographical Note

Steven John Leverette was born and raised in Miami, Florida. He attended Southwest Miami Senior High School, graduating in June 1968. He attended Gettysburg College and received a B.A. in physics in June 1972. Steve worked with the Reactor Engineering Division of the Oak Ridge National Laboratory as a summer fellow in 1971 and as a consultant in 1972. In June 1972 he entered the MIT/WHOI Joint Program in Ocean Engineering, and is a candidate for the Ph.D. in August 1977. During the period from January 1974 to June 1977 he helped develop much of the processing system for the WHOI multi-channel seismic system. Steve is a member of S.E.G. and Sigma Xi.